

AD-A165 003

NUMERICAL HEAT TRANSFER MODEL FOR A HEAT-BARRIER-PISTON
ENGINE WITH HYPER.. (U) NAVAL ACADEMY ANNAPOLIS MD DIV
OF ENGINEERING AND WEAPONS D A BLANK FEB 86

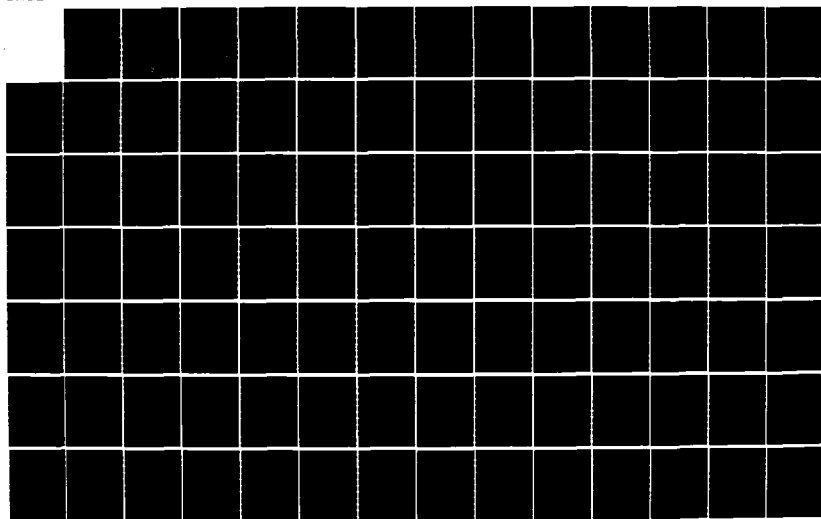
1/3

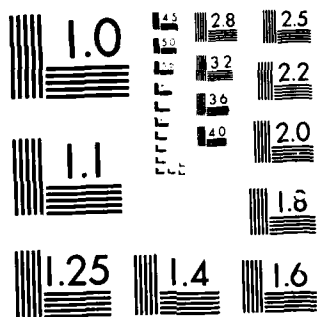
UNCLASSIFIED

USNA-EN-8-86

F/G 21/7

NL





MICROCOPY RESOLUTION TEST CHART
NATIONAL BUREAU OF STANDARDS 1963-A

20

AD-A165 083

NUMERICAL HEAT TRANSFER MODEL FOR A
HEAT-BARRIER-PISTON ENGINE WITH
HYPERGOLIC COMBUSTION

David A. Blank, LCDR, USN

UNITED STATES NAVAL ACADEMY
Annapolis, MD 21402

February 1986

Report No. EW-8-86

UNITED STATES NAVAL ACADEMY
DIVISION OF
ENGINEERING AND WEAPONS
ANNAPOLIS, MARYLAND

DTIC FILE COPY

DTIC
ELECTE
MAR 10 1986

DISTRIBUTION STATEMENT A
Approved for public release
Distribution Unlimited

B

86 3 6 0

NUMERICAL HEAT TRANSFER MODEL FOR A
HEAT-BARRIER-PISTON ENGINE WITH
HYPERGOLIC COMBUSTION

David A. Blank, LCDR, USN

UNITED STATES NAVAL ACADEMY
Annapolis, MD 21402

February 1986

Report No. EW-8-86

DTIC
ELECTE
MAR 10 1986
B

DISTRIBUTION STATEMENT A
Approved for public release
Distribution Unlimited

Work sponsored by Naval Academy Research Council (NARC)

UNCLASSIFIED

SECURITY CLASSIFICATION OF THIS PAGE (When Data Entered)

REPORT DOCUMENTATION PAGE		READ INSTRUCTIONS BEFORE COMPLETING FORM
1. REPORT NUMBER USNA EW-8-86	2. GOVT ACCESSION NO. AD-A165833	3. RECIPIENT'S CATALOG NUMBER
4. TITLE (and Subtitle) Numerical Heat Transfer Model for a Heat-Barrier-Piston Engine with Hypergolic Combustion		5. TYPE OF REPORT & PERIOD COVERED Progress, 1982-1986
7. AUTHOR(s) David Alan Blank, LCDR, USN		6. PERFORMING ORG. REPORT NUMBER EW-8-86
9. PERFORMING ORGANIZATION NAME AND ADDRESS U.S. Naval Academy Naval Systems Engineering Department Annapolis, MD 21402		8. CONTRACT OR GRANT NUMBER(s)
11. CONTROLLING OFFICE NAME AND ADDRESS Research Office Office of the Academic U.S. Naval Academy, Annapolis, MD 21402		10. PROGRAM ELEMENT, PROJECT, TASK AREA & WORK UNIT NUMBERS
14. MONITORING AGENCY NAME & ADDRESS (if different from Controlling Office)		12. REPORT DATE February 1986
		13. NUMBER OF PAGES 189
		15. SECURITY CLASS. (of this report) Unclassified
		15a. DECLASSIFICATION/DOWNGRADING SCHEDULE
16. DISTRIBUTION STATEMENT (of this Report) <div style="border: 1px solid black; padding: 5px; text-align: center;">DISTRIBUTION STATEMENT A Approved for public release Distribution Unlimited</div>		
17. DISTRIBUTION STATEMENT (of the abstract entered in Block 20, if different from Report) Distribution Unlimited		
18. SUPPLEMENTARY NOTES		
19. KEY WORDS (Continue on reverse side if necessary and identify by block number) Numerical Heat Transfer Internal Regeneration Adiabatic Engine Adiabatic Piston Engine Heat Barrier Piston Engine		
20. ABSTRACT (Continue on reverse side if necessary and identify by block number) Axisymmetric turbulent combustion flow with heat transfer has been modeled for a four-stroke engine exhibiting hypergolic combustion and containing a heat barrier within the piston. The boundaries of the solution scheme extend fixed distances into the piston and cylinder lining. In the model, a valve was simulated which has thickness for the purpose of heat transfer calculations and is infinitely thin for the purpose of fluid flow field calculations. A fuel injector was numerically modeled which gave good simulation of the type of —>		

DD FORM 1 JAN 73 1473

EDITION OF 1 NOV 65 IS OBSOLETE
S/N 0102-LF-014-6601

UNCLASSIFIED

SECURITY CLASSIFICATION OF THIS PAGE (When Data Entered)

UNCLASSIFIED

SECURITY CLASSIFICATION OF THIS PAGE (When Data Entered)

injector used in current hypersonic combustion research. The implicit finite-difference solution of the governing equations for the primitive variables was conducted in three regions, one fixed in space with time, one utilizing a stretching and compressing computational mesh and one which moved with time without stretching and compressing. An accuracy check of the computational code for the five primitive variables representing the non-combustion case was conducted by specifying an analytic expression for each of these variables and changing the source terms of the corresponding governing equations to make these analytic expressions into the solution for the resultant set of modified equations. Comparison of the numerically computed solution with the specified analytic solution gave excellent agreement. A further check was made to ensure the accuracy of the work by comparing the results of the solution of a two-stroke motored engine with the numerical results of another researcher whose work for the same engine configuration gave reasonable correlation with recent experimental data. The model was used to simulate the compression stroke and fuel injection portion of the power stroke, as well as the initial portion of the exhaust stroke of a four-stroke engine using hypersonic combustion and with a weak barrier placed a distance below the surface of the piston. For the final runs a 20 x 26 mesh was used to solve the conjugate heat transfer problem in the fluid flow field as well as in a thin portion of the adjacent cylinder and piston regions and a 17 x 20 mesh was used for the other flow field calculations.

The overall objective of the analysis was the development of a comprehensive computer code to be used as a tool in directing and interpreting future experimental work. Because very little experimentation has been done in the area of hypersonic combustion to date, the numerical results generated for the combusting case were not compared with experimental data.

RE: Distribution Statement
Unlimited per CDR David A. Blank, U. S.
Naval Academy, Division of Engineering and
Weapons

Accession For	
NTIS GRA&I	<input checked="checked" type="checkbox"/>
DTIC TAB	<input type="checkbox"/>
Unannounced	<input type="checkbox"/>
Justification	<input type="checkbox"/>
By	
Distribution	
Availability Codes	
AVAIL & FOR	
Dist	Special
A-1	

S N 0102- LF- 014- 6601

UNCLASSIFIED

SECURITY CLASSIFICATION OF THIS PAGE (When Data Entered)

TABLE OF CONTENTS

	<u>Page</u>
ACKNOWLEDGEMENTS	iii
LIST OF TABLES	iv
LIST OF FIGURES	v
LIST OF SYMBOLS	vii
 Chapter 1 <u>INTRODUCTION</u>	 1
1.1 Preliminary Remarks	1
1.2 Previous Investigations	2
1.3 Scope and Contributions of the Present Investigation	7
 Chapter 2 <u>GOVERNING EQUATIONS</u>	 13
2.1 Flow Field Equations in Primitive Coordinates	14
2.2 Transformation of Flow Field Equations	18
2.3 Flow Field Equations in Transformed Coordinates	21
2.4 Non-flow Energy Equation	21
2.5 Boundary Conditions	23
2.5.1 Velocity Boundary Conditions	27
2.5.2 k- ϵ Boundary Conditions	31
2.5.3 Temperature Boundary Conditions	36
2.5.4 Fuel Species and Mixture Fraction Boundary Conditions	44
 Chapter 3 <u>COMBUSTION MODEL</u>	 47
3.1 Species Mass Fraction and Mixture Fractions	48
3.2 Energy Equation Combustion Source Term Model	49
3.3 Variation of the Specific Heat (C_p) Due to Combustion	50
 Chapter 4 <u>NUMERICAL PROCEDURES</u>	 54
4.1 Discretization of Governing Equations	54
4.1.1 Discretization of the Transformed Continuity Equation	55
4.1.2 Discretization of the Transformed General Transport Equation	58
4.1.3 Discretization of transformed source terms	61
4.1.4 Discretization of the Non-flow (NF) Energy Equation	68
4.2 Special Procedure for Calculating the Pressure Field	69
4.3 Perturbation of Continuity Equation	74
4.4 Solution Procedure	76

	<u>Page</u>
Chapter 5 <u>VALVE MODEL</u>	79
5.1 Solution Regions	81
5.2 Valve Inlet and Valve Boundary Conditions	83
5.3 Effects of Fluid Entrainment Due to Valve Motion on Time Dependent Properties	90
Chapter 6 <u>NOZZLE MODEL</u>	94
Chapter 7 <u>ERROR ANALYSIS OF THE SOLUTION SCHEME</u>	106
7.1 Error Analysis Technique	106
7.2 Formulation of Error Analysis Test	109
Chapter 8 <u>DISCUSSION OF RESULTS</u>	112
8.1 Error Analysis Results	112
8.2 Case 3 Results	114
8.3 Case 5 Results	117
8.4 Concluding Remarks	120
 <u>APPENDICES</u>	
A. Energy Equation	123
B. Piston Displacement and Velocity	126
C. Non-Flow Region Temperature Transformation Technique	127
D. Solution Region Interface Code Modifications	130
E. Results	133
 Bibliography	 170

ACKNOWLEDGEMENTS

The author is in debt to many persons for their assistance toward his progress in the completion of this study. Without their help this work never could have been completed.

The excellent guidance, the wise advice and strong encouragement of Dr. Tien-Mo Shih and Professor Eugene L. Keating during the past five years in relation to this research is especially appreciated. The trust and friendship shown the author by these two individuals will never be forgotten.

The author is in deep gratitude for the support given him by David Meeks and his wife Sandra W. Blank during the final stages of the project. Both of these individuals sacrificed much in helping the author to finish.

The author owes alot to his friend and fellow graduate student Associate Professor John Allen for his encouragement and pertinent counsel during the duration of this work. The outstanding advice of Richard Chute, Dave Scharnweber and Lyle Hoppie of Eaton Corporation is much appreciated. Their assistance played a major role in the formulation of the problem and in several aspects of the modeling.

The author also appreciates the support given him by the Naval Systems Engineering Department of the U.S. Naval Academy in helping him to obtain funding and providing him time to do the work. The assistance of the Naval Systems secretarial staff and of Ms. Inez Johnson in the typing of the manuscript is greatly appreciated.

Finally, and most importantly, the author is in deep gratitude to his Lord Jesus Christ, whose divine guidance and strength made all of this effort possible.

LIST OF TABLES

	<u>Page</u>
2-1 Transformed Governing Equations for the Flow Field	22
3-1 Heats of Formation	52
3-2 Specific Heat at Constant Pressure	53
5-1 Valve Velocity Profile	93
6-1 Modification to Equation (4-2) and (4-54) for solution of various ϕ 's and P' at the nodal points adjacent to the throat opening of the fuel injector shown in figure 6-4	105
7-1 $R_{anal\phi}$ for various ϕ 's	111
E-1 u-velocity equation error analysis	135
E-2 v-velocity equation error analysis	136
E-3 Turbulent kinetic energy equation error analysis	137
E-4 Turbulent kinetic energy dissipation rate equation error analysis	138
E-5 Flow energy equation error analysis	139
E-6 Error analysis for combined u, v, k, ϵ , T equations	140-142
E-7 Error analysis for combined u, v and k equations	143-144

LIST OF FIGURES

	<u>Page</u>
1-1 Heat Barrier Piston Engine Configuration	8
2-1 Engine Geometry and Coordinate Systems	20
2-2 Nomenclature for Geometry of Near Wall Boundary Conditions	25
2-3 Velocity Law of Wall for Viscous Sublayer	26
2-4 Temperature Boundary Conditions, for Outer Nonflow borders	37
2-5 Nonflow Solution Region	42
4-1 Geometry for Control volumes of primitive variables except u and v	56
4-2 Geometry for control volumes of primitive variables u and v	57
4-3 Overview of Solution Code	77
5-1 Solution Regions	80
5-2 Open valve from viewpoints of both flow and nonflow energy equations	86
6-1 Diesel Fuel Injector	95
6-2 Nozzle Fuel Injector Model	96
6-3 Detailed Description of Nozzle Fuel Injector Model	100
6-4 Blow-up of Control Volume for Various Primitive Variables Adjacent to Fuel Nozzle	102
7-1 Boundary Conditions used in error analysis	108
C-1 Comparison of Region 4 nodal points at times (n-1)/rpm and n/rpm	127
D-1 Solution region interfaces	132
E-1 Case 3 Velocity vector plot for a crank shaft angle of 300°	145
E-2 Comparison of u-velocity profiles for case 3 run with an identical run performed by Ramos and Sirignano ⁶⁹	146

E-3	Case 3 temperature profile for a crank shaft angle of 300°	147
E-4	Case 5 temperature profile for $\theta = 300^\circ$, run 1	148
E-5	Case 5 temperature profile for $\theta = 360^\circ$, run 1	149
E-6	Case 5 temperature profile for $\theta = 372^\circ$, run 1	150
E-7	Case 5 temperature profile for $\theta = 384^\circ$, run 1	151
E-8	Case 5 temperature profile for $\theta = 360^\circ$, run 2	152
E-9	Case 5 temperature profile for $\theta = 366^\circ$, run 2	153
E-10	Case 5 temperature profile for $\theta = 570^\circ$, run 3	154
E-11	Case 5 velocity vector plot for $\theta = 300^\circ$, run 1	155
E-12	Case 5 velocity vector plot for $\theta = 360^\circ$, run 1	156
E-13	Case 5 velocity vector plot for $\theta = 372^\circ$, run 1	157
E-14	Case 5 velocity vector plot for $\theta = 384^\circ$, run 1	158
E-15	Case 5 velocity vector plot for $\theta = 360^\circ$, run 2	159
E-16	Case 5 velocity vector plot for $\theta = 366^\circ$, run 2	160
E-17	Case 5 velocity vector plot for $\theta = 570^\circ$, run 3	161
E-18	Case 5 product mass fraction distribution for $\theta = 366^\circ$, run 2	162
E-19	Case 5 fuel mass fraction distribution for $\theta = 366^\circ$, run 2	163
E-20	Case 5 specific heat values at $\theta = 366^\circ$, run 2	164
E-21	Case 5 turbulent kinetic energy distribution at $\theta = 366^\circ$, run 2	165
E-22	Case 5 turbulent kinetic energy dissipation rate distribution at $\theta = 366^\circ$, run 2	166
E-23	Case 5 effective viscosity (μ_{eff}) profile for $\theta = 366^\circ$, run 2	167
E-24	Case 5 pressure (P) versus crankshaft angle (θ), run 2	168
E-25	Case 5 piston surface heat transfer rate versus crankshaft angle (θ), run 2	169

LIST OF SYMBOLS

A	Area of the wall of the control volume
A	Van Driest constant (= 26.0)
A	Empirical reaction rate coefficient (=20)
a_m	Coefficient of combined convective/conductive flux through the designated wall of the control volume ($m = n, s, e, w$)
a_p	Sum of coefficients of combined convective/conductive flux through control volume walls
B	Empirical reaction rate coefficient (=0.5)
C_1, C_2, C_μ	Constants of turbulence model, assigned values 1.44, 1.92 and 0.09 respectively
C_6, C_7	Arbitrary constants used in error analysis
C	Clearance
C	Number equal to 1 when solving using error analysis formulation of Chapter 7; equal to 0 otherwise.
C	Specific heat
c	Flux of momentum per unit area
C_D	Constant of turbulence model, assigned value of 1.0
C_D	Discharge coefficient
C_p	Specific heat at constant pressure
D	Dissipation
D	Diameter of fuel injector orifice openings
dist1	Axial length of solution region 1
dist2	Axial length of solution region 3
d_n, d_s, d_e, d_w	Defined by equations (4-49) - (4-52)
E	Turbulence model constant, assigned a value of 9.793
f	Mixture fraction
G	Generation of turbulent kinetic energy
\bar{G}	Transformed expression for generation of turbulence kinetic energy

h	Combined convective and radiative heat transfer coefficient
h	Enthalpy
h_j^0	Heat of formation of species j
i	Indicy corresponding to axial (x or z) direction
J	Flux
j	Indicy corresponding to radial (r) direction
K	Thermal conductivity
K	Von Karmen constant (= .4187)
k	Turbulent kinetic energy
L	Length of the connecting rod
λ	Semi-stroke
M	Mass in a finite difference cell-volume divided by the computational time increment
\dot{m}	Flux of mass through a wall of a cell-volume
\dot{m}	Mass flow rate
\dot{m}_i	Rate of consumption/production of species i per unit volume
m_i	Mass fraction of species i
p	Pressure
P_m	Peclet number ($m = e, w, n$ or s)
Pr_λ, Pr_t	Laminar and turbulent Prandtl numbers assigned values of 1.0 and 1.0 respectively
\dot{q}'''	Rate heat flux per unit volume
R_j	Gas constant for species i
\bar{R}	Universal gas constant
R_j	Rate of consumption/production of species j
r	Radial coordinate

r_v	Radius of the valve
S, \bar{S}	Source term in untransformed and transformed governing differential equations respectively
S_c	Schmidt number (value of 1.0 used)
S_p	Portion of integrated source term which is multiplied by ϕ_p (see section 4.1.2)
S_u	Portion of integrated source term (see section 4.1.2)
s	Stoichiometric oxygen requirement per unit mass of fuel
T	Temperature
t	Time
u	Axial velocity in Eulerian frame
\bar{u}	Axial velocity relative to moving coordinate frame
U	Velocity
u_v	Valve velocity
V	Cell volume
v	Radial velocity
W_i	Molecular weight of species i
x	Non-dimensional axial coordinate
y	General coordinate, either z or r
z	Axial coordinate
z_p	Instantaneous distance between cylinder and piston heads
z_v	Valve position

Greek Symbols

β	$= (\partial \rho / \partial T)_p$
γ	$= (\partial \rho / \partial p)_T$
γ	$= \frac{\mu}{Pr}$

Γ	Effective diffusivity
δ	Increment
∇	General operator
∇	Divergence operator
Δt	Time increment
δp	Instantaneous axial length of solution region 2
ϵ	Dissipation rate of turbulent kinetic energy
θ	Crank shaft angle
θ	Angular coordinate in cylindrical coordinates
μ	Dynamic viscosity
μ_{eff}	Effective viscosity equal to the sum of the dynamic and turbulent viscosities
μ_t	Turbulent viscosity
ρ	Density
$\sigma_k, \sigma_\epsilon$	Constants of turbulence for turbulent energy and energy dissipation rate, assigned values 1.0 and 1.2 respectively.
τ	Shear stress
ω	Angular velocity of the engine

Subscripts

a	air
P,N,S,E,W	Nodal points of finite-difference grid
n,s,e,w	Cell boundary locations of finite-difference grid
eff	Effective
F	Field
f	Fuel
g	Gas

in	Inert
ℓ, l	Laminar
O_2	Oxygen
p	Piston
pr	Product
t	Turbulent
v	Valve
vs	Valve seat
w	Wall

Superscripts

-	overbar - denotes average or global value
'	correction
*	Approximate or temporary value
*	Throat valve for nozzle
n	New time level
o, n-1	Old time level

CHAPTER 1
INTRODUCTION

1.1 Preliminary Remarks.

The present global energy situation has greatly increased the demand for the creation of more highly efficient energy conversion methods. Because of the preponderant use of reciprocating internal combustion engines in converting the world's fossil fuels into useful work, the need for innovations in internal combustion engine design is paramount.

Until very recently, the means by which such innovations could be developed was limited largely to experimentation. The theoretical understanding of the internal combustion process was based on classical thermodynamics and combustion theory. The properties of the working substance within the engine were viewed as being homogeneous throughout, and the fluid dynamics of the gases within the combustion chamber was not considered. With the advent of great progress in the area of turbulent modeling, the development of several powerful numerical methods for solving fluid and energy flow within enclosed boundaries, and the significant advances made in combustion modeling, it is now possible to begin to analyze with much more realism, the processes taking place inside internal combustion (IC) engines. The objective of the research effort recorded in this report, was to bring to bear a select array of these recent developments on a specific IC engine innovation in order to create a flexible solution code for use in assisting future experimental work on a new and unique engine concept.

The diesel engine for which this model has been developed, has two significant innovations. A barrier placed a distance below the surface

of the piston retards heat flow through the bottom of the piston. As a result, the metal between the surface of the piston and this barrier stores and re-adds energy to the working substance during the engine cycle. The second innovation involves the use of a new combustion method called hypergolic combustion. In this method the fuel is pre-heated to above its activation temperature, so that as soon as a fuel radical comes in contact with a radical of oxygen after the fuel has been sprayed into the engine, the complete combustion of the fuel radical takes place immediately. Thus the heat release rate is much faster than in normal diesel engines and high compression ratios are not required.

Due primarily to the need to limit the scope of the present study coupled with the fact that only one experimental analysis of hypergolic combustion has been conducted to date [1], the thrust of the work reported herein is the development and validation of a working computer code for use in future engine development. An analysis of these engine concepts using the code developed will be the subject of follow on research.

1.2 Previous Investigations Leading Up to the Present Analysis.

A review of the past decade and a half of literature pertaining to the numerical modeling of combustion in IC engines and on related topics reveals that there are a maze of approaches being pursued that have applicability to this problem. Included are five major areas:

1. The degree of geometric dimension used in the analysis: Zero dimensional models average the spatially varying quantities and use only time as the independent variable. One dimensional models use time along with only one spacial coordinate and involve averaging along the other coordinates. The multi-dimensional approach, also referred to as full simulation

approach, involves the simulation of all processes which occur in the engine including fluid motion.

2. The engine feature simulations considered: This includes a variety of items such as valve models, fuel injection models, spark models, flame propagation models, wall quenching, piston motion, etc.
3. The fluid dynamics assumptions made: This includes such items as whether the flow is considered viscid or inviscid, laminar turbulent, having uniform gas properties such as specific heat and diffusivity or properties that vary spacially, etc.
4. The type of combustion model employed: Turbulent mixing models and chemical kinetics models are in use. The chemical kinetics models vary from use of single equation models to use of detailed chemical kinetics which considers the myriad of branch reactions involved in hydrocarbon combustion.
5. The numerical method employed to solve the resultant set of model equations: The approaches in use vary greatly.

A complete accounting of the references pertaining to all the permutations of these five major areas would be excessive. Instead, a literature route which briefly describes the wake of significant work behind the present study of hypergolic combustion in a heat barrier piston engine will be given.

Work begun by Blaser and added to by Pouring, Failla, Rankin, et al,²⁻⁵ lead to the development of an innovative internal combustion engine referred to as the "Heat Balanced" engine, which was found to give efficiency increases of over 40 percent compared to conventional IC engines under certain operating conditions. The major feature of this

design is the carving out of a volume from the piston just below its top and along its outside radius creating, in effect, a second chamber. It was found that with this design a portion of the heat which normally would have been lost through the bottom of the piston was instead re-added to the air mixture during the intake and compression strokes of the combustion cycle.

The discovery of this phenomenon, called internal regeneration, led to a series of follow on studies. Work by Adams^{6,7} to study heat transfer in the "cap" portion of this piston by modeling the cap as a radial fin gave insight into this phenomenon. A theoretical study was conducted by Keating, et al,^{8,9} on the potential effects of several assumed mechanisms on engine performance using the air standard cycle as the basis for the description of engine stroke processes. The model described herein is the result of a parallel effort which was begun at about the same time. It was developed for the ultimate purpose of studying the mechanism of internal regeneration and represents a solution to the conjugate heat transfer problem between the piston and the engine gases. It uses a full simulation approach to model the engine stroke processes.

In the search for an adequate engine model for this study, it was determined advantageous to configure the engine as shown in figure 1-1, with a heat barrier placed in the piston a distance below its surface making it a heat barrier piston engine. The heat barrier piston engine, a type of adiabatic piston engine, also stores and re-adds thermal energy to the engine cycle and is considered optimum for the study of this concept because of the simplified geometry involved. For reasons explained in the next paragraph, it was also decided best to configure the engine for hypergolic combustion. There has been much recent

investigation [10 - 18] of engine modifications similar to those considered in this present work. The thrust of the research dealing with low heat rejection (adiabatic) engines has been experimental only [10 - 16].

A key to the study of cycle processes is the proper modeling of spatial heat release throughout the combustion stroke. The problems with adequately modeling combustion in IC engines are immense. The desire to create a model which could be confirmed by future experimental work, coupled with the desire to overcome the combustion problems associated with the overall higher operating temperatures of the heat barrier engine led to the adoption of a potentially significant combustion technique envisioned by Hoppie¹⁹ and demonstrated to be feasible by Scharnweber^{1,18}. The adoption of this technique called hypergolic combustion made possible the use of the fast chemistry model described by Lockwood in [20] with the expectation of good comparative results with future experimental work.

The advent of the full simulation approach is fairly recent. Previous workers modeled engine processes using zero dimensional [21,22] and one dimensional [23 - 30] approaches. Though much work along these lines continues [31 - 35], the use of the multi-dimensional approach is increasing in combustion engine analysis. Significant pioneering work in the development of this approach was conducted by groups at the University of Maryland [36 - 40], Imperial College [41 - 49], Princeton [50 - 54], Los Alamos [55 - 57], Lawrence Livermore [50,52,58], Science Application Inc. [59 - 61], etc. The group headed by Anderson at the University of Maryland was the first to simulate all 4-strokes in a

firing spark ignition engine using an explicit finite-difference procedure by MacCormack⁶². They also developed the first 3-dimensional engine simulation. Gosman, et al, at Imperial College developed a code called RPM based on an implicit, iterative, finite-difference scheme and has used the code to perform calculations for a number of engine configurations. The work by Bracco, Gupta, et al, at Princeton as well as Butler, et al, at Los Alamos was based on the RICE (Reactive Implicit Continuous-Fluid Eulerian) technique of Rivard, et al,⁶³. Work by Boni, et al, of Science Application used a semi-implicit Arbitrary Lagrangian-Eulerian (ALE) method of Hirt, Amsden, et al,⁶⁴ in calculations for combustion in a stratified-charge engine.

More recently, Haselman⁵⁸ of Lawrence Livermore has produced a method called "TDC" for use in the study of reacting flow using an explicit numerical scheme. Other workers of note in the field include Raimos and Sirignano^{65 - 70} who, using a computational scheme vary similar to Gosman's, carried out among the other things a detailed analysis of flow in the valve region of a motored engine. Bernard⁷¹ applied his turbulence closure method given in reference [72] to examine non-reacting turbulent flow in the compression stroke of an IC engine. At General Motors, Diwakar^{73,74} has used the "CONCHAS SPRAY" method of Butler, et al,⁷⁵ to study the Direct-Injector Stratified-Charge (DISC) engine.

Of those works among the above in which reacting flows was considered, most modeled the combustion process using an Arrhenius kinetics formulation, applicable to the laminar combustion process. Gosman, et al,⁴⁴⁻⁴⁸ has pursued an alternative approach explained in reference [20] by assuming that in most instances turbulence mixing, and

not chemical kinetics, dominates the local combustion rate. In the case of hypergolic combustion, this assumption would be even more valid and is thus the approach adopted in the present analysis.

The emphasis of all of the full simulation models mentioned above was the flow field of the engine only. No consideration was given to heat conduction inside the cylinder walls and piston of the engine. Thus, prior to the beginning of the work reported on herein the need for modeling this conjugate heat transfer problem using a full simulation approach existed in order to study the flow of heat in low heat rejection engines.

1.3 Scope and Contributions of the Present Investigation

As mentioned in section 1.1 the objective of this investigation is the development of a comprehensive computer code for use in the study of heat transfer in an IC engine configured with a heat barrier inside the piston and powered by fuel which is sprayed into the engine at a temperature above the fuel's activation temperature. The approach taken to the work has been to adapt, where possible, current developments in numerical heat transfer [76], turbulent flow modeling [41,66,77,78], combustion modeling for the case of fast chemistry [20,48,79], turbulent boundary layer theory [80], etc, in the formulation of the computational model in order to develop as accurate a code as possible. Compromises had to be made in light of the need for computational efficiency. Where no available developments were suitable for the code, original modeling was conducted. Also included in the work was the development of a graphics package for use in displaying and analyzing data generated by the code.

The following major assumptions were made in the development of the model (See figure 1-1):

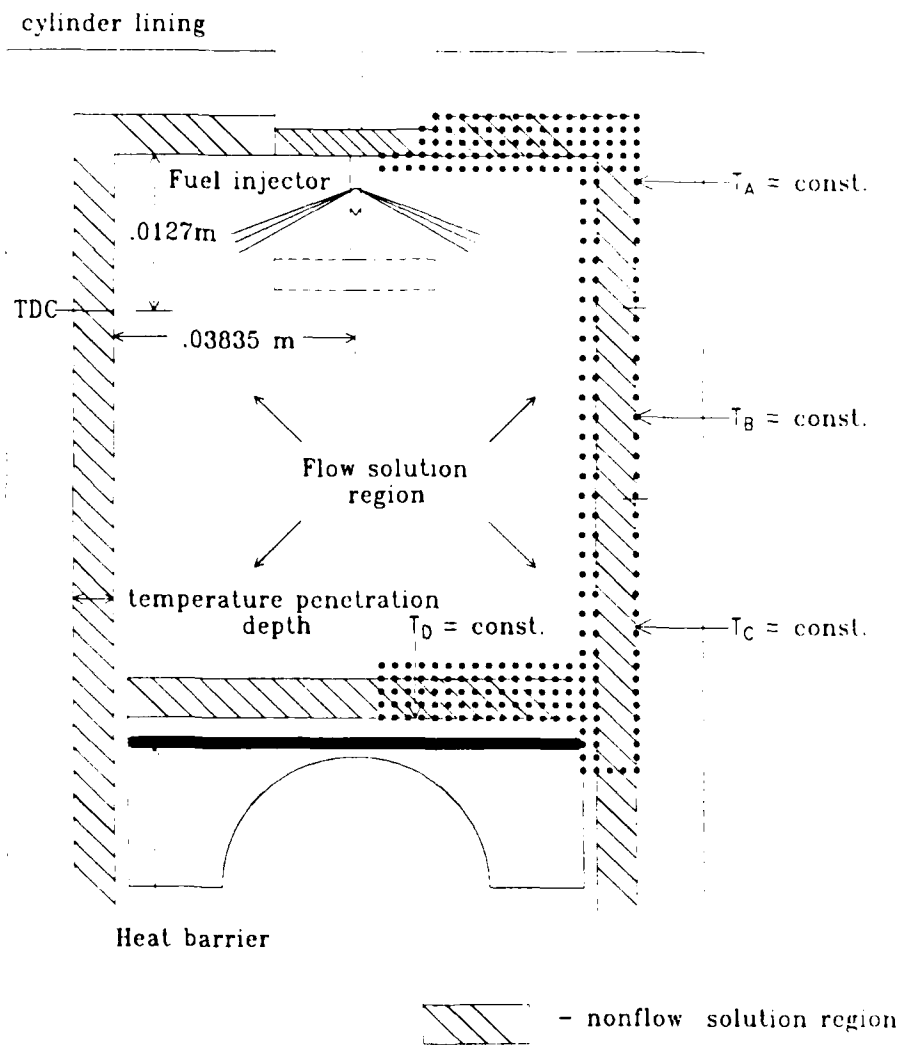


Figure 1-1. Heat Barrier Piston Engine Configuration.

- 1) Axisymmetric fluid flow.
- 2) Effects of swirl neglected.
- 3) Effects of radiation neglected (not a good assumption if the barrier in the piston strongly retards heat flow through the bottom of the piston). The barrier used in the present analysis is weak and thus makes this assumption reasonable.
- 4) Use of one valve placed along the symmetry axis for both intake and exhaust.
- 5) Use of law of the wall for specification of momentum and energy equation boundary conditions. (This specification only really valid for steady, 1-D flow with a zero pressure gradient in the boundary layer.)
- 6) Effects of wall flame quenching neglected. Higher wall temperatures due to the heat-barrier make this a reasonable assumption.
- 7) The time scale of the chemical kinetics is considered infinitely greater than the time scale of turbulent mixing and thus makes a fast chemistry model usable throughout. Note that because of the hypergolic nature of the combustion this is believed to be what is actually happening.
- 8) Specification of constant temperatures at a given distance within the piston and cylinder linings. This is based on experimental findings of Eaton Corporation [81]. See chapter 2 for the details.
- 9) Use of Perfect Gas Law.
- 10) Use of $k-\epsilon$ turbulence model due to Jones and Launder⁷⁷. (This model assumes turbulent kinetic energy is isotropic which is

not the case during the rapid expansion and compression processes taking place in IC engines.)

The above assumptions served to focus the development of the code toward a very specific problem. However, the necessary considerations taken into account in the development of this code made its scope very broad. For this reason, to limit the extent of the present work to within reason an indepth analysis of this special engine was not included. It will be the object of future research.

The resultant code was verified for accuracy by two means. The first of these, explained in Chapter 7, is an extension of an error analysis technique developed by Shih⁸². Details of the results of this comparison are contained in Chapter 8. The second verification was the comparison of the results of a computation for a given engine configuration with those of another researcher in the field whose results for this same computation gave good correlation with experimental results [69]. Details of this comparison are also given in Chapter 8.

The resultant model described on the pages that follow contains a number of innovations which may serve to advance the field of IC engine research. A summary of these contributions listed below serves not only to highlight the results of the work, but also to add clarification to the exact scope of the research effort:

1. The development of a method of simultaneously solving heat flow due to conduction within the metal of the cylinder and piston linings and heat flow within the engine's gas mixture:

Previous to the beginning of this work, researchers in the field using a full simulation approach specified a constant

wall temperature and neglected heat conduction within the engine wall linings. This particular development makes possible a parametric study of the effect of varying the strength of the barrier in the piston. Also, it makes possible the study of the effects of placing barriers at other locations in the engine. In order to complete this development it was necessary to solve the problem of how to transform the non-flow coordinate system for the energy equation to facilitate the matching of boundary condition nodal points with the transformed flow region equations. This matching was required because the nodal points used in the solution of the governing flow field equations are moving due to piston motion.

2. The development of a governing equation transformation technique which enables the distances of the near wall boundary nodal points to the walls of the piston and cylinder surfaces to remain unchanged throughout the engine cycle: This involved the breaking of the flow fluid into three solution regions.
3. The development of a detailed working valve model which enables the analysis of heat transfer within as well as to and from the valve when it is both seated, and while it is moving through the flow field region: The only serious valve modeling done prior to the beginning this work modeled the valve as infinitely thin for the purpose of heat transfer and neglected energy equation boundary conditions in the vicinity of the open valve [69].
4. The development of a model for the injection process of fuel under hypersonic conditions: Because the gaseous fuel at the

injection orifice openings was determined to be entering the combustion chamber at Mach 1; this was by far the most time consuming and challenging of the obstacles to overcome in the solution of the problem. Involved in the modeling process was the development of a special discretization scheme for the nodal points adjacent to the fuel entry point. Also involved was the detailed analysis and modification of governing equation source terms in the vicinity of the injection point.

5. The validation of the numerical accuracy of the power law discretization scheme for the convection diffusion problem developed by Patankar⁷⁶: An extension of the computational scheme error analysis technique developed by Shih⁸² was made to the computer code solution of the five applicable discretized governing equations for the non-reacting case. This analysis resulted not only in the verification of the accuracy of the code but also pointed to the preferred utility of Patankar's power law discretization scheme in the discretization of the total flux terms of the property transport equations. See section 4.1.2, chapter 7 and chapter 8 for details.
6. The determination of a baseline combustion engine model for use in the future study of low heat rejection engines: Not only can this model be used to study the specific engine innovations outlined earlier, but because of its simplistic geometry it may also be used as the basis for comparison of works dealing with more complex geometries, such as the heat balanced engine [2-5] or various other types of low heat rejection engines [10-16]. Also it can be used as a basis for comparison of the heat flow characteristics of low heat rejection engines using other combustion schemes.

Chapter 2

GOVERNING EQUATIONS

Calculation of heat flow in the fluid flow field of an internal combustion engine is governed by a coupled set of partial differential equations that account for mass continuity, mass momentum, energy and pertinent chemical species mass fractions for compressible turbulent reacting gas flow. Accounting for turbulence using the $k - \epsilon$ model requires the addition of two more equations. In the non-flow portion of the engine (i.e., cylinder lining, piston and valve) only the energy equation is required.

Piston motion within the engine necessitates a special transformation of the governing equations to facilitate the convenient use of a control volume approach in the numeric solution of the governing equations. The axisymmetric geometry of the engine and the neglecting of the effects of swirl made possible the solution of the problem in cylindrical coordinates using only the r and z directions and two components of velocity.

The aim of the present chapter is to delineate the governing differential equations along with their boundary conditions used in the formulation of the problem. Not included are the specifics of the combustion model, and all the boundary conditions associated with the valve and fuel injector. Also, not included is the procedure for determining pressure. These items will be covered later. The governing equations are presented in both their untransformed and transformed forms for completeness.

2.1 Flow Field Equations in Primitive Coordinates

Continuity Equation

$$\frac{\partial \rho}{\partial t} + \frac{\partial}{\partial z} (\rho u) + \frac{1}{r} \frac{\partial}{\partial r} (r \rho v) = 0 . \quad (2-1)$$

Axial Momentum Equation [41, 67]

$$\frac{\partial}{\partial t} (\rho u) + \frac{\partial}{\partial z} (\rho u^2) + \frac{1}{r} \frac{\partial}{\partial r} (r \rho u v) = \frac{\partial}{\partial z} \left(\mu_{\text{eff}} \frac{\partial u}{\partial z} \right) + \frac{1}{r} \frac{\partial}{\partial r} \left(r \mu_{\text{eff}} \frac{\partial u}{\partial r} \right) + S_u , \quad (2-2)$$

where

$$\mu_{\text{eff}} = \mu_1 + \mu_t ,$$

$$\mu_1 = 1.78 \times 10^{-5} \frac{\text{N-s}}{\text{m}^2} ,$$

$$\mu_t = c_\mu \rho \frac{k^2}{\varepsilon} ,$$

$$c_\mu = .09 ,$$

$$S_u = - \frac{\partial p}{\partial z} + \frac{\partial}{\partial z} \left[\mu_{\text{eff}} \frac{\partial u}{\partial z} \right] + \frac{1}{r} \frac{\partial}{\partial r} \left[r \mu_{\text{eff}} \frac{\partial v}{\partial z} \right] - \frac{2}{3} \frac{\partial}{\partial z} \left[\mu_{\text{eff}} \nabla \cdot \underline{u} + \rho k \right]$$

and

$$\nabla \cdot \underline{u} = \frac{\partial u}{\partial z} + \frac{v}{r} + \frac{\partial v}{\partial r} .$$

Radial Momentum Equation [41, 67]

$$\frac{\partial}{\partial t} (\rho v) + \frac{\partial}{\partial z} (\rho u v) + \frac{1}{r} \frac{\partial}{\partial r} (r \rho v^2) = \frac{\partial}{\partial z} \left[\mu_{\text{eff}} \frac{\partial v}{\partial z} \right] + \frac{1}{r} \frac{\partial}{\partial r} \left[r \mu_{\text{eff}} \frac{\partial v}{\partial r} \right] + S_v , \quad (2-3)$$

where

$$S_v = - \frac{\partial p}{\partial r} + \frac{\partial}{\partial z} \left[\mu_{\text{eff}} \frac{\partial u}{\partial r} \right] + \frac{1}{r} \frac{\partial}{\partial r} \left[r \mu_{\text{eff}} \frac{\partial v}{\partial r} \right] - 2 \mu_{\text{eff}} \frac{v}{r^2} - \frac{2}{3} \frac{\partial}{\partial r} \left[\mu_{\text{eff}} \nabla \cdot \underline{u} + \rho k \right] .$$

k-ε Turbulence Model Equations [41,67,77,78]

For the turbulent kinetic energy (k):

$$\frac{\partial}{\partial t} (\rho k) + \frac{\partial}{\partial z} (\rho u k) + \frac{1}{r} \frac{\partial}{\partial r} (r \rho v k) = \frac{\partial}{\partial z} \left[\frac{\mu_{eff}}{\sigma_k} \frac{\partial k}{\partial z} \right] + \frac{1}{r} \frac{\partial}{\partial r} \left[r \frac{\mu_{eff}}{\sigma_k} \frac{\partial k}{\partial r} \right] + S_k, \quad (2-4)$$

where

$$\sigma_k = 1.00,$$

$$S_k = -C_D \rho \epsilon + G,$$

$$G = 2 \mu_{eff} \left(\left[\frac{\partial u}{\partial z} \right]^2 + \left[\frac{\partial v}{\partial r} \right]^2 \left[\frac{v}{r} \right]^2 + \frac{1}{2} \left[\frac{\partial u}{\partial r} + \frac{\partial v}{\partial z} \right]^2 \right) - \frac{2}{3} \nabla \cdot \underline{u} (\mu_{eff} \nabla \cdot \underline{u} + \rho k)$$

and

$$C_D = 1.00.$$

For the turbulent kinetic energy dissipation rate (ε):

$$\frac{\partial}{\partial t} (\rho \epsilon) + \frac{\partial}{\partial z} (\rho u \epsilon) + \frac{1}{r} \frac{\partial}{\partial r} (r \rho v \epsilon) = \frac{\partial}{\partial z} \left[\frac{\mu_{eff}}{\sigma_\epsilon} \frac{\partial \epsilon}{\partial z} \right] + \frac{1}{r} \frac{\partial}{\partial r} \left[r \frac{\mu_{eff}}{\sigma_\epsilon} \frac{\partial \epsilon}{\partial r} \right] + S_\epsilon, \quad (2-5)$$

where

$$S_\epsilon = \frac{\epsilon}{k} (C_1 G - C_2 \rho \epsilon) + \rho \epsilon \nabla \cdot \underline{u},$$

$$\sigma_\epsilon = \frac{k^2}{(C_2 - C_1) C_\mu^{1/2}} = 1.2,$$

$$C_1 = 1.44,$$

$$C_2 = 1.92$$

and

$$K = .4187.$$

Energy Equation [66,67,77]

$$\frac{\partial}{\partial t} (\rho T) + \frac{\partial}{\partial z} (\rho u T) + \frac{1}{r} \frac{\partial}{\partial r} (r \rho v T) = \frac{\partial}{\partial z} \left[\gamma_{eff} \frac{\partial T}{\partial z} \right] + \frac{1}{r} \frac{\partial}{\partial r} \left[r \gamma_{eff} \frac{\partial T}{\partial r} \right] + S_T, \quad (2-6)$$

where

$$\gamma_{eff} = \frac{\mu_l}{P_{r_l}} + \frac{\mu_t}{P_{r_t}},$$

$$P_{r_l} = 1.,$$

$$P_{r_t} = 1.,$$

$$S_T = \frac{1}{\bar{C}_p} \left[\frac{\partial P}{\partial t} + u \frac{\partial P}{\partial z} + v \frac{\partial P}{\partial r} + G + \dot{q}_c''' + \dot{q}_r''' \right],$$

\dot{q}_c''' = heat addition due to combustion defined in Appendix A and modeled in Chapter 3,

\dot{q}_r''' = heat addition due to radiation (neglected in present analysis)

and

\bar{C}_p = specific heat (defined in Chapter 3).

The basis for formulation of equation (2-6) is given in Appendix A.

Species mass fraction and mixture fraction [20,44,47,48]

For the mass fraction of i (m_i):

$$\frac{\partial}{\partial t} (\rho m_i) + \frac{\partial}{\partial z} (\rho u m_i) + \frac{1}{r} \frac{\partial}{\partial r} (r \rho v m_i) = \frac{\partial}{\partial z} \left[\frac{\mu_{eff}}{S_c} \frac{\partial m_i}{\partial z} \right] + \frac{1}{r} \frac{\partial}{\partial r} \left[r \frac{\mu_{eff}}{S_c} \frac{\partial m_i}{\partial r} \right] + S_{m_i}, \quad (2-7)$$

where

$S_c = 1.$ (Schmidt number),

$$S_{m_i} = \rho \dot{m}_i$$

and

\dot{m}_i = rate of species generation per unit volume (modeled in Chapter 3).

For reasons discussed in Chapter 3, only an equation for the mass fraction of the fuel (m_f) in conjunction with an equation for the determination of the mixture fraction (f) are required to account for all of the species concentrations of concern in this problem.

The governing equation for the mixture fraction is:

$$\frac{\partial}{\partial t} (\rho f) + \frac{\partial}{\partial z} (\rho u f) + \frac{1}{r} \frac{\partial}{\partial r} (r \rho v f) = \frac{\partial}{\partial z} \left[\frac{\mu_{eff}}{S_c} \frac{\partial f}{\partial z} \right] + \frac{1}{r} \frac{\partial}{\partial r} \left[r \frac{\mu_{eff}}{S_c} \frac{\partial f}{\partial r} \right] . \quad (2-8)$$

Thus, for this governing equation, the source term is:

$$S_f = 0 .$$

Note that f is defined and explained in Chapter 3.

General Transport Equation [41,43,76]

Equations (2-2) through (2-8) all have the same general form and can thus be represented compactly by a more general transport equation in terms of the primitive variable ϕ as:

$$\frac{\partial}{\partial t} (\rho \phi) + \frac{\partial}{\partial z} (\rho u \phi) + \frac{1}{r} \frac{\partial}{\partial r} (r \rho v \phi) = \frac{\partial}{\partial z} \left[\Gamma \phi \frac{\partial \phi}{\partial z} \right] + \frac{1}{r} \frac{\partial}{\partial r} \left[r \Gamma \phi \frac{\partial \phi}{\partial r} \right] + S_\phi , \quad (2-9)$$

where

$$\phi = u, v, k, \epsilon, T, m_f, \text{ or } f ,$$

S_ϕ = corresponding source terms

and

$\Gamma \phi$ = corresponding diffusion coefficients.

Equation of State

Adequate in internal combustion analysis as an equation of state is the generalized state equation for a multi-component ideal gas [83]:

$$\rho = \frac{P}{T \sum_{i=1}^n m_i R_i}, \quad (2-10)$$

where

$$R_i = \frac{\tilde{R}}{W_i} \frac{N-m}{\text{Kg-K}},$$

\tilde{R} = Universal Gas constant

and

W_i = molecular weight of species i .

2.2 Transformation of flow field equations. [67]

Piston motion necessitates the transformation of the z coordinate of the computational mesh into a coordinate system which does not change with time. In order to ensure optimum treatment of the boundary conditions at the piston and cylinder head surfaces however, it was determined preferable not to have the adjacent nodal points change in their relative distances to these surfaces. Further, to accommodate valve motion, it was determined necessary to create a region in which the actual mesh point spacing is constant in time in the z direction. These three problems generated the need to solve the governing equations in three separate solution regions, one in which the equations are not transformed, one in which the spacing of the computational mesh changes with time in accordance with piston motion, and one in which the actual spacing between grid points in the z direction is fixed but the actual positions of these nodal points are changing in the z direction with piston motion. Further

discussion of this three region approach is contained in Chapter 5 along with an indepth description of the regions. The purpose of this section is to describe the mathematical formulation of the transformation only.

Namely -

$$\phi(z, r, t) \rightarrow \phi(x, r, t')$$

within the applicable domain of transformation.

Between the lines $x = 0$ and $x = 1$ on the geometric representation of our engine flow field solution region depicted in figure 2-1, one can see that:

$$x = \frac{z - \text{dist1}}{\delta_p}, \quad (2-11)$$

where

$$\delta_p \equiv z_p - \text{dist1} - \text{dist2} \quad (2-12)$$

and

$z_p \equiv$ distance of piston face from the z origin. z_p is a function of time and is described analytically by equation (B-1) in Appendix B.

Note that

$$\frac{\partial}{\partial z} = \frac{1}{\delta_p} \frac{\partial}{\partial x} \quad (2-13)$$

and

$$\frac{\partial}{\partial t} = \frac{\partial}{\partial t'} - \frac{x}{\delta_p} u_p \frac{\partial}{\partial x}, \quad (2-14)$$

where

$$u_p = \frac{d\delta_p}{dt} = \frac{dz_p}{dt} \text{ and is the piston velocity.}$$

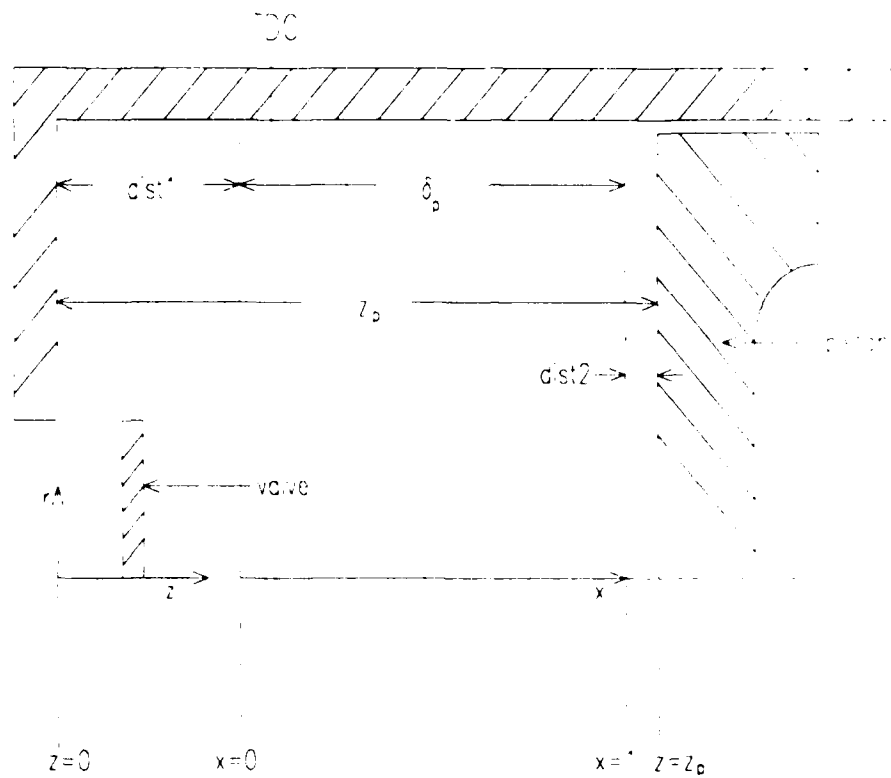


Figure 2-1. Engine Geometry and Coordinate Systems.

u_p is expressed as a function of time by equation (B-2) in Appendix B.
Letting

$$\bar{u} = u - x u_p \quad (2-15)$$

and substituting equations (2-13) through (2-15) into equations (2-1) and (2-9) results in the following:

Transformed Continuity Equation

$$\frac{1}{\delta_p} \frac{\partial}{\partial t} (\rho \delta_p) + \frac{1}{\delta_p} \frac{\partial}{\partial x} (\rho \bar{u}) + \frac{1}{r} \frac{\partial}{\partial r} (r \rho v) = 0 \quad (2-16)$$

Transformed General Transport Equation

$$\begin{aligned} \frac{1}{\delta_p} \frac{\partial}{\partial t} (\rho \delta_p \phi) + \frac{1}{\delta_p} \frac{\partial}{\partial x} (\rho \bar{u} \phi) + \frac{1}{r} \frac{\partial}{\partial r} (r \rho v \phi) = \frac{1}{\delta_p} \frac{\partial}{\partial x} \left[\frac{\Gamma \phi}{\delta_p} \frac{\partial \phi}{\partial x} \right] + \frac{1}{r} \frac{\partial}{\partial r} (r \Gamma \phi \frac{\partial \phi}{\partial r}) \\ + \bar{S}_\phi, \end{aligned} \quad (2-17)$$

where

\bar{S}_ϕ is the transformed source term for a given ϕ .

2.3 Flow Field Equations in Transformed Coordinates.

The application of the coordinate transformation described in section 2.2 to the specific governing flow field equations of our problem was simplified by the fact that use of equation (2-17) made necessary only the transformation of the source terms. The results of this transformation are given in Table 2-1. Thus Table 2-1 used in conjunction with equation (2-17) gives a compact summary of the transformation of equations (2-1) through (2-8).

2.4 Non-Flow Energy Equation

The analysis of heat transfer in the non-flow portion of our engine, consisting of the piston, valve and cylinder lining, involves the solution of only one equation, the unsteady heat conduction equation:

TABLE 2-1 Transformed Governing Equations for the Flow Field*

Equation	ϕ	Γ_ϕ	S_ϕ
Continuity	1	0	0
Axial Momentum	u	μ_{eff}	$-\frac{1}{\delta_p} \frac{\partial p}{\partial x} + \frac{1}{\delta_p} \frac{\partial}{\partial x} \left[\frac{\mu_{eff}}{\delta_p} \frac{\partial u}{\partial x} \right] + \frac{1}{r} \frac{\partial}{\partial r} \left[r \frac{\mu_{eff}}{\delta_p} \frac{\partial v}{\partial r} \right] - \frac{2}{3\delta_p} \frac{\partial}{\partial x} (\mu_{eff} v \cdot \underline{u} + \rho k)$
Radial Momentum	v	μ_{eff}	$-\frac{\partial p}{\partial r} + \frac{1}{\delta_p} \frac{\partial}{\partial x} \left[\frac{\mu_{eff}}{\delta_p} \frac{\partial u}{\partial x} \right] + \frac{1}{r} \frac{\partial}{\partial r} \left[r \frac{\mu_{eff}}{\delta_p} \frac{\partial v}{\partial r} \right] - 2 \mu_{eff} \frac{v}{r^2} - \frac{2}{3} \frac{\partial}{\partial r} (\mu_{eff} v \cdot \underline{u} + \rho k)$
Turbulent Kinetic Energy	k	$\frac{\mu_{eff}}{\sigma_k}$	$-C_D \rho \epsilon + \bar{G}$ (see transformed G below)**
Turbulent Kinetic Energy Dissipation Rate	ϵ	$\frac{\mu_{eff}}{\sigma_\epsilon}$	$\frac{\epsilon}{k} (C_1 \bar{G} - C_2 \rho \epsilon) + \rho \epsilon v \cdot \underline{u}$
Energy	T	γ_{eff}	$\frac{1}{C_p} \left[\frac{\partial p}{\partial t} - \frac{x}{\delta_p} \frac{\partial p}{\partial x} + \frac{u}{\delta_p} \frac{\partial p}{\partial x} + \frac{v}{\delta_p} \frac{\partial p}{\partial r} + \bar{G} - \rho \sum_{i=1}^n h_i \dot{m}_i \right]$
Fuel Species Mass Fraction	m _f	$\frac{\mu_{eff}}{S_c}$	$\rho [\dot{m}_f]$
Mixture Fraction	f	$\frac{\mu_{eff}}{S_c}$	0

* For use in conjunction with equation (2-17)

$$** \bar{G} = 2 \mu_{eff} \left(\left| \frac{\partial \underline{u}}{\partial x} \right|^2 + \left(\frac{v}{r} \right)^2 + \frac{1}{2} \frac{\partial u}{\partial r} + \frac{1}{\delta_p} \frac{\partial v}{\partial x} \right) - \frac{2}{3} v \cdot \underline{u} (\mu_{eff} v \cdot \underline{u} + \rho k)$$

$$v \cdot \underline{u} = \frac{1}{\delta_p} \frac{\partial u}{\partial x} + \frac{v}{r} + \frac{\partial v}{\partial r}$$

$$\rho C \frac{\partial T}{\partial t} = \frac{\partial}{\partial z} \left[K \frac{\partial T}{\partial z} \right] + \frac{1}{r} \frac{\partial}{\partial r} \left[r K \frac{\partial T}{\partial r} \right] , \quad (2-18)$$

where

C = specific heat (specified as 465 J/Kg-K)

and

K = thermal conductivity (specified as 50 J/Kg-m-s).

The density ρ is specified as 7800 Kg/m³. Note that because the sides of the cylinder do not move with piston motion, the transformation employed in sections 2.2 and 2.3 does not apply here. Instead, a special technique is used to match boundary conditions between the flow and non-flow regions, and equation (2-18) is solved in the z coordinate system. For details of this special procedure see section 2.5.4 and Appendix C.

2.5 Boundary Conditions

The general expressions for the flux of a primitive variable (ϕ) at a wall boundary is given by:

$$J_w(\phi) = - \Gamma_{\phi w} \left(\frac{\partial \phi}{\partial y} \right)_w , \quad (2-19)$$

where

ϕ = can be either u , v , T , m_f or f in our case,

$J_w(\phi)$ = flux of ϕ at wall,

$\Gamma_{\phi w}$ = diffusion coefficient of ϕ at wall,

and

y = the direction perpendicular to the wall and may be either z or r in our solution scheme.

For the momentum equations (i.e., for $\phi = u$ or v), $\Gamma_{\phi} = \mu_{\text{eff}}$ and $J_w = \tau_w$, the shear stress of the wall. In the case of the energy equation ($\phi = T$), $\Gamma_{\phi} = \gamma_{\text{eff}}$ and $J_w = \dot{q}_w$, the rate of heat flux per unit area perpendicular to the wall. For the species mass fraction equations

$(\phi = m_i)$, $\Gamma_\phi = \frac{\mu_{eff}}{Sc}$ and $J_w = J_i$, the diffusion flux of species i .

Similarly, for the mixture fraction equations ($\phi = f$), $\Gamma_\phi = \frac{\mu_{eff}}{Sc}$ and $J_w = J_f$, the diffusion flux of the mixture fraction. The values of k , ϵ and P do not act in accordance with equation (2-18) near the wall and must be given specialized treatment.

In the discretization of the general transport equations to be carried out in section 4.1.2 using a finite difference approach, the flux of a primitive variable across a control volume boundary will include the sum of both the convection and diffusion of that variable. However, at the wall surfaces within our engine, there is obviously no convection and the finite difference approximation of the wall flux is given by: [84]

$$J_w(\phi) = -\Gamma_{\phi_w} \frac{(\phi_g - \phi_w)}{\delta y_{w \rightarrow g}}, \quad (2-20)$$

where (see figure 2-2)

ϕ_g = value of ϕ at the flow field nodal point immediately adjacent to the wall,

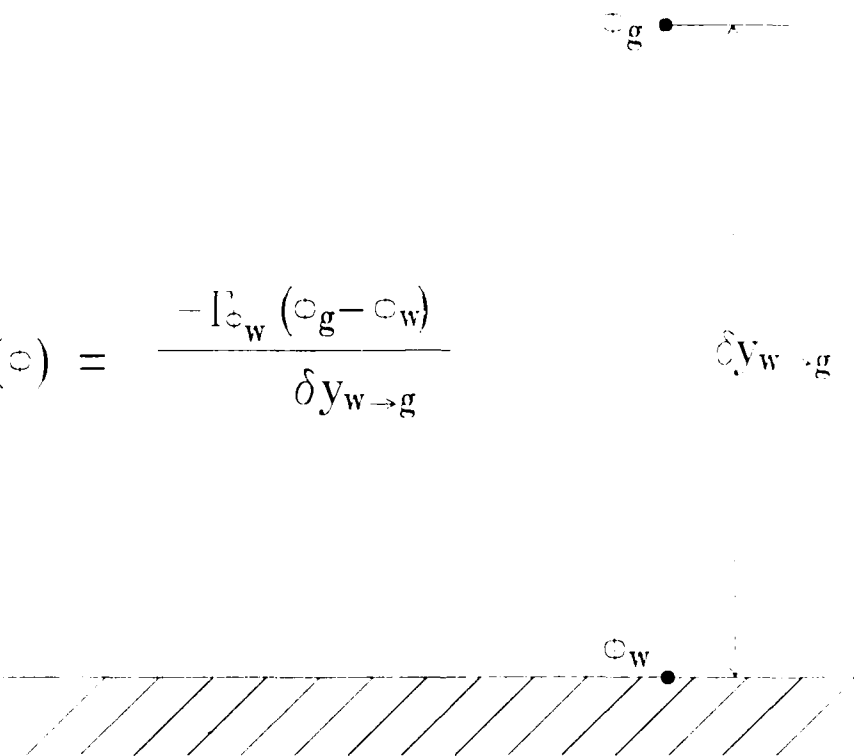
ϕ_w = value of ϕ at the wall,

$\delta y_{w \rightarrow g}$ = distance between the wall and the adjacent flow field nodal point

and

Γ_{ϕ_w} = value of diffusion coefficient at the wall obtained by assuming that the law of the wall expressions for steady, zero pressure gradient and incompressible flow are applicable.

figure 2-3 depicts the law of the wall profile for velocity used in this analysis. Note that we are using a two region approach by defining a



$$J_w(c) = \frac{-l_w (c_g - c_w)}{\delta y_{w \rightarrow g}} \quad \delta y_{w \rightarrow g}$$

*y can be in either the z or r direction.

Figure 2-2. Nomenclature for Geometry of Near Wall Boundary Conditions.

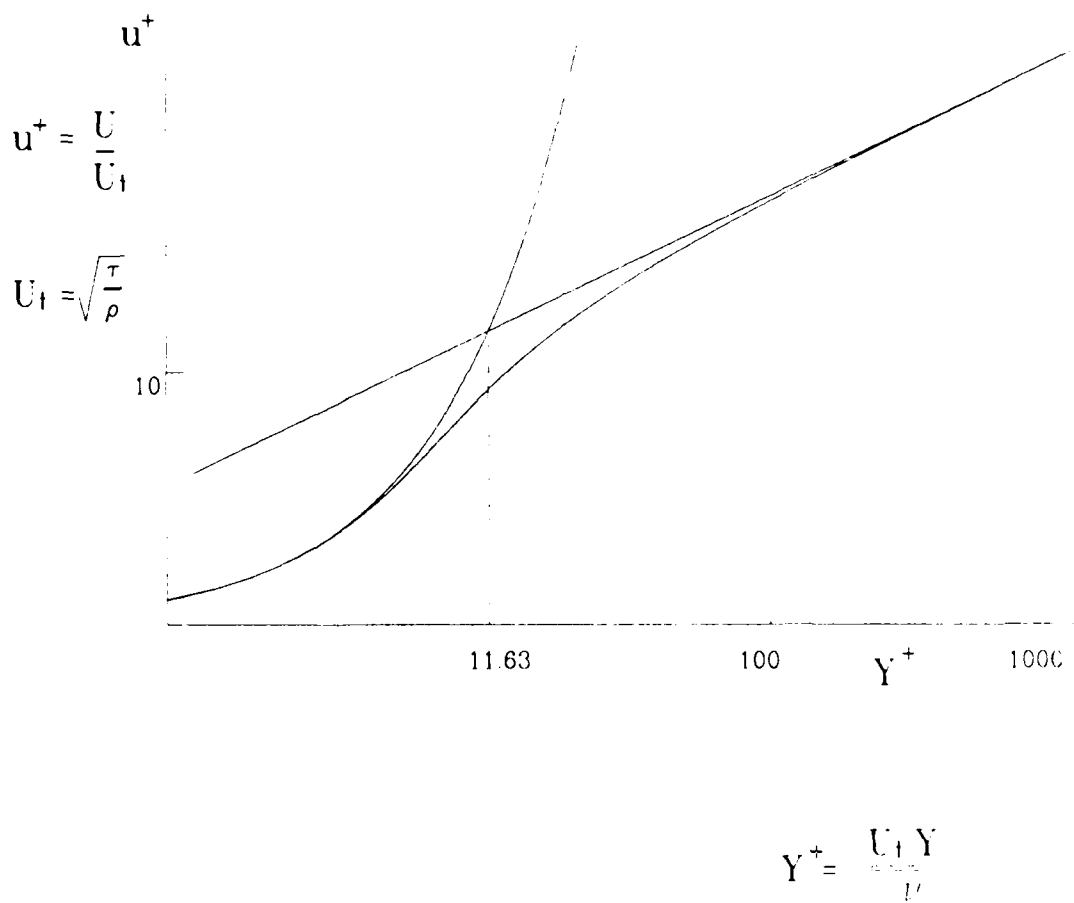


Figure 2-3. Velocity Law of Wall for Viscous Sublayer.

point $y^+ = 11.63$ and assuming the flow to be purely turbulent above this value and purely viscous below this point. The profile for temperature is depicted similarly.

2.5.1 Velocity Boundary Conditions [78]

The value for τ_w is found by assuming that the law of the wall relationships apply for our case. Close to the wall it is assumed that:

$$\tau = \tau_w .$$

The quantity y^+ used in the law of the wall formulation is evaluated in this analysis by using the value of the sheer stress in the inertial sub-layer (τ_I) for τ_w so that:

$$y^+ = \frac{\delta y_{w+g} \sqrt{\frac{\tau_w}{\rho}}}{u} = \frac{\delta y_{w+g} \rho g C_\mu^{1/4} k_g^{1/2}}{\mu g}, \quad (2-21)$$

where

k_g = value of turbulent kinetic energy at the nodal point adjacent to the wall (see figure 2-2).

This follows from the fact that in the inertial sublayer ($30 < y^+ < 400$) the flow is assumed to be fully turbulent and the local rate of turbulence production is balanced by the rate of viscous dissipation so that:

$$\tau_I = \rho C_\mu^{1/2} k$$

"Strictly speaking" however, the expression for y^+ given in equation (2-21) above is only valid in the inertial sublayer. [78]

Near the wall, a 1-D Couett flow analysis (appropriate for such conditions) tells us that

$$\tau = (\mu_l + \mu_t) \frac{\partial u}{\partial y}$$

For $y^+ < 11.63$ it is assumed that:

$$\mu_l \gg \mu_t$$

and

$$\tau_w = \mu_l \frac{U_g}{\delta y_{w+g}} \quad , \quad (2-22)$$

where

$U_g \equiv$ velocity parallel to the wall at the adjacent nodal point to the wall.

For $y^+ > 11.63$ it is assumed that

$$\mu_t \gg \mu_l$$

and

$$\tau_w = \frac{C_\mu^{1/4} \rho_g k_g^{1/2} K U_g}{\log_e \left[\frac{E C_\mu^{1/4} \rho_g k_g^{1/2} \delta y_{w+g}}{\mu_l} \right]} \quad , \quad (2-23)$$

where

$\rho_g =$ density at nodal point adjacent to wall,

$E \equiv 9.793$ (value of integration constant based on smooth wall conditions)

and

$$K = .4187.$$

To simplify the nomenclature scheme used in the precise presentation of the boundary conditions for not only the U and V momentum equation but also the equations for k , ϵ , T , m_f , f and P the geometry and subscripts shown in figure 2-2 apply with the following modifications:

For the cylinder head which represents the west (w) side of the solution scheme:

$$\phi_w = \phi_w (= \phi_{wall}) ,$$

$$\phi_{gw} = \phi_g ,$$

$$x_{wg} = \delta y_{w+g} ,$$

$$\rho_{gw} = \rho_g ,$$

$$x_w^+ = y^+$$

and

$$J_{w_n}(\phi) = J_w(\phi) .$$

For the cylinder wall (side of cylinder) which represents the north (n) side of the solution scheme:

$$\phi_n = \phi_w ,$$

$$\phi_{gn} = \phi_g ,$$

$$r_{ng} = \delta y_{w+g} ,$$

$$\rho_{gn} = \rho_g ,$$

$$r_n^+ = y^+$$

and

$$J_{w_n}(\phi) = J_w(\phi) .$$

For the piston surface which represent the east (e) side of the solution scheme:

$$\phi_e = \phi_w ,$$

$$\phi_{ge} = \phi_g ,$$

$$x_{eg} = \delta y_{w+g} ,$$

$$\rho_{ge} = \rho_g ,$$

$$x_e^+ = y^+$$

and

$$J_{w_e}(\phi) = J_w(\phi) .$$

For the symmetry axis which presents the south (s) boundary of the solution scheme $\phi_s = \phi$ at the border and the subscript s is used in partial derivatives to indicate south.

The above nomenclature scheme is generalized for ϕ and $J_w(\phi)$, where J_w represents the appropriate wall flux term corresponding to a particular primitive variable ϕ . For other surfaces such as the valve and fuel injector, similar patterns of nomenclature are used. The boundary conditions of the u-momentum equation can now be specified.

Cylinder Head

$$u_w = 0 \quad (2-24)$$

$$x_w = \frac{x_{wg} \rho_{gw} C_\mu^{1/4} k_{gw}^{1/2}}{\mu_{gw}} \quad .$$

For $x_w^+ \leq 11.63$:

$$\tau_{ww} = \frac{\mu_l v_{gw}}{x_{wg}} \quad (2-25)$$

For $x_w^+ > 11.63$:

$$\tau_{ww} = \frac{C_\mu^{1/4} \rho_{gw} k_{gw}^{1/2} K v_{gw}}{\log_e [E x_w^+]} \quad (2-26)$$

Cylinder Wall (Side)

$$v_n = 0 \quad (2-27)$$

$$r_n = \frac{r_{ng} \rho_{gn} C_\mu^{1/4} k_{gn}^{1/2}}{\mu_{gn}} \quad .$$

For $r_n^+ \leq 11.63$:

$$\tau_{wn} = \frac{\mu_l u_{gn}}{r_{ng}} \quad (2-28)$$

For $r_n^+ > 11.63$:

$$\tau_{wn} = \frac{C_\mu^{1/4} \rho_{gn} k_{gn}^{1/2} K u_{gn}}{\log_e [E r_n^+]} \quad (2-29)$$

Piston Face

$$u_e = u_p \quad (2-30)$$

$$x_e^+ = \frac{x_{eg} \rho_{ge} C_\mu^{1/4} k_{ge}^{1/2}}{\mu_{ge}}$$

For $x_e^+ < 11.63$:

$$\tau_{we} = \frac{\mu_l v_{ge}}{x_{eg}} \quad (2-31)$$

For $x_e^+ > 11.63$:

$$\tau_{we} = \frac{C_\mu^{1/4} \rho_{ge} k_{ge}^{1/2} K v_{ge}}{\log_e [E x_e^+]} \quad (2-32)$$

Symmetry Axis

$$\left(\frac{\partial u}{\partial r}\right)_s = 0 \quad (2-33)$$

$$v_s = 0 \quad (2-34)$$

Value Surfaces and Orifice Opening

See Chapter 5.

Fuel Nozzle

See Chapter 6.

2.5.2 k-ε Boundary Conditions [78]

As mentioned in 2.5.1 the approach adopted here is strictly valid only for the inertial sublayer, where the assumption is made that the flow

is completely turbulent such that the local rate of production of turbulence is balanced by the viscous dissipation rate. Thus the value of ϵ at the near wall nodes is fixed as follows:

$$\epsilon_g = \frac{C_\mu^{3/4} k_g^{3/2}}{K \delta y_{w+g}} \quad (2-35)$$

Obviously, at the wall the values of ϵ and k are:

$$\epsilon_w = 0 \quad (2-36)$$

and

$$k_w = 0 \quad (2-37)$$

There is no contributory flux of turbulent kinetic energy from the wall for the k equation near the wall and integration of the source term (\bar{S}_k) in the discretization of this equation requires special consideration at this boundary. Discretization of \bar{S}_k at locations other than at the near wall boundary conditions is explained in Chapter 4. Note that:

$$\int_V \bar{S}_k d(V) = - \int_V (C_D \rho \epsilon - \bar{G}) d(V)$$

The integration of ϵ is modeled as follows in order to extend the k -balance formulation of equation (2-35) into the buffer area in addition to the viscous sublayer:

$$\int_V C_D \rho \epsilon d(V) = \frac{C_D \rho_g C_\mu^{3/4} k_g^{3/2} V}{\delta y_{w+g}} U^+ \quad (2-38)$$

where

for $y^+ < 11.63$ -

$$U^+ = y^+$$

and for $y^+ > 11.63$ -

$$U^+ = \frac{1}{K} \log_e [E y^+] .$$

The integration of G is varied from the discretization conducted in Section 4.1.3 by noting that at the wall the fourth term in the expression for \bar{G} given in Table 2-1 can be integrated as:

$$\int_V u_{\text{eff}} \left(\frac{\partial u}{\partial r} + \frac{1}{\delta_p} \frac{\partial v}{\partial x} \right)^2 dV = \frac{\tau_w (U_g - U_w)}{\delta y_w + g} V . \quad (2-39)$$

Following the same pattern given in 2.5.1 in terms of nomenclature, U^+ is expressed as follows for the various internal surfaces:

$$v_w^+ = U^+ \text{ on the cylinder head,}$$

$$u_n^+ = U^+ \text{ on the cylinder wall}$$

and

$$v_e^+ = U^+ \text{ on the piston surface.}$$

Cylinder Head

For $x_w^+ < 11.63$:

$$v_w^+ = x_w^+ .$$

For $x_w^+ > 11.63$:

$$v_w^+ = \frac{1}{K} \log_e [E x_w^+] .$$

$$\epsilon_w = 0 \quad (2-40)$$

$$\epsilon_{gw} = \frac{C_\mu^{3/4} k_{gw}^{3/2}}{K x_{wg}} \quad (2-41)$$

$$k_w = 0 \quad (2-42)$$

k_{gw} is determined by using the following expression for $\int_V S_k d(V)$ at that nodal point:

$$\begin{aligned} \int_V \bar{S}_{k_{gw}} d(V) = & - \frac{C_D \rho_{gw} C_\mu^{3/4} k_{gw}^{3/2}}{x_{wg}} v_w V + \int_V \bar{G} d(V) \\ & - \int \mu_{eff} \left(\frac{1}{\delta_p} \frac{\partial v}{\partial x} \right)^2 d(V) + \frac{\tau_{w_w} v_{gw}}{x_{wg}} V \end{aligned} \quad (2-43)$$

where

$\int_V \bar{G} d(V)$ specified in 4.1.3.

Cylinder Wall (Side)

For $r_n^+ < 11.63$:

$$u_n^+ = r_n^+$$

For $r_n^+ > 11.63$:

$$u_n^+ = \frac{1}{K} \log_e [E r_n^+] \quad .$$

$$\epsilon_n = 0 \quad (2-44)$$

$$\epsilon_{gn} = \frac{C_\mu^{3/4} k_{gn}^{3/2}}{K r_{ng}} \quad (2-45)$$

$$k_n = 0 \quad (2-46)$$

k_{gn} determined from:

$$\int_V \bar{S}_{k_{gn}} d(V) = - \frac{C_D \rho_{gn} C_\mu^{3/4} k_{gn}^{3/2}}{r_{ng}} u_n^+ V + \int_V \bar{G} d(V) -$$

$$\int_V \mu_{eff} \left(\frac{\partial u}{\partial r} \right)^2 d(V) + \frac{\tau_{wn} u_{gn}}{x_{ng}} V. \quad (2-47)$$

Piston Face

For $x_e^+ < 11.63$:

$$v_e^+ = x_e^+.$$

For $x_e^+ > 11.63$:

$$v_e^+ = \frac{1}{K} \log_e [E x_e^+].$$

$$\epsilon_e = 0. \quad (2-48)$$

$$\epsilon_{ge} = 0. \quad (2-49)$$

$$k_e = 0. \quad (2-50)$$

k_{ge} determined from:

$$\int_V \bar{S}_{k_{ge}} d(V) = - \frac{C_D \rho_{ge} C_\mu^{3/4} k_{ge}^{3/2} v_e^+}{x_{eg}} V + \int_V \bar{G} d(V) -$$

$$\int_V \mu_{eff} \left(\frac{1}{\delta p} \frac{\partial v}{\partial x} \right)^2 d(V) + \frac{\tau_{we} v_{ge}}{x_{eg}} V \quad (2-51)$$

Symmetry Axis

$$\left(\frac{\partial \epsilon}{\partial r} \right)_s = 0. \quad (2-52)$$

$$\left(\frac{\partial k}{\partial r}\right)_s = 0 . \quad (2-53)$$

$$\int_V S_{kgs} d(V) = -(C_D \rho \epsilon - \overline{G}) V - \int_V \mu_{eff} \left(\frac{\partial u}{\partial r}\right) d(V) . \quad (2-54)$$

Value Surfaces and Orifice Opening

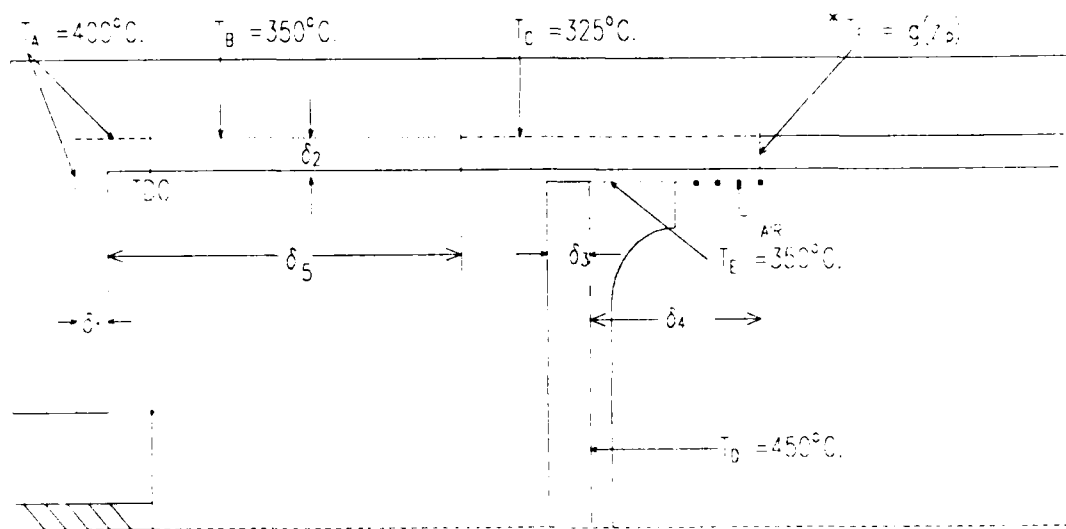
See Chapter 5.

Fuel Nozzle

See Chapter 6.

2.5.3 Temperature Boundary Conditions

The boundary conditions for the energy equation are specified at a fixed distance within the interior metal surfaces from the borders of the flow field solution region. Work done by Eaton Corporation [81] indicates that for an IC engine, at a specific distance δ inside the metal of the cylinder or piston from the combustion chamber, the temperature will not vary over 1% during the engine cycle. This distance varies depending on the thermal conductivity of the metal and the RPM of the engine. For the cylinder wall (side of cylinder) it also varies with the distance from the cylinder head (i.e., varies in the z direction). The actual thickness and values of the corresponding temperatures can be determined experimentally. Because experimental data does not exist for our engine, assumed values are used. See figure 2-4 for the values of the temperatures specified for this analysis. The values of the various penetration δ 's are as follows: $\delta_1 = .0004$ m; $\delta_2 = .0003$ m; and $\delta_3 = .0005$ m. The other two δ 's shown in figure 2-4 are used for specification of the limits of the temperature borders and are as follows: $\delta_4 = .03735$ m; $\delta_5 = .05065$ m. Note that these values will also change for the heat



$$g(z_0) = \begin{cases} 350 & \text{if } z_0 \geq \delta_5 - \delta_3 - \delta_4 \\ 325 & \text{if } z_0 < \delta_5 - \delta_3 - \delta_4 \end{cases}$$

Figure 2-4. Temperature Boundary Conditions.
for Outer Nonflow borders.

barrier piston engine with the degree of barrier which is placed within the piston.

The temperature boundary conditions at the perimeter of the fluid flow field are thus not specified. The heat flux is determined at this border using the same procedure as was used in the solution of the momentum-transport equations. The wall fluid boundary layer is assumed to have a constant heat flux throughout so that:

$$\dot{q}'' = \dot{q}_w'' ,$$

where for 1-D analysis (Couette flow)

$$\dot{q}'' = (\gamma_l + \gamma_t) C_p \frac{\partial T}{\partial y} .$$

Note that:

$$\gamma_l \equiv \frac{\mu_l}{Pr_l}$$

and

$$\gamma_t = \frac{\mu_t}{Pr_t} .$$

Using Reynolds' analogy and assuming that the viscous sublayer and thermal viscous sublayer are the same thickness, for $y^+ < 11.63$ it is assumed that [66,78,80]:

$$\gamma_l \gg \gamma_t$$

and

$$\dot{q}_w'' = - \frac{\mu_l}{\delta y_{w+g} Pr_l} (T_g - T_w) . \quad (2-55)$$

Also, for $y^+ > 11.63$

$$\gamma_t \gg \gamma_l$$

and

$$\dot{q}_w'' = - \frac{\rho_g \bar{c}_{pg} C_u^{1/4} k_g^{1/2} (T_g - T_w)}{\frac{Pr_t}{K} \log_e (E y^+) + Pr_t (P + \frac{Pr_l}{Pr_t})} , \quad (2-56)$$

where [80]

$$P + \frac{\sigma_\phi}{\sigma_{\phi,t}} = \frac{\frac{\pi}{4}}{\sin(\frac{\pi}{4})} \left(\frac{A}{K} \right)^{1/2} \left(\frac{\sigma_\phi}{\sigma_{\phi,t}} - 1 \right) \left(\frac{\sigma_{\phi,t}}{\sigma_\phi} \right)^{1/4} ,$$

A = Van Driest Constant

= 26.0 for smooth wall

and

$\sigma_\phi = Pr, Sc, \text{ etc.}, \text{ depending on } \phi .$

Thus for the various inner metal surfaces, the flow field and non-flow energy equation heat flux boundary conditions can be specified:

Cylinder Head

For $x_w^+ < 11.63$:

$$\dot{q}_{ww}'' = - \frac{\mu_l}{x_{wg} Pr_l} (T_{gw} - T_w) . \quad (2-57)$$

For $x_w^+ > 11.63$:

$$\dot{q}_{ww}'' = - \frac{\rho_{gw} \bar{c}_{pgw} C_u^{1/4} k_{gw}^{1/2} (T_{gw} - T_w)}{\frac{Pr_t}{K} \log_e (E x_w^+) + Pr_t (P + \frac{Pr_l}{Pr_t})} . \quad (2-58)$$

Cylinder Wall (Side)

For $rn^+ < 11.63$:

$$\dot{q}''_{wn} = - \frac{\mu_l}{r_{ng} Pr_l} (T_{gn} - T_n) . \quad (2-59)$$

For $r_n^+ > 11.63$:

$$\dot{q}''_{wn} = - \frac{\rho_{gn} \bar{c}_{pgn} C_{\mu}^{1/4} k_{gn}^{1/2} (T_{gn} - T_n)}{\frac{Pr_t}{K} \log_e (E r_n^+) + Pr_t \left(P + \frac{Pr_l}{Pr_t} \right)} . \quad (2-60)$$

Piston Face

For $x_e^+ \leq 11.63$:

$$\dot{q}''_{we} = - \frac{\mu_l}{x_{eg} Pr_l} (T_{ge} - T_e) . \quad (2-61)$$

For $x_e^+ > 11.63$:

$$\dot{q}''_{we} = - \frac{\rho_{ge} \bar{c}_{pge} C_{\mu}^{1/4} k_{ge}^{1/2} (T_{ge} - T_e)}{\frac{Pr_t}{K} \log_e (E x_e^+) + Pr_t \left(P + \frac{Pr_l}{Pr_t} \right)} . \quad (2-62)$$

Symmetry Axis

$$\left(\frac{\partial T}{\partial r} \right)_s = 0 . \quad (2-63)$$

Valve Surface and Orifice Opening

See Chapter 5.

Fuel Nozzle

See Chapter 6.

Non-Flow Outer Borders

See figure 2-4 for specifics.

Piston, Cylinder Interface

Heat flux between the nodal points of the side of the piston (ps) and the side of the cylinder wall (cw) at the interface shown in figure 2-5 is modeled as:

$$\dot{q}''_{p \rightarrow c} = h_{p \rightarrow c} (T_{ps} - T_{cw}) , \quad (2-64)$$

where

$h_{p \rightarrow c}$ = The combined convective and radiative heat transfer coefficient between the piston side and cylinder wall. It must be determined experimentally and is a function of RPM, pressure, temperature, etc. For our analysis a fixed value was selected.

Note that the value of T_{ps} varies along the left portion of the piston cylinder interface and is a fixed value (T_E - See figure 2-4) along the right portion of the interface. Obviously T_{cw} and the left portion of T_{ps} vary with position and time and are computed iteratively along with $\dot{q}''_{p \rightarrow c}$ in the solution of the non-flow energy equations. As can be seen in figure 2-5, below the piston, a portion of the cylinder lining considered in the non flow solution region is bordered by air. At these nodal points, the boundary conditions are specified by equation (2-59).

Valve, Valve Seat Interface

A detailed description of heat transfer within the valve is given in Chapter 5 as previously indicated. Heat flux at the interface of the valve seat (vs) and the closed valve is given by

$$\dot{q}''_{v \text{ side} \rightarrow vs} = h_{v \text{ side} \rightarrow vs} (T_{v \text{ side}} - T_{vs}) , \quad (2-65)$$

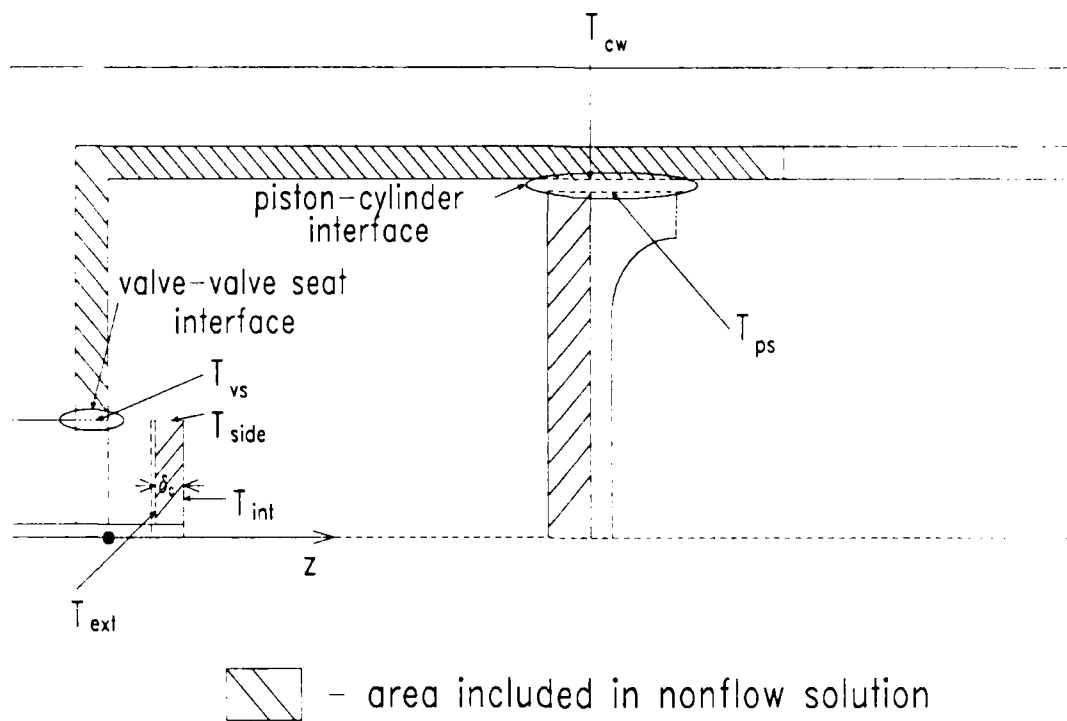


Figure 2-5. Nonflow Solution Region.

where

$h_{v\text{side}\rightarrow vs}$ = combined convective and radiative heat transfer coefficient between the valve side and the valve seat.

Comments for equation (2-64) for $h_{p\rightarrow c}$ apply here also.

When the valve is open, air flow through the valve may either be into or out of the engine. When the flow is into the engine

$$r_{vs}^+ = \frac{r_{vs\rightarrow g} \rho_{in} C_\mu^{1/4} k_{in}^{1/2}}{\mu_{in}},$$

where

$$\mu_{in} = \mu_l + \frac{C_\mu \rho_{in} k_{in}^2}{\epsilon_{in}}$$

and

ρ_{in} , k_{in} and ϵ_{in} - are the near wall inlet values of ρ , k , and ϵ respectively as specified in Chapter 5.

Heat flux from the adjacent gas to the valve seat is as follows:

For $r_{vs}^+ < 11.63$:

$$\dot{q}_{gvs\rightarrow vs}'' = \frac{\mu_l}{\delta r_{vs\rightarrow g} Pr_l} (T_{gin} - T_{vs}), \quad (2-66)$$

where

T_{gin} = temperature of atmosphere.

For $r_{vs}^+ > 11.63$:

$$\dot{q}''_{g_{VS} \rightarrow VS} = \frac{\rho_{in} \bar{c}_{pin} C_{\mu}^{1/4} k_{in}^{1/2} (T_{g_{VS}} - T_{VS})}{\frac{Pr_t}{K} \log_e (Er_{VS}) + Pr_t \left(P + \frac{Pr_1}{Pr_t} \right)} \quad (2-67)$$

If the flow of air is out of the engine, the substitution of the near wall out flow values of ρ , k , μ , ϵ , T are made for the corresponding in flow values in the above equations (equation (2-66) - (2-67)) to obtain equivalent expressions for $\dot{q}''_{g_{VS} \rightarrow VS}$ in the out flow case. See Chapter 5 for a specification of these values.

2.5.4 Fuel Species and Mixture Fraction Boundary Conditions

The flow can be assumed to be non-reacting at and very near the walls due to the cooling effects of the wall. This is normally true for the piston surface also, assuming the barrier used in the piston is such that the surface temperatures remain cool enough. Under such conditions, the specification of the flux of m_f and f can be specified in a manner identical to that used for the energy equation [80]. However, to use these relationships, the values of m_f and f must be known at the wall throughout the engine cycle. A simple approach is to assume that m_f and f are both zero at the walls and to proceed exactly as for the case of the energy equation. In this approach $J_{f_{ue1}}$ and J_f are found by the use of identical equations to equations (2-57) through (2-63), by using Sc in place of Pr and m_f or f in place of T to find $J_{f_{ue1}}$ or J_f in place of q''_w . Initial analysis utilized this formulation. However, neither m_f or f are zero at all wall locations throughout the entire engine cycle. If their actual values could be known, a solution using this formulation would be optimum. Later in the analysis it was determined better to assume that

the values of m_f and f are the same at the near wall and wall nodal points. This assumption, though not optimum, was found to lend itself to a much more accurate solution and is used in the analysis presented herein.

Cylinder Head

$$J_{fuel_w} = 0 . \quad (2-68)$$

$$m_{f_w} = m_{f_{gw}} . \quad (2-69)$$

$$J_{f_w} = 0 . \quad (2-70)$$

$$f_w = f_{gw} . \quad (2-71)$$

Cylinder Wall

$$J_{fuel_n} = 0 . \quad (2-72)$$

$$m_{f_n} = m_{f_{gn}} . \quad (2-73)$$

$$J_{f_n} = 0 . \quad (2-74)$$

$$f_n = f_{gn} . \quad (2-75)$$

Piston Face

$$J_{fuel_e} = 0 . \quad (2-76)$$

$$m_{f_e} = m_{f_{ge}} . \quad (2-77)$$

$$J_{f_e} = 0 . \quad (2-78)$$

$$f_e = f_{ge} . \quad (2-79)$$

Symmetry Axis

$$\left(\frac{\partial m_f}{\partial r}\right)_s = 0 . \quad (2-80)$$

$$\left(\frac{\partial f}{\partial r}\right)_s = 0 . \quad (2-81)$$

Valve Surface and Orifice Opening

See Chapter 5.

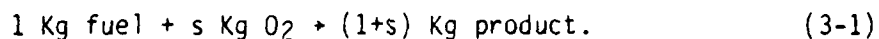
Fuel Nozzle

See Chapter 6.

Chapter 3

COMBUSTION MODEL

In the engine model under investigation, the rate of combustion is controlled by turbulent mixing and not chemical kinetics. This is a consequence of the fact that the fuel enters the engine at a temperature above the fuel's reaction activation temperature. Under such conditions (hypergolic conditions), relative to the rate of turbulent mixing, the rate of chemical reaction is so fast, it can be viewed as occurring instantaneously once a radical of fuel and oxygen are mixed [1,18,19,20]. As a consequence, the array of intermediate chemical reactions which occur in the combustion process can be ignored. The only reaction equation of concern is the overall heat-releasing reaction given by:



Due to its high injection temperature, the fuel is assumed to react irreversibly with the oxygen.

The effect of the formation of nitrogen oxides during the combustion process have relatively little effect on the global heat release process within the engine and as a consequence is neglected [47]. Also, to simplify analysis, the mass diffusion coefficients of each species are assumed equal. This last assumption is well satisfied for the case of fully turbulent flow [20].

As a consequence of the above, our combustion model, in addition to the local rate of fuel combustion ($-\dot{m}_f$), need only be concerned with the computation of the local mass fractions of the fuel (m_f), oxygen (m_{O_2}), and combined combustion products (m_{pr}). With the rate of fuel com-

bustion specified, the rate of heat release per unit volume \dot{q}_c''' can be determined for use in the solution of the energy equation. The sections which follow delineate this model.

3.1 Species Mass Fraction and Mixture Fractions

The general species mass fraction equation (given in its untransformed form in equation (2-7)), need only be solved for one species by observing first of all that a passive scalar f , defined as

$$f = \frac{m_f - \frac{m_{O_2}}{s} + \frac{m_{O_2,a}}{s}}{1 + \frac{m_{O_2,a}}{s}} \quad (3-2)$$

obeys the transformed general transport equation with its source term (\bar{S}_f) equal to zero, and by noting that given f and one species mass fraction, all the other mass fractions can be determined algebraically. In the above expression $m_{O_2,a}$ is mass fraction of O_2 in air under atmospheric conditions and s is defined by equation (3-1). Once f is determined, the mass fraction of oxygen (m_{O_2}) can be determined. The mass fraction of inert gas (m_{in}) is obtained from the fact that f and m_{in} have the simple linear relationship given by [20,48]:

$$m_{in} = m_{in,a} (1-f) \quad (3-3)$$

where $m_{in,a}$ is the mass fraction of inerts in air.

The mass fraction of the fuel (m_f) is obtained by solving the transformed version of equation (2-7) for m_f (see Table 2-1). Needed in

this calculation is a model for \dot{m}_f , the rate of change of the mass fraction of fuel per unit volume. An eddy-dissipation combustion model developed by Mangussen and Hjertager⁷⁹ for a single step irreversible global reaction is given by:

$$\dot{m}_f = -A \left(\frac{\epsilon}{K} \right) \min \left(m_f, \frac{m_{O_2}}{s}, \frac{B m_{pr}}{1 + s} \right), \quad (3-4)$$

where

$A = 4$ (obtained experimentally),

$B = .5$ (obtained experimentally),

and

$\min(,,) \equiv$ minimum numerical value of the expressions contained in parenthesis.

This is considered to be a reasonable model for hydrocarbon fuels at engine conditions and its utility in internal combustion engine research is demonstrated in reference [48]. The values for A and B may require some adjustments in order to further refine this expression (equation (3-4)) for engine use. Also, this model is not applicable in the case of either an excessively lean or rich mixture.

The final mass fraction needed for our solution is that of the combined products (m_{pr}) which is calculated by use of the fact that the sum of the mass fractions must equal one.

$$m_{pr} = 1 - m_f - m_{O_2} - m_{in}. \quad (3-5)$$

3.2 Energy Equation Combustion Source Term Model

As shown in Appendix A, the untransformed form of \dot{q}_c''' , the contribution of combustion to the energy equation's source term, is

given by the expression

$$\dot{q}_c'' = -\rho \sum_{i=1}^n \dot{m}_i h_i^0 \quad (3-6)$$

when the Prandtl and Schmidt (and thus Lewis) numbers are equal to one. In our case, "i" in the above expression can represent either fuel, oxygen or products.

The rate of production of fuel per unit volume (\dot{m}_f) is given in the preceding section. Equation (3-1) dicates that

$$\dot{m}_{O_2} = s \dot{m}_f \quad (3-7)$$

and

$$\dot{m}_{pr} = - (1 + s) \dot{m}_f. \quad (3-8)$$

The tabular values $h_{O_2}^0$, h_f^0 and h_{pr}^0 are given in Table 3-1 for the use of $C_{12}H_{26}$ as a fuel. Note that $h_{O_2}^0$ equals zero. Thus our expression for \dot{q}_c'' reduces to

$$\dot{q}_c'' = -\rho \dot{m}_f (h_f^0 - (1 + s) h_{pr}^0). \quad (3-9)$$

3.3 Variation of the Specific Heat (C_p) Due to Combustion.

In the formulation of an energy equation based on temperature instead of enthalpy (see appendix A), the specific heat of the gas at constant pressure (\bar{C}_p) was introduced. \bar{C}_p varies with both temperature and species concentration in accordance with the relationship

$$\bar{C}_p = \sum_{i=1}^n m_i C_{p_i}(T) \quad (3-10)$$

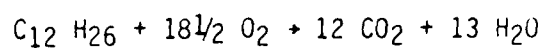
where

$$C_{p_i}(T) = \sum_{j=0,1,2,3,-1/2} a_{ji} T^j ,$$

and

a_{ji} is given in Table 3-2.

TABLE 3-1 Heats of Formation [85]



<u>Species (i)</u>	<u>Heat of Formation (h_i^0)</u>	<u>Molecular Weight (W_i)</u>
$C_{12}H_{26}$	- 71,014 cal/ g mole	170.34
O_2	0	31.9988
$CO_2(g)$	- 94,051 cal/ g mole	44.0099
$H_2O(g)$	- 57,798 cal/ g mole	18.016
Product	$\frac{12 h_{CO_2}^0 + 13 h_{H_2O}^0}{25} = - 75,199.4 \frac{\text{cal}}{\text{g mole}}$	30.49

Conversion Factor:

$$h_i^0 \left(\frac{\text{J}}{\text{Kg}} \right) = (h_i^0 \left(\frac{\text{cal}}{\text{g mole}} \right)) \times \left(\frac{4187}{W_i} \right)$$

TABLE 3-2 Specific Heats at Constant Pressure

$$\bar{C}_p = a_0 + a_1 T + a_2 T^2 + a_3 T^3 + a_{-1/2} T^{-1/2} \frac{\text{cal}}{\text{g mole K}}$$

Species	a_0	$10^3 a_1$	$10^6 a_2$	$10^9 a_3$	$a_{-1/2}$	Range K	% Error
Air*	6.557	1.477	-.2148	0	0	273-3800	1.64
O ₂ *	6.732	1.505	-1.791	0	0	273-3800	3.24
CO ₂ *	18.036	-.04474	0	0	-158.08	273-3800	2.65
H ₂ O*	6.970	3.464	-.4833	0	0	273-3800	2.03
C ₁₂ H ₂₆ **	-2.13245	273.87	-150.689	31.9581		250-1500*	.244

* From Tribus, Myron, "Thermostatics and Thermodynamics" Van Nostrand Co., Princeton, page 184 [86]

** Curve fit of data from Keating, E. L., "Internal and External Combustion Science: Principles and Applications" - Lecture Notes, 1980-81, page B-19. [85]

The specific heats for the product and inerts are found from the above specific heats using the following expressions:

$$C_{p_{\text{prod}}} = \frac{12 C_{p_{\text{CO}_2}} + 13 C_{p_{\text{H}_2\text{O}}}}{25} \frac{\text{cal}}{\text{g mole K}}$$

$$C_{p_{\text{inert}}} = \frac{C_{p_{\text{air}}} - .232 C_{p_{\text{O}_2}}}{.768} \frac{\text{J}}{\text{kg K}}$$

Chapter 4

NUMERICAL PROCEDURES

The numerical method employed in the solution of the governing equations is a finite difference scheme based on the Teach - T code [78] with major modifications. The code was converted from a self-selecting hybrid central/upwind spacial differencing scheme to a power law spacial differencing scheme [76]. The latter scheme uses an expression which almost exactly approximates the solution of the steady one-dimensional convection diffusion problem in the discretization of total flux across each of the surfaces of the control volume. The code was modified from one which handled only steady non-reacting flow to one which handles unsteady flow with combustion. The source terms of the governing equations used in the codes for u , v , k , ϵ , and T were significantly modified to reflect the more extensive source terms listed in Table 2-1. Additionally, the code was only usable for uniform spacing in the r direction, used coarse averaging techniques for viscosity at the border of the staggered velocity control volumes, contained errors in the computation of some of the source terms, etc. These problems were resolved through code modifications.

Details of the discretization and solution of the governing equations are given in the succeeding subsections of this chapter, including the procedures used in the computation of pressure throughout the flowfield.

4.1 Discretization of Governing Equations

The finite-difference method employed in this analysis uses a staggered grid. In this formulation, the majority of the dependent variables are calculated at the center point (P) of the control volume. The u and v velocities are displaced so as to lie half way between the

pressures that drive them and are thus on the faces of the control volumes used in the calculations of the other primitive variables. See figure 4-1. The control volumes used in the finite-difference formulation of the momentum equations for u and v are shown in figures 4-2 and 4-3 respectively.

4.1.1. Discretization of the Transformed Continuity Equation

The transformed continuity equation given in equation (2-16) is discretized by integrating each term over the control volume shown in figure 4-1. Refer to this figure for a definition of the geometrical terms and subscript nomenclature that follow.

$$\int_V \frac{1}{\delta p} \frac{\partial}{\partial t} (\rho \delta p) \delta p r \partial x = \frac{(\rho_p V)^n - (\rho_p V)^o}{\Delta t},$$

$$= M_p^n - M_p^o$$

where

$n \equiv$ present time step,

$o \equiv$ previous time step

$V = \delta p r_d \delta r_{ns} \delta x_{ew}.$

$$\int_V \frac{1}{\delta p} \frac{\partial}{\partial x} (\rho \bar{u}) \delta p r \partial x = [(\rho \bar{u})_e - (\rho \bar{u})_w] A_{ew}$$

$$= m_e^n - m_w^n,$$

where

$A_{ew} = r_d \delta r_{ns}.$

$$\int_V \frac{1}{r} \frac{\partial}{\partial r} (r \rho v) \delta p r \partial x = (\rho v)_n A_n - (\rho v)_s A_s$$

$$= m_n^n - m_s^n,$$

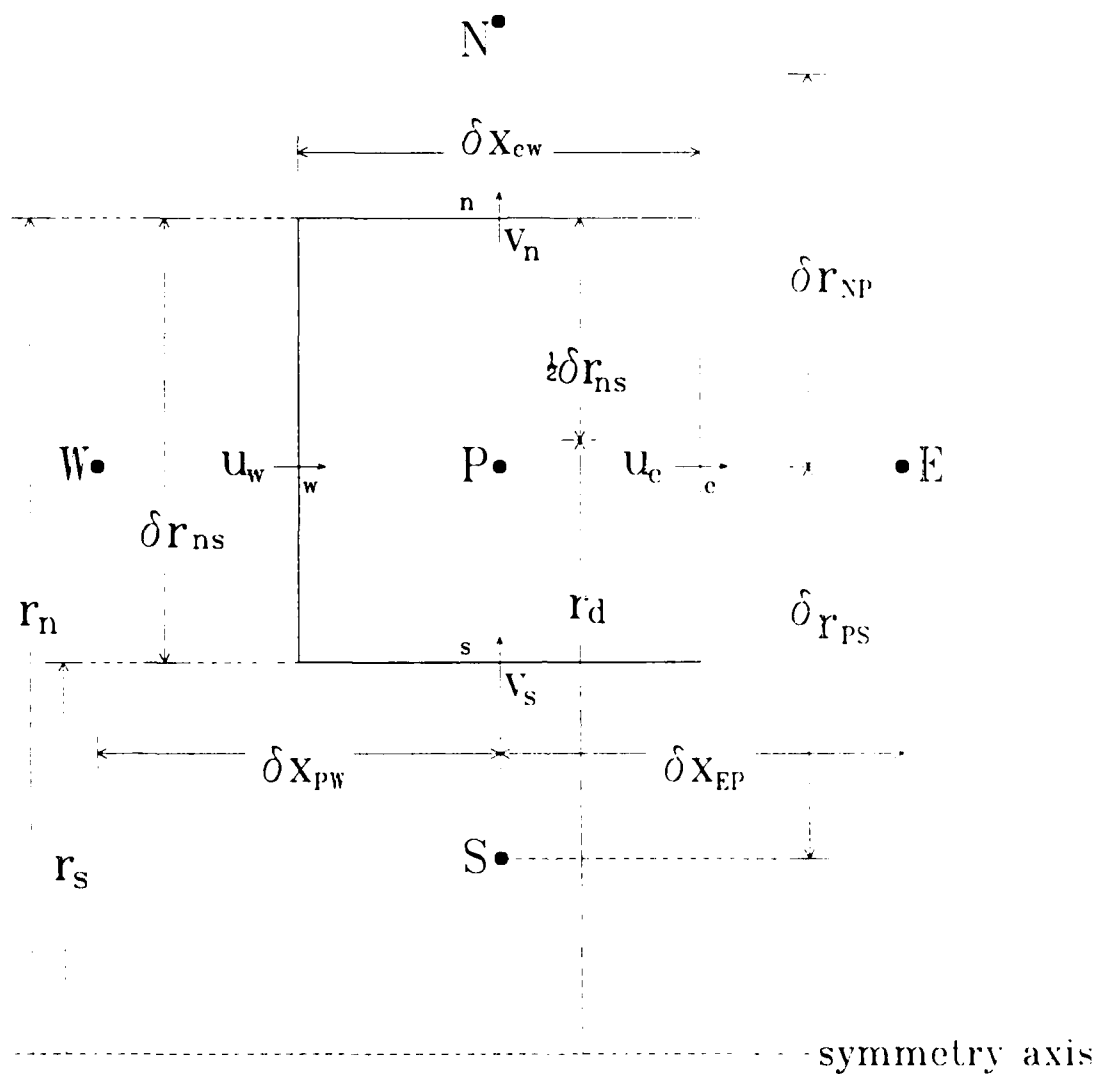
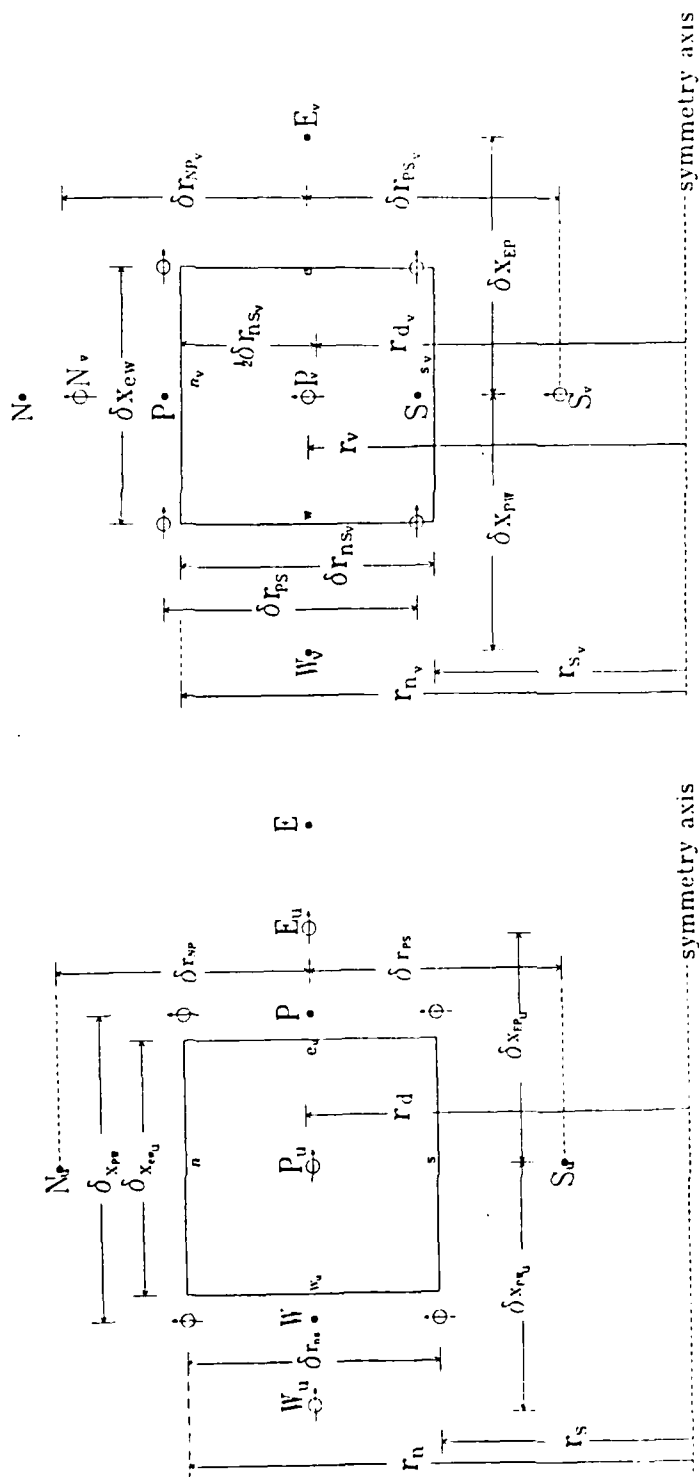


Figure 4-1. Geometry for control volumes of primitive variables except u and v .



A. Geometry for control volume of primitive variable u.

B. Geometry for control volume of primitive variable v.

Figure 4-2. Geometry for control volumes of primitive variables u and v.

where

$$A_n = \delta_p r_n \delta x_{ew}$$

and

$$A_s = \delta_p r_s \delta x_{ew} .$$

Adding the above terms results in the discretized form of the continuity equation:

$$\dot{M}_p^n - \dot{M}_p^0 + \dot{m}_n^n - \dot{m}_s^n + \dot{m}_e^n - \dot{m}_w^n = 0 \quad (4-1)$$

4.1.2 Discretization of the Transformed General Transport Equation

Equation (2-17) is integrated over a general control volume after combining several of its terms. If $\phi = k, \epsilon, T, m_f$, or f , the geometry and subscript nomenclature appropriate to figure 4-1 is used. If $\phi = u$, the geometry and subscript nomenclature for figure 4-2a is used instead. If $\phi = v$, that for figure 4-2b is used.

$$\begin{aligned} \int_{V_\phi} \frac{1}{\delta_p} \frac{\partial}{\partial t} (\rho \delta_p \phi) \delta_p r \, dr \, dx &= \frac{[(\rho \phi V)_\phi^n - (\rho \phi V)_\phi^0]}{\Delta t} \\ &= \dot{M}_\phi^n - \dot{M}_\phi^0 \\ \int_{V_\phi} \frac{1}{\delta_p} \frac{\partial}{\partial x} \left(\rho \bar{u} \phi - \frac{\Gamma_\phi}{\delta_p} \frac{\partial \phi}{\partial x} \right) \delta_p r \, dr \, dx &= \left[(\rho \bar{u} \phi - \frac{\Gamma_\phi}{\delta_p} \frac{\partial \phi}{\partial x})_{e_\phi} \right. \\ &\quad \left. - (\rho u \phi - \frac{\Gamma_\phi}{\delta_p} \frac{\partial \phi}{\partial x})_{w_\phi} \right] A_{ew_\phi} \\ &= J_{e_\phi} - J_{w_\phi} \\ \int_{V_\phi} \frac{1}{r} \frac{\partial}{\partial r} \left(r \rho v \phi - r \Gamma_\phi \frac{\partial \phi}{\partial r} \right) \delta_p r \, dr \, dx &= (\rho v \phi - \Gamma_\phi \frac{\partial \phi}{\partial r})_{n_\phi} A_{n_\phi} \\ &\quad - (\rho v \phi - \Gamma_\phi \frac{\partial \phi}{\partial r})_{s_\phi} A_{s_\phi} \\ &= J_{n_\phi} - J_{s_\phi} \end{aligned}$$

$$\int_V \int_{\phi} \bar{S}_{\phi} d(V_{\phi}) = Sp_{\phi} \phi_p + Su_{\phi} ,$$

where

Sp_{ϕ} , Su_{ϕ} - are specified for various ϕ in section 4.1.3

Collecting terms yields -

$$M_{p\phi}^n \phi_{p\phi}^n - M_{p\phi}^o \phi_{p\phi}^o + J_{e\phi} - J_{w\phi} + J_{n\phi} - J_{s\phi} = Sp_{\phi} \phi_p + Su_{\phi} ,$$

Note that if equation (4-1) is re-derived for a generalized control volume in a manner identical to the formulation of the above equation, and the result is first multiplied by $\phi_{p\phi}^n$ and then subtracted from the above equation, the following expression results:

$$\begin{aligned} M_{p\phi}^o (\phi_{p\phi}^n - \phi_{p\phi}^o) + (J_{e\phi} - m_{e\phi}^n \phi_{p\phi}^n) - (J_{w\phi} - m_{w\phi}^n \phi_{p\phi}^n) + \\ (J_{n\phi} - m_{n\phi}^n \phi_{p\phi}^n - (J_{s\phi} - m_{s\phi}^n \phi_{p\phi}^n)) = Sp_{\phi} \phi_{p\phi} + Su_{\phi} . \end{aligned}$$

The above result is simplified by using the power law spatial differencing scheme developed by Patanker⁷⁶ to approximate the total flux terms

$(J - m_{n\phi}^n \phi_p)$. The total flux terms become:

$$(J_{e\phi} - m_{e\phi}^n \phi_{p\phi}^n) = a_{E\phi} (\phi_{p\phi} - \phi_{E\phi}) ,$$

$$(J_{w\phi} - m_{w\phi}^n \phi_{p\phi}^n) = a_{W\phi} (\phi_{W\phi} - \phi_{p\phi}) ,$$

$$(J_{n\phi} - m_{n\phi}^n \phi_{p\phi}^n) = a_{N\phi} (\phi_{p\phi} - \phi_{N\phi})$$

and

$$(J_{s\phi} - m_{s\phi}^n \phi_{p\phi}^n) = a_{S\phi} (\phi_{S\phi} - \phi_{p\phi}) .$$

Substitution of the above four expressions into our previous equation results in the final version of the discretized general transformed transport equation in compact form:

$$(a_{p\phi} + M_{p\phi}^o - Sp_{\phi}) \phi_{p\phi}^n = \sum_m a_{m\phi} \phi_m^n + Su_{\phi} + M_{p\phi}^o \phi_{p\phi}^o \quad (4-2)$$

where [76]

$$m = N_\phi, S_\phi, E_\phi, W_\phi,$$

$$a_{p_\phi} = a_{E_\phi} + a_{W_\phi} + a_{N_\phi} + a_{S_\phi}, \quad (4-2a)$$

$$a_{E_\phi} = D_{e_\phi} A(|P_{e_\phi}|) + \max(-c_{e_\phi}, 0), \quad (4-2b)$$

$$a_{W_\phi} = D_{w_\phi} A(|P_{w_\phi}|) + \max(c_{w_\phi}, 0), \quad (4-2c)$$

$$a_{N_\phi} = D_{n_\phi} A(|P_{n_\phi}|) + \max(-c_{n_\phi}, 0), \quad (4-2d)$$

$$a_{S_\phi} = D_{s_\phi} A(|P_{s_\phi}|) + \max(c_{s_\phi}, 0), \quad (4-2e)$$

$$D_{e_\phi} = \frac{\Gamma_{\phi e_\phi} A_{ew_\phi}}{\delta p \delta x_{EP_\phi}}, \quad c_{e_\phi} = \dot{m}_{e_\phi}^n, \quad P_{e_\phi} = \frac{c_{e_\phi}}{D_{e_\phi}}, \quad (4-2f)$$

$$D_{w_\phi} = \frac{\Gamma_{\phi w_\phi} A_{ew_\phi}}{\delta p \delta x_{PW_\phi}}, \quad c_{w_\phi} = \dot{m}_{w_\phi}^n, \quad P_{w_\phi} = \frac{c_{w_\phi}}{D_{w_\phi}}, \quad (4-2g)$$

$$D_{n_\phi} = \frac{\Gamma_{\phi n_\phi} A_{n_\phi}}{\delta r_{NP_\phi}}, \quad c_{n_\phi} = \dot{m}_{n_\phi}^n, \quad P_{n_\phi} = \frac{c_{n_\phi}}{D_{n_\phi}}, \quad (4-2h)$$

$$D_{s_\phi} = \frac{\Gamma_{\phi s_\phi} A_{s_\phi}}{\delta r_{PS_\phi}}, \quad c_{s_\phi} = \dot{m}_{s_\phi}^n, \quad P_{s_\phi} = \frac{c_{s_\phi}}{D_{s_\phi}}, \quad (4-2i)$$

$$A(|P|) = \max(0, (1 - |P|)^5)$$

and

$\max(,)$ \equiv maximum positive value of quantities contained inside parenthesis

For clarity it should be noted that the generalized expression for the discretized transport equation given above (equation (4-2)) applies for all ϕ . For ϕ other than u or v, expressions (4-2a) through (4-2i) are derived using the control volume shown in figure 4-1 and the nomenclature is exactly as given in these expressions with the ϕ 's removed. For $\phi = u$ the terms a_{M_u} ($M = N, S, E, W$), D_{m_u} , c_{m_u} , $\dot{m}_{m_u}^n$, and P_{m_u} (for $m = e, w, n, s$) are derived instead using the geometry given in figure 4-2a. Similarly, for ϕ

= v, the terms a_{mV} , D_{mV} , C_{mV} , m_{nV} and P_{mV} are used in expressions (4-2a) through (4-2i) and are defined in terms of the geometry given in figure 4-2b.

4.1.3 Discretization of Transformed Source Terms

The source terms of the transformed governing equations (summarized in Table 2-1) are discretized by integrating each over its appropriate control volume.

u-Momentum Equation Source Term

The expression for the transformed u-velocity transport equation source term (\bar{S}_u) repeated below is integrated a term at a time over the control volume given in Figure 4-2a.

$$\bar{S}_u = - \frac{1}{\delta_p} \frac{\partial P}{\partial x} + \frac{1}{\delta_p} \frac{\partial}{\partial x} \left[\frac{\mu_{eff}}{\delta_p} \frac{\partial u}{\partial x} \right] + \frac{1}{r} \frac{\partial}{\partial r} \left[\frac{r \mu_{eff}}{\delta_p} \frac{\partial v}{\partial x} \right] - \frac{2}{3\delta_p} \frac{\partial}{\partial x} (\mu_{eff} \nabla \cdot \underline{u} + \rho k) .$$

$$\begin{aligned} US1 &\equiv \int \int_{V_u} \left(- \frac{1}{\delta_p} \frac{\partial P}{\partial x} \right) \delta_p r dr dx \\ &= - \frac{1}{\delta_p} \frac{(P_p - P_w)}{\delta x p_w} V_u , \end{aligned} \quad (4-3)$$

where

$$\begin{aligned} V_u &= \delta_p r_d \delta r_{ns} \delta x_{ew_u} . \\ US2 &\equiv \int \int_{V_u} \left(\frac{1}{\delta_p} \frac{\partial}{\partial x} \left[\frac{\mu_{eff}}{\delta_p} \frac{\partial u}{\partial x} \right] \right) d(V_u) \\ &= \frac{\left[\frac{\mu_{eff}}{\delta_p} \frac{\partial u}{\partial x} \right]_p - \left[\frac{\mu_{eff}}{\delta_p} \frac{\partial u}{\partial x} \right]_w}{\delta_p \delta x p_w} V_u \end{aligned} \quad (4-4)$$

$$\begin{aligned}
 US3 &\equiv \int \int_{V_U} \left(\frac{1}{r} \frac{\partial}{\partial r} \left[\frac{r}{\delta_p} \mu_{eff} \frac{\partial v}{\partial x} \right] \right) \delta_p r \partial r \partial x \\
 &= \left(\left[r \mu_{eff} \frac{\partial v}{\partial x} \right]_n - \left[r \mu_{eff} \frac{\partial v}{\partial x} \right]_s \right) \delta x_{ewU} .
 \end{aligned} \tag{4-5}$$

$$\begin{aligned}
 US4 &\equiv \int \int_{V_U} \left(- \frac{2}{3 \delta_p} \frac{\partial}{\partial x} \left(\mu_{eff} \left[\frac{1}{\delta_p} \frac{\partial u}{\partial x} + \frac{v}{r} + \frac{\partial v}{\partial r} \right] + \rho k \right) \right) d(V_U) \\
 &= - \frac{2}{3} \frac{(\mu_{eff} \left[\frac{v}{r} + \frac{\partial v}{\partial r} \right] + \rho k)_p - (\mu_{eff} \left[\frac{v}{r} + \frac{\partial v}{\partial r} \right] + \rho k)_W}{\delta_p \delta x_{pw}} V_U \\
 &\quad - \frac{2}{3} US2 .
 \end{aligned} \tag{4-6}$$

$$Su_U = US1 + US2 + US3 + US4 . \tag{4-7}$$

$$Sp_U = 0 \tag{4-8}$$

v - Momentum Equation Source Term

The expression for the transformed v-velocity transport equation source term (\bar{S}_v) is integrated term by term over the control volume given in figure 4-2b.

$$\begin{aligned}
 \bar{S}_v &= - \frac{\partial P}{\partial r} + \frac{1}{\delta_p} \frac{\partial}{\partial x} \left[\mu_{eff} \frac{\partial u}{\partial r} \right] + \frac{1}{r} \frac{\partial}{\partial r} \left[r \mu_{eff} \frac{\partial v}{\partial r} \right] - 2 \mu_{eff} \frac{v}{r^2} - \\
 &\quad \frac{2}{3} \frac{\partial}{\partial r} (\mu_{eff} \nabla \cdot \underline{u} + \rho k) .
 \end{aligned}$$

$$\begin{aligned}
 VS1 &\equiv \int \int_{V_V} \left(- \frac{\partial P}{\partial r} \right) \delta_p r \partial r \partial x \\
 &= - \frac{(P_p - P_s)}{\delta r_{ps}} V_V ,
 \end{aligned} \tag{4-9}$$

where

$$V_V = \delta p r_{dV} \delta r_{nsV} \delta x_{ew} .$$

$$\begin{aligned} VS2 &\equiv \int_{V_V} \int \left(\frac{1}{\delta p} \frac{\partial}{\partial x} \left[\mu_{eff} \frac{\partial u}{\partial r} \right] \right) \delta p r \partial r \partial x \\ &= \left(\left[\mu_{eff} \frac{\partial u}{\partial r} \right]_e - \left[\mu_{eff} \frac{\partial u}{\partial r} \right]_w \right) r_{dV} \delta r_{nsV} . \end{aligned} \quad (4-10)$$

$$\begin{aligned} VS3 &\equiv \int_{V_V} \int \left(\frac{1}{r} \frac{\partial}{\partial r} \left[r \mu_{eff} \frac{\partial v}{\partial r} \right] \right) \delta p r \partial r \partial x \\ &= \left(\left[r \mu_{eff} \frac{\partial v}{\partial r} \right]_{nV} - \left[r \mu_{eff} \frac{\partial v}{\partial r} \right]_{sV} \right) \delta p \delta x_{ew} . \end{aligned} \quad (4-11)$$

$$\begin{aligned} VS4 &\equiv \int_{V_V} \int \left(-2 \mu_{eff} \frac{v}{r^2} \right) d(V_V) \\ &= -2 \mu_{eff} p_V \frac{v}{r_V^2} V_V . \end{aligned} \quad (4-12)$$

$$VS4' \equiv - \frac{VS4}{v} . \quad (4-13)$$

$$VS5 \equiv \int_{V_V} \int \left(- \frac{2}{3} \frac{\partial}{\partial r} \left(\mu_{eff} \left[\frac{1}{\delta p} \frac{\partial u}{\partial x} + \frac{v}{r} + \frac{\partial v}{\partial r} \right] + \rho k \right) \right) d(V_V) .$$

$$VS5 = - \frac{2}{3} \frac{\left(\mu_{eff} \left(\frac{1}{\delta p} \frac{\partial u}{\partial x} + \rho k \right) \right)_p - \left(\mu_{eff} \left(\frac{1}{\delta p} \frac{\partial u}{\partial x} + \rho k \right) \right)_s}{\delta r_{ps}} V_V$$

$$- \frac{2}{3} \frac{(\mu_{eff} (\frac{v}{r} + \frac{\partial v}{\partial r}))_{n_v} - (\mu_{eff} (\frac{v}{r} + \frac{\partial v}{\partial r}))_{s_v}}{\delta r_{ns_v}} V_v . \quad (4-14)$$

$$Su_v = VS1 + VS2 + VS3 + VS5 . \quad (4-15)$$

$$Sp_v = VS4' \quad (4-16)$$

Turbulent Kinetic Energy Equation Source Term

$$\begin{aligned} \overline{S_k} &= - C_D \rho \epsilon + \overline{G} \\ &= - C_D \rho \epsilon + 2 \mu_{eff} \left(\left[\frac{1}{\delta_p} \frac{\partial u}{\partial x} \right]^2 + \left[\frac{\partial v}{\partial r} \right]^2 + \left(\frac{v}{r} \right)^2 + \frac{1}{2} \left[\frac{\partial u}{\partial r} + \frac{1}{\delta_p} \frac{\partial v}{\partial x} \right]^2 \right) - \\ &\quad - \frac{2}{3} \nabla \cdot \underline{u} (\mu_{eff} \nabla \cdot + \rho k) . \end{aligned}$$

The above is integrated a term at a time over the control volume given in figure 4-1 to obtain Su_k and Sp_k .

$$\begin{aligned} kS1 &\equiv \int_V (- C_D \rho \epsilon) d(V) \\ &= - C_D \rho_p \epsilon_p V \\ &= \frac{- C_D C_\mu \rho_p^2 k_p^2 V}{(\mu_{effp} - \mu_l)} . \end{aligned} \quad (4-17)$$

$$kS1' \equiv \frac{kS1}{k} . \quad (4-18)$$

$$\begin{aligned} kS2 &= \int_V \left(2 \mu_{eff} \left(\left[\frac{1}{\delta_p} \frac{\partial u}{\partial x} \right]^2 + \left[\frac{\partial v}{\partial r} \right]^2 + \left(\frac{v}{r} \right)^2 + \frac{1}{2} \left[\frac{\partial u}{\partial r} + \frac{1}{\delta_p} \frac{\partial v}{\partial x} \right]^2 \right) \right) d(V) \\ &= 2 \mu_{effp} \left(\left[\frac{1}{\delta_p} \frac{\partial u}{\partial x} \right]_p^2 + \left[\frac{\partial v}{\partial r} \right]_p^2 + \left[\frac{v}{r} \right]_p^2 + \frac{1}{2} \left[\frac{\partial u}{\partial r} + \frac{1}{\delta_p} \frac{\partial v}{\partial x} \right]_p^2 \right) V . \end{aligned} \quad (4-19)$$

$$\begin{aligned}
 kS3 &= \int_V \int \left(-\frac{2}{3} \nabla \cdot \underline{u} (\mu_{eff} \nabla \cdot \underline{u} + \rho k) \right) d(V) \\
 &= -\frac{2}{3} \left(\frac{1}{\delta_p} \frac{\partial u}{\partial x} + \frac{v}{r} + \frac{\partial v}{\partial r} \right)_p \left[\mu_{effp} \left(\frac{1}{\delta_p} \frac{\partial u}{\partial x} + \frac{v}{r} + \frac{\partial v}{\partial r} \right)_p + \rho_p k_p \right] V .
 \end{aligned}$$

$$kS3' = -\frac{2}{3} \left(\frac{1}{\delta_p} \frac{\partial u}{\partial x} + \frac{v}{r} + \frac{\partial v}{\partial r} \right)_p \rho_p V . \quad (4-20)$$

$$kS3'' = kS3 - (kS3') k_p . \quad (4-21)$$

$$Su_k = kS2 + kS3'' . \quad (4-22)$$

$$Sp_k = kS1' + kS3' . \quad (4-23)$$

$$\overline{G_p} = \frac{kS2 + kS3}{V} . \quad (4-24)$$

Turbulent Kinetic Energy Dissipation Rate Equation Source Term

$$\overline{S_\epsilon} = \frac{\epsilon}{k} (C_1 \overline{G} - C_2 \rho \epsilon) + \rho \epsilon \nabla \cdot \underline{u}$$

Su_k and Sp_k are obtained by integrating the above expression over the control volume depicted in Figure 4-1.

$$\begin{aligned}
 eS1 &\equiv \int_V \int \left(C_1 G \frac{\epsilon}{k} \right) d(V) \\
 &= \frac{C_1 G_p C_u \rho_p k_p}{\mu_{eff} - \mu_l} V .
 \end{aligned} \quad (4-25)$$

$$eS2 \equiv \int_V \int \left(-C_2 \frac{\rho \epsilon^2}{k} \right) d(V)$$

$$= - \frac{C_2 \rho_p \epsilon_p^2 V}{k_p} . \quad (4-26)$$

$$eS2' = \frac{eS2}{\epsilon_p} . \quad (4-27)$$

$$eS3 = \int_V \rho \epsilon \left(\frac{1}{\delta_p} \frac{\partial u}{\partial x} + \frac{v}{r} + \frac{\partial v}{\partial r} \right) d(V)$$

$$= \rho_p \epsilon_p \left(\frac{1}{\delta_p} \frac{\partial u}{\partial x} + \frac{v}{r} + \frac{\partial v}{\partial r} \right)_p V . \quad (4-28)$$

$$eS3' = \frac{eS3}{\epsilon_p} . \quad (4-29)$$

$$Su_\epsilon = eS1 . \quad (4-30)$$

$$Sp_\epsilon = eS2' + eS3' . \quad (4-31)$$

Energy Equation Source Term

$$\bar{S}_T = \frac{1}{\bar{C}_p} \frac{\partial P}{\partial t} - \frac{x}{\delta_p} u_p \frac{\partial P}{\partial x} + \frac{u}{\delta_p} \frac{\partial P}{\partial x} + v \frac{\partial P}{\partial r} + \bar{G} - \rho \sum_{i=1}^n h_i^0 \dot{m}_i$$

Integrating this expression over the control volume shown in figure 4-1 results in Su_T and Sp_T .

$$TS1 \equiv \int_V \left(\frac{1}{\bar{C}_p} \left[\frac{\partial P}{\partial t} - \frac{x}{\delta_p} u_p \frac{\partial P}{\partial x} + \frac{u}{\delta_p} \frac{\partial P}{\partial x} \right] \right) \delta_p r \, dr \, dx$$

$$= \int_V \left(\frac{1}{\bar{C}_p} \left[\frac{\partial}{\partial t} (P \delta_p) - \frac{P \partial \delta_p}{\partial t} + \frac{\bar{u}}{\delta_p} \frac{\partial P}{\partial x} \right] \right) \delta_p r \, dr \, dx$$

$$= \frac{1}{\bar{C}_{pp}} \left(\left[\frac{P_p^0 - P_p^{\Delta t}}{\Delta t} \right] V^0 + \left[\frac{\bar{u}}{\delta_p} \frac{\partial P}{\partial x} \right] V^n \right) , \quad (4-32)$$

where

V^0 = volume of control volume of previous time step

and

$$V^n = V$$

= volume of control volume at present time step.

$$\begin{aligned} TS2 &\equiv \int_V \int \left(\frac{1}{\bar{C}_p} v \frac{\partial P}{\partial r} \right) d(V) \\ &= \frac{v_p}{\bar{C}_{p_p}} \left(\frac{\partial P}{\partial r} \right)_p V . \end{aligned} \quad (4-33)$$

$$\begin{aligned} TS3 &\equiv \int_V \int \left(\frac{\bar{G}}{\bar{C}_{p_p}} \right) d(V) \\ &= \frac{G_p}{C_{p_p}} V \end{aligned} \quad (4-34)$$

where

\bar{G}_p - given in equation (4-24).

$$TS4 \equiv \int_V \int \left(\frac{\dot{q}_c'''}{\bar{C}_p} \right) d(V)$$

where

$$\dot{q}_c''' = - \rho \sum_{i=1}^n h_i^0 (\dot{m}_i)$$

and from equation (3-11)

$$\dot{q}_c''' = - \rho [h_f^0 - (1+s) h_{pr}^0] (\dot{m}_f) .$$

Thus

$$TS4 = - \frac{\rho_p}{C_{p_p}} [h_f^0 - (1+s) h_{pr}^0] \dot{m}_{fp} V . \quad (4-35)$$

Fuel Species Mass Fraction Equation Source Term

$$\bar{S}_{mf} = \rho \dot{m}_f$$

\bar{S}_{mf} is integrated over the control volume shown in figure 4-1.

$$\begin{aligned} fmS1 &\equiv \int_V \rho \dot{m}_f d(V) \\ &= \rho p \dot{m}_{fp} V \end{aligned} \quad (4-36)$$

$$Su_{mf} = fmS1 \quad (4-37)$$

$$Sp_{mf} = 0 \quad (4-38)$$

Mixture Fraction Equation Source Term

Since $\bar{S}_f = 0$.

$$Su_f = Sp_f = 0 \quad (4-39)$$

4.1.4 Discretization of the Non-Flow (NF) Energy Equation

Equation 2-18 is integrated over the control volume shown in figure 4-1 with the non-dimensional x distances replaced by the corresponding dimensional z distances.

$$\int_V \rho \frac{\partial T}{\partial t} dV = \frac{T_p^n - T_p^o}{\Delta t} \rho V = M_p \frac{T_p^n - T_p^o}{\Delta t}$$

$$\int_V \frac{K}{C} \left[\frac{\partial}{\partial z} \frac{\partial T}{\partial z} \right] r \varphi \Delta z = \frac{K}{C} \left[\left(\frac{\partial T}{\partial z} \right)_e - \left(\frac{\partial T}{\partial z} \right)_w \right] A_{ew} = J_{eT_{NF}} - J_{wT_{NF}}$$

$$\int_V \frac{K}{C} \frac{1}{r} \frac{\partial}{\partial r} \left[r \frac{\partial T}{\partial r} \right] r \varphi \Delta z = \frac{K}{C} \left[\left(\frac{\partial T}{\partial r} \right)_n A_n - \left(\frac{\partial T}{\partial r} \right)_s A_s \right] = J_{nT_{NF}} - J_{sT_{NF}}$$

Note that:

$$J_{eT_{NF}} = a_{ET_{NF}} (T_E - T_p), \quad a_{ET_{NF}} = \frac{K}{C} \frac{A_{EW}}{\delta z_{EP}},$$

$$J_{wTNF} = a_{wTNF}(T_P - T_E) , \quad a_{wTNF} = \frac{K A_{Ew}}{C \delta z_{pw}} ,$$

$$J_{nTNF} = a_{nTNF}(T_N - T_P) , \quad a_{nTNF} = \frac{K A_n}{C \delta r_{NP}} ,$$

$$J_{sTNF} = a_{sTNF}(T_P - T_S) \quad \text{and} \quad a_{sNF} = \frac{K A_s}{C \delta r_{PS}} .$$

Substituting the above results into the integrated version of equation (2-18) results in the discretized non-flow energy equation:

$$(a_{PTNF} + M_P)T_P = \sum_m a_{mTNF} T_{mTNF} + M_P T_P^0 \quad (4-40)$$

where,

$$m = N_{TNF}, S_{TNF}, E_{TNF}, W_{TNF}$$

and

$$a_{PTNF} = \sum_m a_{mTNF} .$$

4.2 Special Procedure for Calculating the Pressure Field

In order to solve the u and v momentum equations and the energy equation the local flow pressure must be specified. Two algorithms exist which lend themselves to calculation of P for the present analysis: SIMPLE [76,78] and SIMPLER [78,87]. Though the second algorithm has the potential of accelerating the convergence rate of the solution scheme for each time step, it was found arduous to use in this analysis. This was due to the complexity of the source terms and the time variations of the boundary conditions. SIMPLE (Semi - Implicit - Method for Pressure - Linked Equations) on the other hand proved itself to be "simpler" to use in this analysis and was therefore incorporated. For completeness, an outline of the details are given below for the transformed flow field.

The continuity equation (equation 4-1) restated in a less compact form is:

$$\dot{M}_p^n - \dot{M}_p^o + (\rho v)_n A_n - (\rho v)_s A_s + (\rho \bar{u})_e A_{ew} - (\rho \bar{u})_w A_{ew} = 0 . \quad (4-41)$$

At the outset of a specific time iteration, P , u and v can only be guessed. The actual pressure (P) at a nodal point is equal to the guessed pressure (P^*) plus the local pressure correction (P') and the global pressure correction (\bar{P}'). The present section deals with the pressure correction due to local velocity variations only. Section 4.3 will cover the global pressure correction. Therefore, for the present, we will define P as:

$$P = P^* + P' . \quad (4-42)$$

Similarly,

$$\begin{aligned} u &= u^* + u' , \\ \bar{u} &= \bar{u}^* + \bar{u}' \end{aligned} \quad (4-43)$$

and

$$v = v^* + v' , \quad (4-44)$$

where

$$\bar{u} = \text{transformed velocity defined by equation (2-15).}$$

From equation (4-42) we can define \bar{u}_w as follows:

$$\bar{u}_w = \bar{u}_w^* + \bar{u}_w' ,$$

where

$$\bar{u}_w^* = u_w^* - x_w u_p ,$$

and

$$\begin{aligned}\bar{u}_w' &= \frac{\partial \bar{u}_w}{\partial (P_w' - P_p')} (P_w' - P_p') \\ &\equiv dw (P_w' - P_p') .\end{aligned}$$

Thus we can express \bar{u}_w

$$\bar{u}_w = u_w^* + dw (P_w' - P_p') . \quad (4-45)$$

Similarly, we can define:

$$\bar{u}_w = \bar{u}_e^* + de (P_p' - P_e') , \quad (4-46)$$

$$v_n = v_n^* + dn (P_p' - P_n') , \quad (4-47)$$

and

$$v_s = v_s^* + ds (P_s' - P_p') , \quad (4-48)$$

where dw , de , dn and ds are determined from the discretized momentum equations for the control volume surrounding the appropriate specified flow field velocity. For example, the discretized equation for the momentum equation for u_w , where u_w is at the center of the control volume given in figure 4-2, is given by:

$$(a_{p_u}^n + M_{p_u}^n - S_{p_u}) u_w = \sum_m A_m u_m + \frac{1}{\delta p} \frac{P_w - P_p}{\delta x_{pw}} V_{u_w} + b_{p_u} , \quad (4-49)$$

where

$$\begin{aligned}m &= N_u, S_u, E_u, W_u , \\ b_{p_u} &= US2 + US3 + US4 + M_{p_u}^o u_{p_u}^o\end{aligned}$$

and

$V_{u_w} = V_u$ is the volume of the control volume around u_w (see figure 4-2).

and

u_w^* = guessed value of u_w which is
labeled in figures 4-1 and 4-2.

Note that because -

$$\bar{u}_w = u_w - x_w u_p$$

and neither x_w nor u_p vary with respect to a change in the expression
($P_w - P_p$):

$$dw = \frac{\partial \bar{u}_w}{\partial (P_w - P_p)} = \frac{\partial u_w}{\partial (P_w - P_p)}$$

Solving equation (4-49) for u_w and taking the partial derivative of
the result with respect to the expression ($P_w - P_p$) results in:

$$dw = \frac{\frac{V_{u_w}}{\delta x p_w}}{\frac{n}{a p_u} + \frac{o}{M p_u} - S p_u} \quad (4-50)$$

Similarly,

$$de = \frac{\frac{V_{u_e}}{\delta x e p}}{\frac{o}{a p_{u_e}} + \frac{M p_{u_e}}{M p_{u_e}} - S p_{u_e}} \quad (4-51)$$

where

V_{u_e} - is the volume of the control volume used in the discretization
of the u -momentum equation about u_e in an identical manner to the
formulation of V_{u_w} about u_w

P_{u_e} - center nodal point of control volume for u_e which is equivalent
to the point E_u in figure 4-2.

For clarity, as shown in figure 4-1, u_e is the velocity vector passing through the east face of the unstaggered control volume while u_w passes through the west face, v_n the north face and v_s the south face of this control volume. Identical formulations to the above result in the following similar terms for v_n and v_s :

$$dn = \frac{\frac{v_{v_n}}{\delta r_{NP}}}{A_{p_{v_n}} + M_{p_{v_n}}^0 - S_{p_{v_n}}} \quad (4-52)$$

$$ds = \frac{\frac{v_{v_s}}{\delta r_{PS}}}{A_{p_{v_s}} + M_{p_{v_s}}^0 - S_{p_{v_s}}} \quad (4-53)$$

Substitution of equations (4-50) through (4-53) into equations (4-45) through (4-48) respectively, and substitution of the resulting four expressions into equation (4-41) yields in compact form the following:

$$a_{pp} \dot{p}_p = \sum_{m=w,e,n,s} a_{mp} \dot{p}_m + S_{u_p}, \quad (4-54)$$

where

$$a_{mp} = \rho_m A_m d_m$$

$$a_{pp} = a_{wp} + a_{ep} + a_{np} + a_{sp}$$

$$S_{u_p} = M_p^0 - M_p^n - (\rho v)_n A_n + (\rho v)_s A_s - (\rho \bar{u})_e A_{ew} + (\rho \bar{u})_w A_{ew} \text{ (this is modified in Section 4.3 by equation (4-59))}$$

and

M - subscript on P_M' which indicates capital value of the corresponding little m (i.e., when $m = w$, $P_M' = P_W'$, etc).

In the overall solution scheme, the u and v momentum equations are solved first and all four dm's calculated for use in equation (4-54). Then equation (4-54) is solved and the P' values obtained are used in equations (4-42), (4-47), (4-48) as well as equation (4-55) and (4-56) below to obtain updated values of P, u_w , w_e , v_n and v_s .

$$u_w = u_w^* + dw (P_W' - P_p) \quad (4-55)$$

$$u_e = u_e^* + de (P_p - P_E') \quad (4-56)$$

4.3 Perturbation of Continuity Equation

Inside internal combustion engines, pressure variations are produced by both fluid motion and by the expansion and compression of the air due to piston motion. The formulation given in section 4.2 describes the local pressure correction due to spatial variations in the fluid velocities. The procedure used to determine the global variation of pressure due to piston motion involves the perturbation of the continuity equation and is the subject of this section.

With the assumption of a perfect gas, density is a function of T and P.

$$\rho = \rho (P, T) \quad .$$

Earlier researchers perturbed the expression for density with respect to both P and T and obtained global correction terms for the temperature and pressure using both the energy and continuity equations [41,67]. These formulations required a global conservation of both energy and mass for

convergence. However, it has been found that the energy equation, using the discretization for TS1 given in equation (4-32) will correct itself globally for changes in temperature due to piston motion, and that it is sufficient to only require a global conservation of mass [68]. Thus the expression:

$$\rho = \rho^* + \left(\frac{\partial \rho}{\partial P}\right) \bar{P}' \quad (4-57)$$

is used in our present analysis where

ρ^* = guessed value of density obtained from use of equation (2-10),

\bar{P}' = global pressure correction defined below in equation (4-58),

$$\left(\frac{\partial \rho}{\partial P}\right)_T = \frac{1}{R_{\text{gas}} T} \text{ for a perfect gas}$$

and

$$R_{\text{gas}} = \sum_{i=1}^n m_i R_i \quad (\text{see equation 2-10}).$$

Note that:

$$\begin{aligned} M_p^n &\equiv \rho \frac{V}{\Delta t} \\ &= \left(\rho^* + \left(\frac{\partial \rho}{\partial P}\right)_T \bar{P}'\right) \frac{V}{\Delta t} \\ &= M_p^* + \beta_p^* \bar{P}' \end{aligned}$$

Substitution of this result into equation (4-10) yields:

$$M_p^* + \beta_p^* \bar{P}' - \overset{0}{M_p} + \overset{n}{\dot{m}_n} - \overset{n}{\dot{m}_s} + \overset{n}{\dot{m}_e} - \overset{n}{\dot{m}_w} = 0$$

Summing the above equation over the entire flowfield (F) and solving for the global pressure correction yield:

$$\bar{p}' = \frac{\sum_F [M_p^0 - M_p^* - (\dot{m}_n^n - \dot{m}_s^n + \dot{m}_e^n - \dot{m}_w^n)]}{\sum_F B_p^*} . \quad (4-58)$$

This correction is incorporated into the solution scheme in two places. It is inserted into the source term of equation (4-54) so that Su_p modified to

$$Su_p' = M_p^0 - M_p^* - B_p^* \bar{p}' - (\rho v)_n A_n + (\rho v)_s A_s - (\rho u)_e A_{ew} + (\rho u)_w A_{ew} . \quad (4-59)$$

Also \bar{p}' is used to correct P as follows:

$$P = P^* + \bar{p}' . \quad (4-60)$$

It should be noted that the global correction is made first in the iteration scheme. Then equation (4-54) is solved with the equation (4-59) modification of Su_p , to obtain the local pressure correction values (P'). Then equation (4-42) is used to adjust the values of the flow field pressure locally.

4.4 Solution Procedure

An overview of the logic of the code used in the solution of this problem is given in figure 4-4. The general solution technique used to solve the discretized form of the governing equations for each variable is an iterative line-by-line method in which an initial guess of the flow field values is made and then is improved upon from one line to another [78,88]. The equations for the points along a particular line are solved by temporarily assuming that the most recently calculated values of the terms on the neighboring lines are known, reducing the equation for each point along the line (either N-S and E-W) to only three unknowns.

Thus the equations along each line take the form of a tri-diagonal matrix and are solved using a simple Tri-Diagonal Matrix Algorithm

The program which directs the order of the solution of the problem is called CONTROL. Upon running the program, CONTROL calls upon a series of subroutines to set up the initial geometry and specify initial property values. Control then moves the solution into a large time loop which is designed to take the engine through the desired number of complete revolutions. The program proceeds through this time loop a time step at a time until it reaches the final time step (t_{Final}). Within a given time step the solution scheme is directed into a property iteration loop to simultaneously determine all the properties at that time using the method outlined in the previous paragraph. The program will not leave this property iteration loop until the maximum value of the source residuals for each of the u , v , P' , and T equations is less than .005. The values of these residuals are found by first computing the difference between the left and right hand sides of equation (4-2) for all the nodal points of a given property in the flow field. Then these differences are summed over the entire flow field and divided by quantities appropriate to each parameter to obtain the overall source residual for that primitive variable. Once the largest of these residuals goes below .005 and last three iteration values for \bar{P}' are all less than .01, the program is returned to the time loop where various old time values are stored and new geometric values determined in preparation for the next time step. In the event the program exceeds a fixed limit of iterations it is automatically advanced to the next time step, even though these two convergence criteria have not been met yet. At certain prespecified time steps along the way, CONTROL will direct the storage of data into files for future analysis and plotting.

Chapter 5

Valve Model

The problems encountered in the modeling of valve motion in the flow region of the numerical solution scheme were numerous. Several solution attempts were made before the final model contained herein was arrived at.

The primary problem encountered, that of having a moving boundary pass through solution nodal points which were also moving due to the transformation of the governing equations, was solved by dividing the flow field solution scheme into 3 regions as mentioned in Chapter 2.

As can be seen in Figure 5-1 in both region 1 and region 3, the absolute distance of the nodal points in the east-west direction from their nearest north-south boundaries do not change. In region 1 they are slaved to the top of the cylinder while in region 3 they are fixed to the piston even though it is moving. In region 2 the geometric positions of the nodal points in the east-west direction relative to the top of the cylinder are changing in accordance with the transformation given in section 2.2.

The interest in developing a good model for the heat transfer in the valve as well as through the cylinder and piston linings resulted in the development of a method to move a block of nodal points representing the valve back and forth through the solution scheme. However, convergence problems lead to the partial adoption of the use of an infinitely thin valve reported by researchers in [69] instead. It was later realized that extreme underrelaxation procedures may have made the use of a "thick" valve in the flow field feasible. However, the former

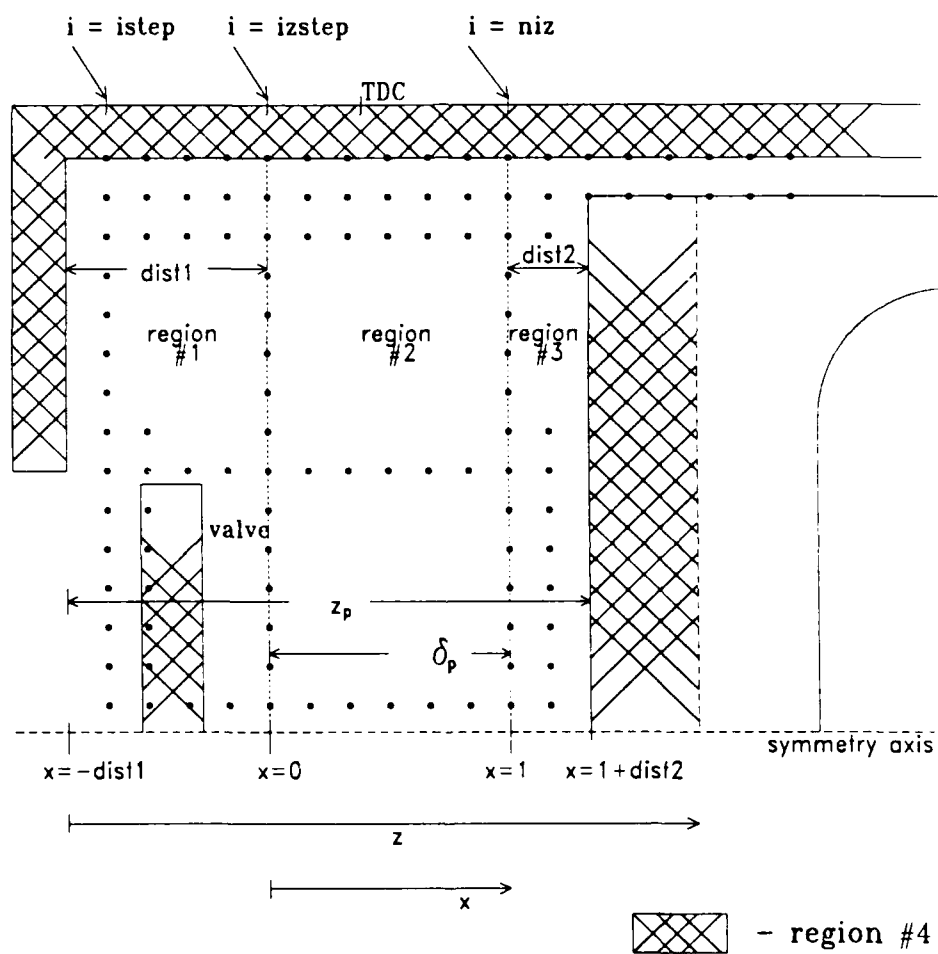


Figure 5-1. Solution Regions.

method was not reverted to, because, in the interim analysis, a method was discovered of giving the valve reasonable thickness for the purpose of solving the conjugate heat transfer problem while allowing it to be infinitely thin for the solution of the other flow field parameters. The approach utilized herein therefore views the valve as infinitely thin in relation to the parameters u , v , k , ϵ , f , m_f and P . The valve is viewed as having thickness from the view point of T . Also, fluid entrainment due to valve motion is considered in the computation of the unsteady terms of the flow field finite difference equations for all parameters. Details of this model are contained in subsequent subsections.

5.1 Solution Regions

Figure 5-1 shows the division of the solution regime into four solution regions, three flow field regions and one non-flow region. Only in region 2 is it necessary to use equations in a transformed state. In regions 1, 3, and 4 the equations are solved in an untransformed state, though special attention must be given to the area of region 4 adjacent to regions 2 and 3 (explained later).

In the actual solution of the entire flow field, the multiple region concept was employed in such a way as to arrive at a simultaneous solution of the flow field variables at all the nodal points at one time without having to iterate back and forth between the flow field regions. However, iteration back and forth between the non-flow field region (region 4) and the flow field regions (regions 1-3) was required. This simultaneous flow field solution was obtained by using the transformed form of the equations (equation (2-17)) throughout all the flow field regions and by noting that for regions 1 and 3 the values for the

NO-A163 003

NUMERICAL HEAT TRANSFER MODEL FOR A HEAT-BARRIER-PISTON
ENGINE WITH HYPER. (U) NAVAL ACADEMY ANNAPOLIS MD DIV
OF ENGINEERING AND WEAPONS D A BLANK FEB 86

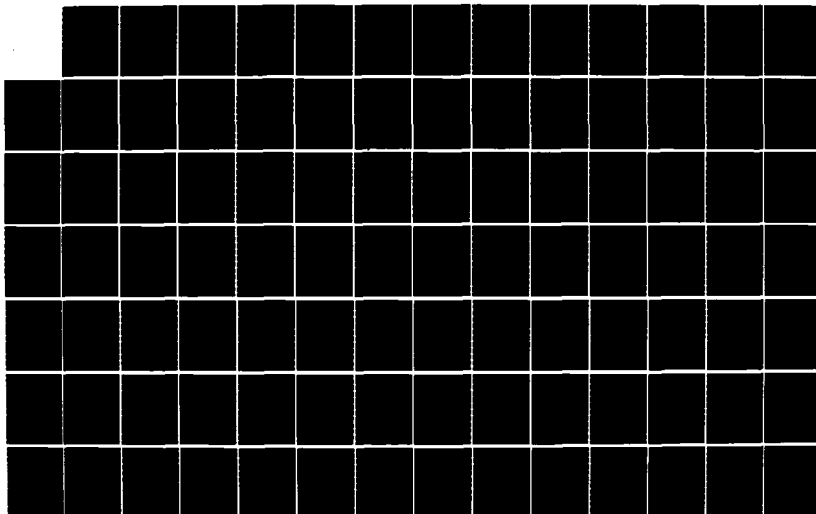
2/3

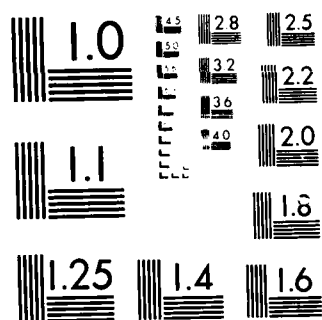
UNCLASSIFIED

USNA-EN-8-86

F/G 21/7

NL





MICROCOPY RESOLUTION TEST CHART
NATIONAL BUREAU OF STANDARDS-1963-A

expression $x \cdot u_p$ used in the computation of \bar{u} (equation 2-15) and in the determination of the transformed source term for the energy equation S_T (see table 2-1) are as follows:

$$\text{region 1: } x \cdot u_p = 0; \quad (5-1)$$

$$\text{region 3: } x \cdot u_p = u_p. \quad (5-2)$$

Use of the transformed equation throughout also necessitated the use of the absolute distances in the computation of the areas (A_{n_ϕ} and A_{s_ϕ}) and the volumes of the control volumes V_ϕ as well as all the other x coordinates distances used in the discretized terms of the governing equations. In the solution computer code the $\delta_p \cdot \delta x$ terms contained in the governing equations were computed as follows (δx is any distance in the x coordinated system, see figures 4-1, 2 and 3):

Regions 1, 2 and 3

$$\delta_p \delta x = \delta_z, \quad (5-3)$$

where for

Region 1:

$$\delta_z \equiv \delta x, \quad (5-3a)$$

Region 2:

$$\delta_z \equiv \delta_p \delta x, \quad (5-3b)$$

and

Region 3:

$$\delta_z \equiv \delta x. \quad (5-3c)$$

At the boundary areas of the nodal points control volumes corresponding to the interfaces between regions 1 and 2 and regions 2 and 3 special attention had to be given in the application of the transformation of the u -momentum equations to obtain an accurate solution.

This was due to the fact that in the solution of the finite difference equations for the u-momentum equation at these interface nodal points, the control volume boundaries at the interface can be moved by our transformation from one region to another. See Appendix D for an explanation of the special procedure used in this case. No special problems arose in the computation of the other primitive variables.

As mentioned in section 2.3 the solution of the Energy Equation in region 4 is carried out without the use of transformed equations. Because the portion of region 4 adjacent to regions 2 and 3 is changing size and the relative positions of the nodal points in this portion of region 4 must be repositioned. This is necessary in order to make possible the matching of the boundary conditions at the interface of regions 2 and 3 with region 4. To accomplish this, a very different procedure had to be employed. See Appendix C for the specifics of this procedure.

5.2 Valve Inlet and Valve Boundary Conditions

To account for the presence of a functioning valve, boundary conditions must be specified for not only both sides of the valve itself, but also for the orifice opening created when the valve is open. The thermodynamic behavior of the gases due to heat loss and heat absorption to and from the cylinder and piston coupled with pressure and velocity changes caused by piston motion slightly complicate the boundary conditions at the orifice. However, with the exception of the energy equation, boundary conditions at the inner and outer surfaces of the valve are easily specified.

Orifice Conditions

The nature of the boundary conditions at the valve orifice vary depending on whether the flow of gas is into or out of the engine. It

was discovered that because of the effects of heat transfer between the gas and the walls, the effects of pressure changes caused by combustion and piston motion, along with other factors, the direction of gas flow did not always correspond with the direction of piston motion. Obviously, the driving function is the difference between the ambient air pressure and the value of the pressure at valve orifice.

If $P_{atm} > P_{orifice}$, the orifice boundary conditions are specified as follows [69]:

$$u = \sqrt{\frac{2 C_D}{\rho} |P_{atm} - P|}, \quad (5-4)$$

$$k = (.03 u)^2, \quad (5-5)$$

$$\epsilon = \frac{k^{3/2}}{.0075 r_{valve}}, \quad (5-6)$$

$$m_f = 0, \quad (5-7)$$

$$f = 0, \quad (5-8)$$

and

$$T = T_{atm} (298. K), \quad (5-9)$$

where

$$C_D = .7.$$

If $P_{atm} < P_{orifice}$ the orifice boundary conditions instead are:

$$u = - \sqrt{\frac{2 C_D}{\rho} |P_{atm} - P|}, \quad (5-10)$$

$$\frac{\partial k}{\partial z} = 0, \quad (5-11)$$

$$\frac{\partial \epsilon}{\partial z} = 0 , \quad (5-12)$$

$$\frac{\partial m_f}{\partial z} = 0 , \quad (5-13)$$

$$\frac{\partial f}{\partial z} = 0 \quad (5-14)$$

and

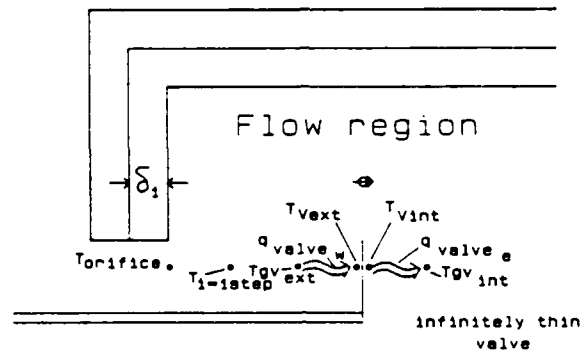
$$\frac{\partial T}{\partial z} = 0 . \quad (5-15)$$

Valve Surface Boundary Conditions

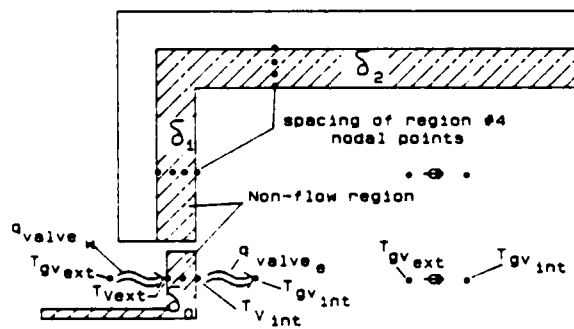
When the valve is closed it is acting in the same geometric capacity as the cylinder head, and with the exception of the energy equation the boundary conditions are those given in section 2.5 for u , v , k , ϵ , m_f and f for the cylinder head. See equations (2-24, 25, 26, 40, 41, 42, 43, 68, 69, 70 and 71).

When the valve is open, for the purpose of fluid flow, it is considered to be an infinitely thin surface. Boundary conditions for v , k , ϵ , m_f and f on each side of this surface are specified in a manner identical to that used in section 2.5 for both sides of the valve. On the interior side of the valve they are specified precisely as for the case when the valve is closed with the exception that the distance x_{wg} (see ∂y_{w+g} in Figure 2-2) is now determined from the new valve surface position to the interior adjacent nodal point. See Figure 5-2.

Obviously the near wall values (ϕ_{gw} , ρ_{gw} , x_w^+ , $J_{w_w}(\phi)$) used in determining these correspond to the properties of the gas at the nodal points immediately adjacent to the interior side of the valve. For the



a. Open valve from viewpoint of flow field energy equation.



b. Open valve from viewpoint of non-flow energy equation.

Figure 5-2 Open valve from viewpoints of both flow and non-flow energy equations

exterior side of the valve (top of valve), the specification of the boundary conditions for these five parameters is identical to the boundary conditions given in section 2.5 for the piston surface with the understanding that the distance x_{eg} and the near wall property values (ϕ_{ge} , ρ_{ge} , x_e^+ , $J_{we}(\phi)$) be properly determined. In other words, that their specification be based on the fluid properties of the gas at the outboard nodal points immediately adjacent to the external side of the valve, and the distance between these nodal points and the external valve surface.

When the valve is functioning the u-momentum equation boundary condition for the valve is specified as follows:

$$u_{valve} = u_{valve}(t), \quad (5-16)$$

where

$u_{valve}(t)$ = the velocity of the valve at time t as specified by the velocity profile for the valve given in Table 5-1.

Though the energy equation boundary conditions for the interior and exterior sides of the valve are also similar to those used for the cylinder head and piston respectively, they differ in the manner in which they are inserted. From the view point of the flow field, for all governing equations, including the energy equation, the valve is assumed to be infinitely thin, but is considered to have thickness for the purpose of solving the heat conduction equations within the valve. See figure 5-2. The procedure for accomplishing this involves solving the heat conduction equations for the valve for a set of special nodal

points located at an imaginary position outside of the flow field. This is done in an iterative manner with the energy equation for the flow field. For convenience, the geometric position of the nodal points used to solve the conduction equations when the valve is in the flow field (ie., is open) are the same points used as for when the valve is closed. In other words, whether the valve is open or closed, its nodal points are considered to be an extension of the cylinder head portion of region 4. The thickness of the valve is assumed to be δ_0 from the viewpoint of the non-flow energy-equation nodal points used to solve heat flow in the valve (see figure 5-2b). In the flow field, though the valve is assumed infinitely thin, it is assumed to have different temperatures on each side of its surface ($T_{v_{int}}$ and $T_{v_{ext}}$). The key to accomplishing the simultaneous solution of the flow and non-flow equations is the cyclic juggling (during each iteration) of the orifice temperature ($T_{orifice}$) and the temperature one nodal point to right of the orifice ($T_{i=istep}$) with the interior surface temperature of the valve ($T_{v_{int}}$) and the temperature of the gas at the nodal point immediately adjacent to the interior valve surface ($T_{gv_{int}}$) respectively. Thus, when the flow field equations are being solved, $T_{orifice}$ and $T_{i=istep}$ are located as shown in figure 5-2a. Later in the iteration, when the non-flow equations are being solved, the temperature values at the nodal points corresponding to $T_{orifice}$ is now $T_{v_{int}}$ and that corresponding to $T_{i=istep}$ is now $T_{gv_{int}}$. Obviously, the spacings, and other properties between and at these nodal points must also be properly represented at the appropriate times within each iteration. Rather than re-specify these spacings and properties in the same cyclic manner as with the temperatures it was found convenient to determine and keep track of the total heat flux

terms for flow of heat from both sides of the valve to the flow field gas ($\dot{q}''_{\text{valve}_w}$ and $\dot{q}''_{\text{valve}_e}$). See figure 5.2. These heat flux terms are used in both the solution of the flow and non-flow equations and are updated once during each iteration. Following the development and nomenclature pattern outlined in section 2.5, these total flux terms are specified below and serve as the boundary conditions for the east and west surface of the valves for both the flow and non-flow regions when the valve is open.

If $x_{\text{valve}_e}^+ < 11.63$:

$$\dot{q}''_{\text{valve}_e} = \frac{-\mu_1}{r_{\text{egv}} Pr_1} (T_{\text{gvint}} - T_{\text{vint}}). \quad (5-17)$$

If $x_{\text{valve}_e}^+ > 11.63$:

$$\dot{q}''_{\text{valve}_e} = \frac{-\rho_{\text{gev}} C_{p\text{gev}} C_{\mu}^{1/4} k_{\text{gev}}^{1/2} (T_{\text{gvint}} - T_{\text{vint}})}{\frac{Pr_t}{K} \log_e (E x_{\text{valve}_e}^+ + Pr_t (P + \frac{Pr_e}{Pr_t}))}. \quad (5-18)$$

If $x_{\text{valve}_w}^+ < 11.63$:

$$\dot{q}''_{\text{valve}_w} = \frac{-\mu_1}{r_{\text{wgV}} Pr_1} (T_{\text{gvext}} - T_{\text{vext}}). \quad (5-19)$$

If $x_{\text{valve}_w}^+ > 11.63$:

$$\dot{q}''_{\text{valve}_w} = \frac{-\rho_{\text{gwV}} C_{p\text{gwV}} C_{\mu}^{1/4} k_{\text{gwV}}^{1/2} (T_{\text{gvext}} - T_{\text{vext}})}{\frac{Pr_t}{K} \log_e (E x_{\text{valve}_w}^+ + Pr_t (P + \frac{Pr_1}{Pr_t}))}. \quad (5-20)$$

The boundary condition for the equation along the side (north border) of the valve is as follows when the valve is open:

$$\left(\frac{\partial T}{\partial r}\right)_{r=\text{valve radius}} = 0 . \quad (5-21)$$

This corresponds to the assumption that the end surface of the valve is adiabatic. This assumption made it possible to match boundary conditions for both the flow region solution when the valve is infinitely thin and the non-flow solution region - where the valve has thickness. Also, this assumption alleviated the paradox of how there can be measurable heat flux through an area which is both zero and finite at the same time.

In the event the valve is closed and thus is seated into the cylinder head the adiabatic assumption is dropped and the boundary condition for the side of the valve becomes that given by equation (2-65). The valve exterior surface boundary condition in this case is identical to that given by equation (5-19) with the value of $T_{gv\text{ext}}$ used in these expressions set equal to atmospheric temperature.

5.3 Effects of Fluid Entrainment Due to Valve Motion on Time Dependent Properties

In the formulation of a finite difference scheme to accommodate valve motion through a set of fixed nodal points, it was noted that, extreme care was necessary in the calculating of the values of the primitive variables on either side of the valve in the current time step using the geometrically corresponding values of these properties at the previous time step. As the infinitely thin valve moves in one direction, the values of v , P , T , k , ϵ , m_f , and f along with density located immediately ahead of the valve "pass through" the valve and are used as

the old time values in the calculation of these variables on the other side of the valve in the next time step. To alleviate this very unrealistic situation, the assumption was made that the fluid property values in the boundary layers on both sides of the valve are entrained between time steps and are available for use in the next time step at the next geometric nodal point in the direction of valve motion. To make this realistic the valve motion and the nodal point spacing in the vicinity of the valve had to be closely coordinated. To simplify computation, the valve was only actually relocated every other time step as shown in Table 5-1, but is considered to have a velocity roughly corresponding to its rate of motion over each two time steps. For the time step in which the valve is actually moved geometrically, the mathematical representation of the specification of the old time values for use in the current time step are as follow:

For an opening valve along both sides of the valve surface -

$$\phi_{old}(i,j,n) = \phi(i-1, j, n-1) , \quad (5-22)$$

where

i = indicy used to locate the position of the nodal point

in the z direction,

$i-1$ = indicy of next nodal point in the solution scheme

immediately to the west of a nodal point at i ,

j = indicy used to locate the position of the nodal point

in the r direction,

n = time index, indicating the current time step,

$n-1$ = previous time step,

and

ϕ - understood here to represent either, v , P , T , k , ϵ , m_f
and ρ .

Similarly, for a closing valve the old time values along both sides of the valve surface are given by:

$$\phi_{old}(i,j,n) = \phi(i+1, j, n-1).$$

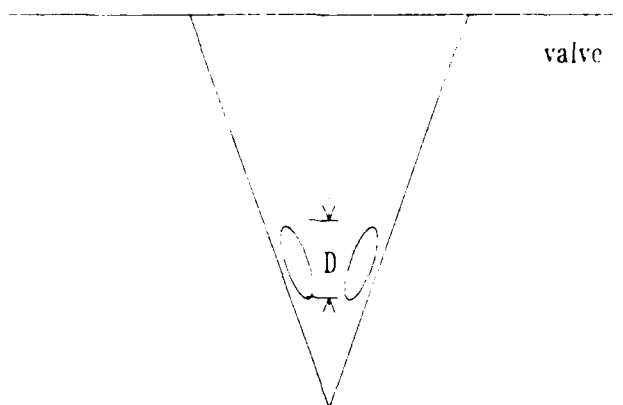
TABLE 5-1 Valve velocity profile

Crank Case Angle (θ)	Valve Position (z_v) (m)	Valve velocity (u_{valve}) (m/s)
0°	.00469	0
6°	.00586	1.17
12°	.00586	1.97
18°	.00686	1.97
24°	.00686	1.17
30° - 114°	.00793	.0
120°	.00686	0.907
126°	.00686	1.307
132°	.00586	1.507
138°	.00586	1.707
144°	.00469	2.107
150°	.00469	2.107
156°	.00335	1.707
162°	.00335	1.507
168°	.00185	1.307
174°	.00185	0.907
180° - 540°	.0	.0
546°	.00185	0.907
552°	.00185	1.307
558°	.00335	1.507
564°	.00335	1.707
570°	.00469	2.107
576°	.00469	2.107
582°	.00586	1.707
588°	.00586	1.507
594°	.00686	1.307
600°	.00686	0.907
606° - 690°	.00793	.0
696°	.00686	-1.17
702°	.00686	-1.97
708°	.00586	-1.97
714°	.00586	-1.17
720°	.00469	.0

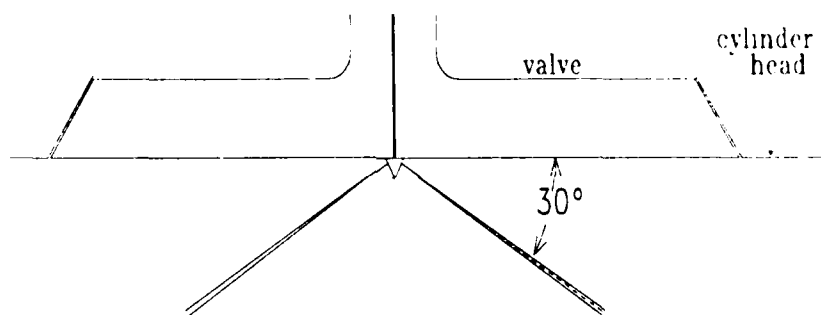
Chapter 6
FUEL NOZZLE MODEL

In hypergolic combustion, fuel is brought into the engine in gaseous form under extremely high pressures. To date, in research conducted with this method of combustion, the same type of orifice openings have been used to inject the fuel as are common in diesel engine construction [1,18]. See figure 6-1. At the exit of the orifice in our case the flow is assumed to be choked flow. This is due to the large pressure drop between just inside the fuel injector and the combustion chamber. Thus the fuel is entering at a Mach number equal to 1.0, which presented numerous problems in the modeling of the nozzle. Rather than attempt to model the actual geometric characteristics of the fuel injector, the object of this analysis instead was to obtain a model which gave a reasonable representation of the fuel injection process.

The fuel injector shown in figure 6-1(a) is made up of 4 orifice holes, each with a diameter (D) equal to .0105 inches. The flow coming out of these orifices is such that after a short period of travel, the streams from each orifice begin to join and form the shape of a cone in the manner shown in figure 6-1(b). To accommodate an axisymmetric analysis, it is reasonable to assume that after a short distance of travel, the fuel flow is uniform at a given radius (i.e., invariant in θ at a given radius where z, r, θ make up the 3-D coordinates). Because of this, it was decided to model the injector as an axisymmetric convergent nozzle in a manner shown in Figure 6-2. This was in consonance with the recommendations of experimental researchers in the field [81]. The dimensions of this nozzle are proportional to the size of the orifices of the injector given in figure 6-1(b) in accordance with the following relationship:

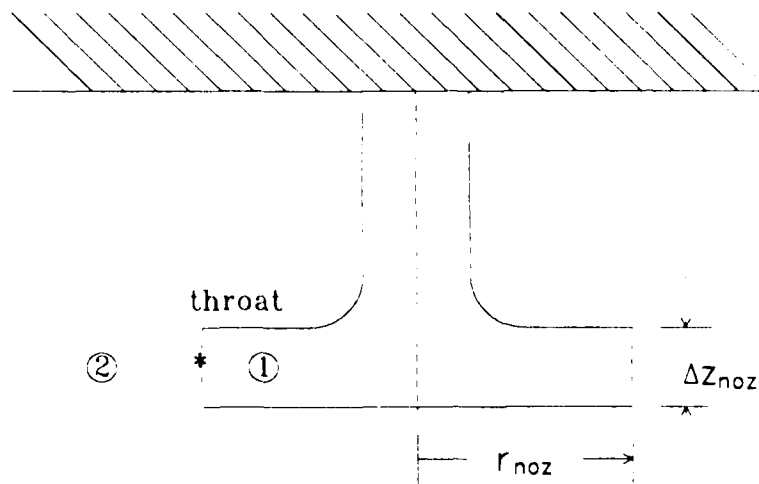


(a.) Fuel Injector showing orifice openings

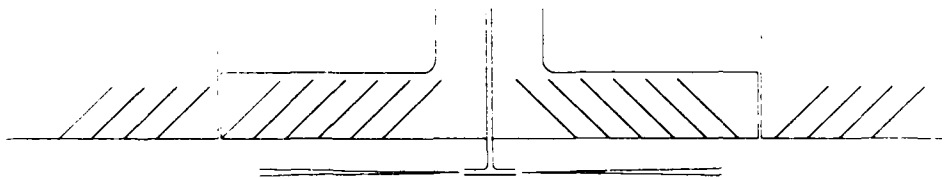


(b.) Fuel Injector with fuel spray path
(ideal path for case of no piston
or valve motion.)

Figure 6-1. Diesel Fuel Injector.



(a.) Fuel injector model



(b.) Nozzle fuel injector with fuel spray path (ideal path for case of no prior internal flow field).

Figure 6-2. Nozzle Fuel Injector Model.

$$\left(\begin{array}{c} \text{flow cross} \\ \text{sectional area} \\ \text{of 4 orifices} \end{array} \right) = 4 \left[\pi \left(\frac{D}{2} \right)^2 \right] = 2 \pi r_{noz} \Delta z_{noz} = \left(\begin{array}{c} \text{flow cross} \\ \text{sectional area of} \\ \text{nozzle assembly} \end{array} \right)$$

Thus,

$$r_{noz} \Delta z_{noz} = \frac{D^2}{2} . \quad (6-1)$$

To be compatible with experimental work, the stagnation values of the temperature and pressure of the fuel entering the injector were set at 2000 psi and 1000°F respectively. Also a compression ratio of 7 to 1 was used.

The flow in the nozzle is assumed isentropic. This assumption makes possible the specification of the pressure at the throat of the nozzle (see figure 6-2(a)) [89].

$$p^* = P_1 \left[\frac{2}{\gamma + 1} \right]^{\frac{\gamma}{\gamma - 1}} , \quad (6-2)$$

where

$$\gamma = \left[\frac{C_p}{C_v} \right]_{T = 1000^\circ F} \\ \approx 1.0147.$$

Also, for this case, the throat boundary condition values for T , ρ , and V can be specified from the following expressions [89]:

$$T^* = T_1 \left[\frac{2}{\gamma + 1} \right] , \quad (6-3)$$

$$\rho^* = \rho_1 \left[\frac{2}{\gamma + 1} \right]^{\frac{1}{\gamma - 1}} , \quad (6-4)$$

and

$$v^* = \sqrt{\gamma R_{fuel} T^*} , \quad (6-5)$$

Also, m_f , f , k and ϵ can be specified as:

$$m_f^* = 1.0, \quad (6-6)$$

$$f^* = 1.0, \quad (6-7)$$

$$k^* = 0.0, \quad (6-8)$$

and

$$\epsilon^* = 0.0. \quad (6-9)$$

The k^* and ϵ^* values above follow from the assumption of isentropic flow in the nozzle and thus no turbulence.

The viscosity of the fuel is estimated as [90]:

$$\mu_{fuel}^* = \mu_{laminar}(T^*, P^*) \approx 1.2 \times 10^{-5} \frac{N \cdot s}{m^2}.$$

The problems created by a) the geometric limitations of the nozzle (equation 6-1), b) the need to specify all the boundary conditions including the velocity at the throat location, c) the need to approximate the 30° spray nozzle, and d) the Mach 1 velocity boundary condition at the throat of the nozzle, were all eventually solved (after many unsuccessful modeling attempts) by the selection of the model shown in figure 6-3 subject to the explanation that follows. This arrangement enabled the values of v_{noz} and Δz_{noz} to be modeled realistically without having to be majorly concerned in regards to grid spacing in the z direction in the vicinity of the nozzle. The injector is located far enough into the flow field so as to be able to deposit the bulk of the fuel in approximately the same "location" as would be accomplished by a spray nozzle with a 30° injection angle positioned much closer to the top of the cylinder. For clarity, it should be noted that after the fuel has traveled a certain distance from the injector, fluid motion caused by piston action becomes the dominant factor in fuel dispersion from that "location" on. Thus, the

fuel injector model concerns itself primarily with the preliminary path of the fuel and in giving adequate specifications of all the primitive variables at and near the throat so that they can in turn be reasonably determined at the deposit location at the end of this preliminary path. Obviously a comparison of the computed flow field with experimental data, could be used to "tune" the values of r_{noz} , z_{noz} and Δz_{noz} , to make this model more compatible with the actual physics of the flow field. Since such data does not exist, this analysis is considered to be a reasonable first cut. The problem of co-specifying boundary conditions for v , along with k , ϵ , T , m_f , f and P all at and near the throat of the nozzle was overcome by varying the discretization of the basic transport equation at the control volume adjacent to the nozzle as explained in the paragraphs that follow. The problem with a velocity of Mach 1 was solved by modifying several of the \bar{S}_ϕ expressions to make them physically compatible with the unique flow conditions in the vicinity of the nozzle. This also will be explained further in later paragraphs in this chapter.

In the finite difference solution of the energy equation, information at nodal point (1) shown in figure 6-3 is not passed to nodal point (2), because the boundary condition of the control volume boundary corresponding to the nozzle throat (*) is known. (Obviously, due to physics of flow, we would not want to use point (1) in the solution of (2) anyway). These two nodal points are decoupled by setting the terms for the total flux between them (a_{S_ϕ} given in equation 4-2e) equal to zero. A correct property flux term which reflect the throat (*) total flux value is inserted into the solution of the governing equation at nodal point (2) through the use of the source terms Su_ϕ and Sp_ϕ [76]. Specific changes to the discretized equation contained in 4.1.2 for use in solution

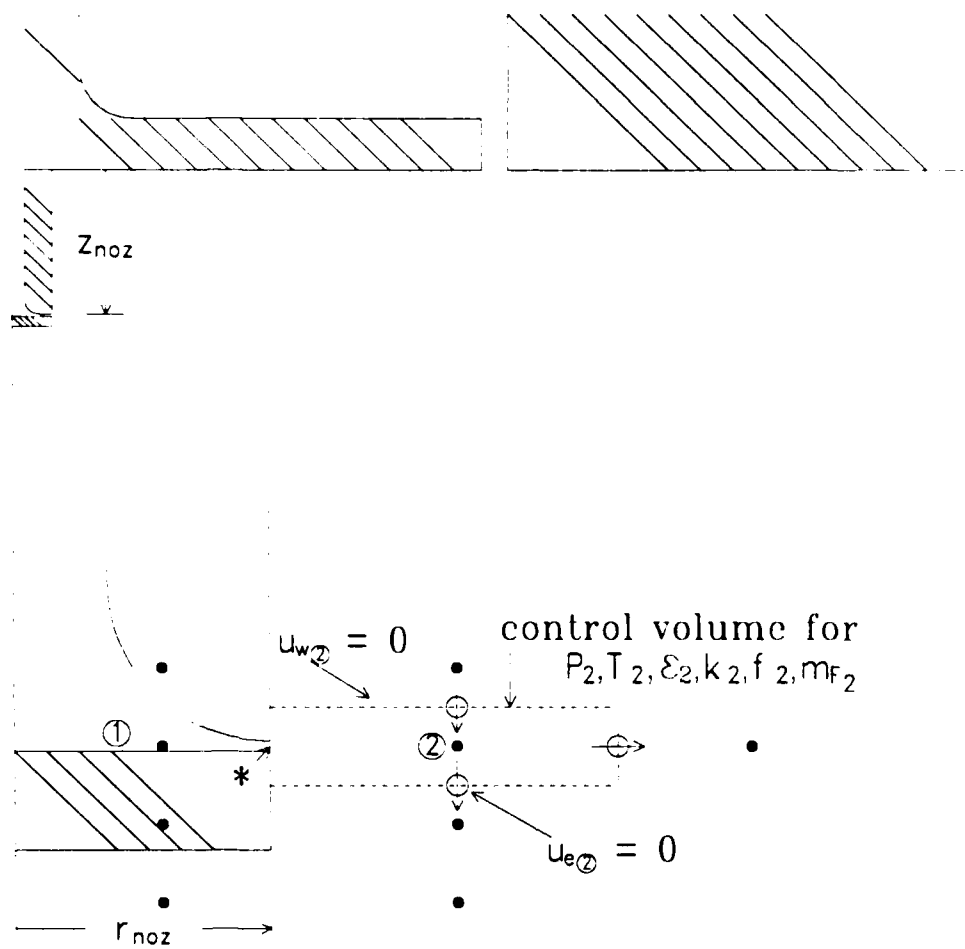


Figure 6-3. Detailed Description of Nozzle Fuel Injector Model.

of temperature at nodal point (2) are summarized in Table 6-1.

The values of u_w and u_e corresponding to nodal point (2) in figure 6-3 (also see figure 6-4) are set equal to zero. This is done for two reasons. First of all, it is necessary to set both values equal to zero in order to ensure that the spray exiting the nozzle is actually perpendicular to the nozzle assembly as desired. Secondly, a flow pattern similar to that which results from the vena contracta effect [76] is assumed for flow between the throat and point (2). For such a flow, there is assumed to be no flow across the outer border of the "modified" vena contracta boundary (see figure 6-4), and a constant mass flow rate (\dot{m}) within its borders. Though this effect does not actually dictate u_w and u_e are both zero, it dictates that the normal velocity on the borders of the vena contracta must be zero. Specifying u_e and u_w velocities for nodal point (2) to be zero not only approximates this, but also ensures that the mass flow rate from the throat (*) to point (2) within the modified vena contracta are equal. Additionally, it ensures that \dot{m}_{sv_3} (the mass rate of flow through the southern boundary of the control volume) for the solution of v_3 (control volume shown in small dashed lines in figure 6-4) is the same as the mass flow rate of fuel at the throat (*). Note, that due to equal spacing, this area ($A_{sv(3)}$) passes through point (2). This arrangement enables us to modify the discretization for the v-momentum equation in the control volume for $v(3)$ in a manner identical to the modification made to the energy equation at point (2). This arrangement also enables us to specify the values of m_f and f at point (2), namely -

$$m_f(2) = 1.0, \quad (6-10)$$

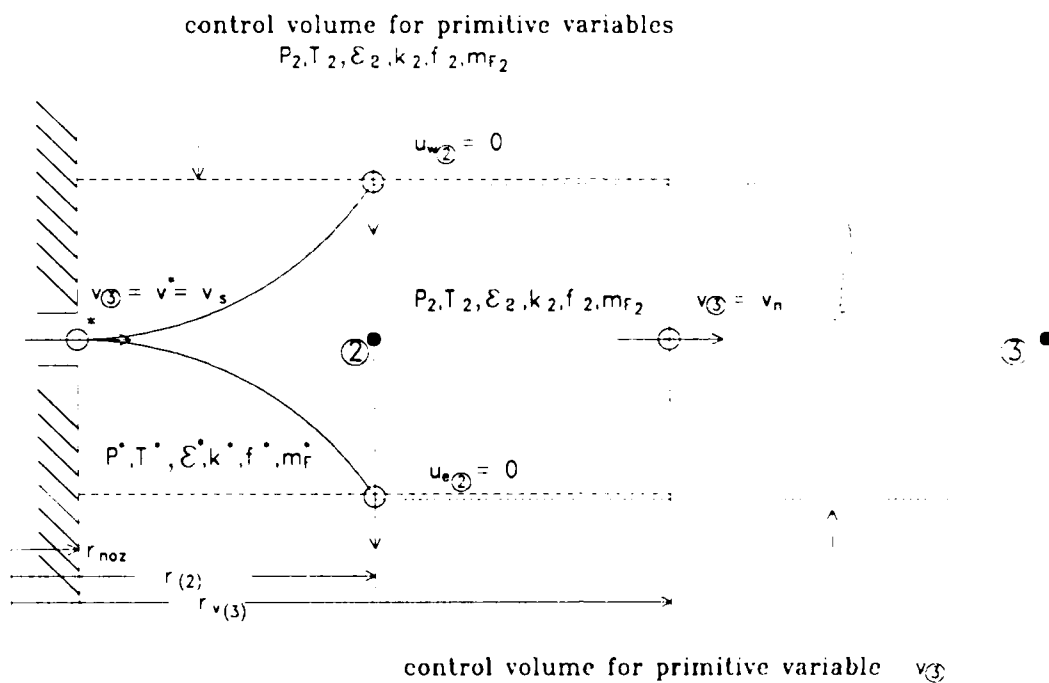


Figure 6-4. Blow-up of Control Volumes for Various Primitive Variables Adjacent to Fuel Nozzle.

and

$$f(2) = 1.0. \quad (6-11)$$

For the case of choked flow, which is assumed here, the expansion process which takes place as the fuel leaves the nozzle is not isentropic. Our k - ϵ equations are not adequate for the computation of k or ϵ in the vicinity of nodal point (2). It was determined best to assume the flow to have reached a reasonable percentage of its full turbulence value at point (2) and to specify appropriate values for k and ϵ at this point. Table 6-1 summarizes the specific changes made to the discretization of the equations used in the solution of the primitive variables at nodal point (2) and its vicinity.

As can be seen from this table, the values of Su_ϕ and Sp_ϕ are modified to incorporate these changes. The effects of compressibility are greater in the control volume adjacent to the nozzle. Thus, the values $Su_{p'}$ and $Sp_{p'}$ are modified as shown in Table 6-1 to give more accurate treatment along the northern area of the control volume of nodal point (2) in the equation scheme used to compute the local pressure correction (P'). The expressions given in Table 6-1 for P' follow from improving the specification of density at this border area to:

$$\rho_n = \rho_n^* + \rho_n', \quad (6-12)$$

where ρ^* is the guessed density and ρ' is a density correction. Note that ρ' can be expressed as:

$$\rho' = \frac{P'}{RT},$$

and thus -

$$\rho'_n = \frac{P_p + P_N}{R(T_p + T_n)} \quad (6-13)$$

Substitution of equation (6-12) and (6-13) into equation (4-54) results in the source term insertion shown in Table 6-1.

TABLE 6-1 Modification to Equation (4-2) and (4-54) for solution of various ρ 's and P ' at the nodal points adjacent to the throat opening of the fuel injector shown in Figure 6-4

ρ	$a_{S\rho}$	$c_{S\rho}$	$D_{S\rho}$	change to $S_{p\rho}$	change to $S_{u\rho}$	Additional Modifications
v	0.0	$(\rho A v)^*$	$\frac{\mu_2 A_{Sv(3)}}{r_v(3) - r(2)}$	$-(c_{Sv} + D_{Sv})$	$+(c_{Sv} + D_{Sv}) \frac{C_{Sv}}{A_{Sv(3)}} \rho p(2)$	1) $\nabla \cdot u = 0$ in vicinity of $v(3)$ 2) $\frac{\partial(\rho v)}{\partial t} = 0$ in $v(3)$ control volume
k	N/A	$(\rho A v)^*$	N/A	$= -10^{30}$	$= +10^{30} \left[\frac{.006 C_{Sk}}{A_{Sv(3)}} \rho p(2) \right]^2$	1) $\nabla \cdot u = 0$ in vicinity of $k(2)$ control volume
ϵ	N/A	N/A	N/A	$= -10^{30}$	$= +10^{30} \left(\frac{k(2)}{z_p} \right) \frac{3/2}{.0075 z_p}$	2) $\frac{\partial(\rho k)}{\partial t} = 0$ in $k(2)$ control volume 3) See note (3) below
T	0.0	$(\rho A v)^*$	$\frac{\mu^*_{fuel} A^*}{Pr_2(r(2) - r_{noz})}$	$-(c_{ST} + D_{ST})$	$+(c_{ST} + D_{ST}) T^*$	1) $\nabla \cdot u = 0$ in vicinity of $T(2)$ control volume 2) $\frac{\partial(\rho T)}{\partial t} = 0$ in $T(2)$ control volume 3) See note (3) below
P	0.0	$(\rho A v)^*$	N/A	$-\frac{.5 v_n}{R_n T_n} A_n$	$-\frac{.5 v_n}{R_n T_n} A_n P_n$	1) Add $\left(\frac{.5 v_s}{R_s T_s} A_s \right)$ to the S_{pg} for point (3) 2) Add $\left(\frac{.5 v_s}{R_s T_s} A_s P_s \right)$ to the S_{pg} for point (3)

(1) * - indicates throat value (2) $\mu_2 = \mu_{eff} - \mu_2 + \mu_{fuel}(2)$ (3) the values of ϵ and k directly to the east and west of point (2) are set equal to zero. Also the u values one and two nodal points to the east and west of point (2) are set at zero.

CHAPTER 7

ERROR ANALYSIS OF THE SOLUTION SCHEME

In the actual discretization of the complex transformed governing equations used in this analysis there is much chance for error. There is also the possibility that mistakes can be made in the programming of the solution code. Additionally, even if these first two evolutions are carried out flawlessly there is the question of just how accurately the discretized equations can be expected to solve the problem. The present chapter deals with these concerns by applying a novel and very powerful error analysis technique developed by Shih⁸².

The analysis was conducted in such a way that the accuracy of the governing equations could be tested both one at a time and in combination with any number of the other primitive variable equations for the non-combustion case. It was conducted for both the untransformed and transformed versions of the governing equations and represents the first known error analysis of this type to the power law discretization formulation of Patankar used herein. [76]

7.1. Error Analysis Technique

The discretization of the general transformed transport equation for the primitive variable ϕ is given by equation (4-2) in section 4.1.2. This represents an algebraic approximation of the actual governing equation for ϕ given in equation (2-17) and can be used to give a good approximation to the actual solution of (2-17). In real life, there is no analytic solution to equation (2-17) for any of its ϕ 's. However, suppose we specify that for the flow field equations in general -

$$\phi = \phi(x, r, t) \quad (7-1)$$

subject to Dirichlet boundary conditions for all primitive variables ϕ . Obviously $\phi(x, r, t)$ can not satisfy equation (4-2) or equation (2-17). But it can be made to solve the modified version of equation (4-2) given below:

$$(\overset{n}{a}p_{\phi} + \overset{o}{M}p_{\phi} - \overset{n}{S}p_{\phi}) \phi p_{\phi} = \sum_m \overset{n}{a}m_{\phi} \phi_m + \overset{o}{S}u_{\phi} + \overset{o}{M}p_{\phi} \phi p_{\phi} + C \cdot R_{anal_{\phi}} V_{\phi}, \quad (7-2)$$

where

$$C = \begin{cases} 1 & \text{when error analysis utilized} \\ & \text{in computer code subject to} \\ & \text{Dirichlet boundary conditions.} \\ 0 & \text{For solution of real problem} \\ & \text{subject to boundary conditions} \\ & \text{specified in Chapter 2.5.} \end{cases}$$

and

$R_{anal_{\phi}}$ = defined by the below development

First we define $\nabla\phi$ as follows:

$$\nabla\phi = \frac{1}{\delta_p} \frac{\partial}{\partial t} (\rho \delta_p \phi) + \frac{1}{\delta_p} \frac{\partial}{\partial x} [\rho \bar{u} \phi - \frac{\Gamma_{\phi}}{\delta_p} \frac{\partial \phi}{\partial x}] + \frac{1}{r} \frac{\partial}{\partial r} [r \rho v \phi - r \Gamma_{\phi} \frac{\partial \phi}{\partial r}]$$

Substitution of this expression into equation (2-17) reduced the transformed version of the general transport equation into the following compact expression:

$$\nabla\phi = \bar{S}_{\phi} \quad (7-3)$$

If we boldly substitute the analytic expression for ϕ , namely $\phi = \phi(x, r, t)$ into equation (7-3), we will obviously not obtain a solution,

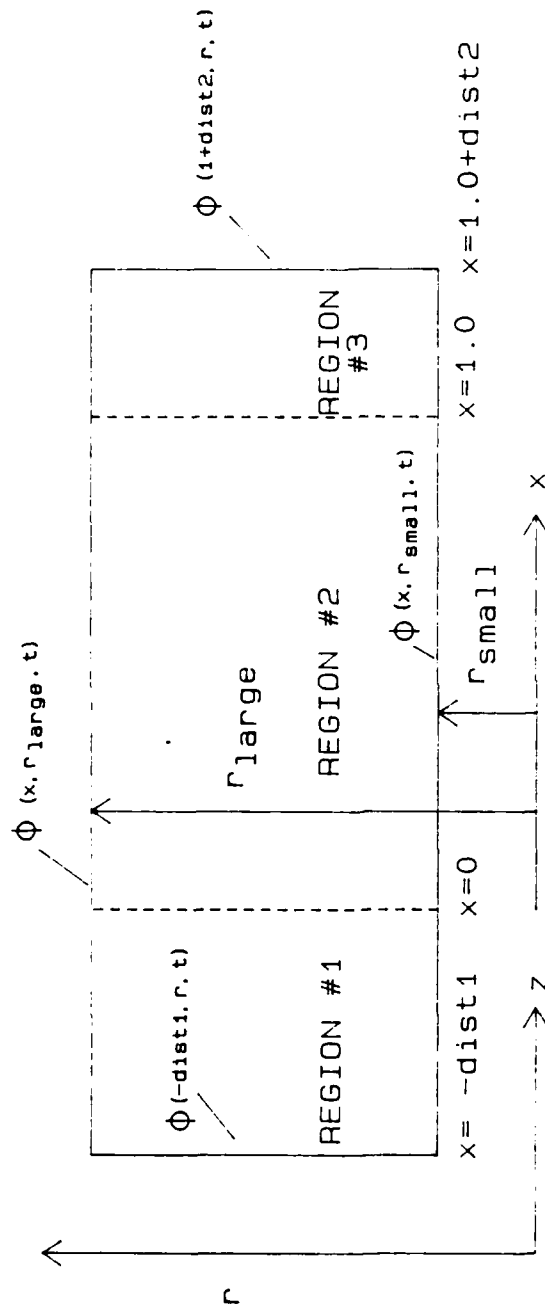


Figure 7-1 Boundary conditions used in error analysis

because (7-3) has no analytic solution. Proceeding anyway we find upon substitution that

$$\nabla\phi(x,r,t) = \bar{S}_\phi(x,r,t) + R_{anal}\phi, \quad (7-4)$$

where

$$R_{anal}\phi \equiv \nabla\phi(x,r,t) - \bar{S}_\phi(x,r,t).$$

Thus, $\phi(x,r,t)$ is the analytic solution of new equation (7-4).

Discretization of equation (7-4) using precisely the same technique as was employed in section 4.1.2 results in equation (7-2) with $C=1$. If we specify Dirichlet boundary conditions we can use equation (7-2) to numerically solve equation (7-4) and can then compare the results of the computation with the "known" (analytic) solution at each of the nodal points in the solution scheme. See figure 7-1 for a specification of these boundary conditions.

7.2 Formulation of Error Analysis Test

After, much trial and error and significant analytic analysis, it was elected to make the following specifications for ϕ for the non-combusting case:

$$u \equiv tx^2r, \quad (7-5)$$

$$v \equiv -2/3 txr^2, \quad (7-6)$$

$$k \equiv c_6 x \cdot r (x + r)t, \quad (7-7)$$

$$\epsilon \equiv c_6^2 x^2 r^2 t c_7, \quad (7-8)$$

and

$$T \equiv t x^2 r^2, \quad (7-9)$$

where

C_6 = arbitrary constant (value of .75 used)

and

C_7 = arbitrary constant (value of .8888 used).

The selection of $\rho = \frac{1}{R}$ was also made corresponding to incompressible flow. The value for R used was that of the gas constant for air. It should be noted that the selection of equation (7-5) in conjunction with equation (7-6) was necessary in order to satisfy the unsteady transformed continuity equation (equation 2-16). It was found that the above formulation coupled with the nature of the SIMPLE algorithm resulted in a decoupling of the primitive variable P from the solution scheme. The $\frac{\partial P}{\partial x}$ term in the u-momentum equation for example was retained as a negative expression in \bar{S}_{u_u} and as a positive expression in R_{anal_u} and was thus cancelled out.

The substitution of equations (7-5) through (7-9) into equation (7-3) resulted in the expressions for R_{anal_u} , R_{anal_v} , R_{anal_k} , R_{anal_ϵ} , and R_{anal_T} summarized in Table 7-1.

For comparison with R_{anal_ϕ} for various ϕ 's the expression R_{num_ϕ} was derived from equation (4-2) with the following result:

$$R_{num} = \frac{1}{V_\phi} \left[a p_\phi^n + M p_\phi^0 - S p_\phi \right] \phi p_\phi^n - \left(\sum_m a_{m\phi} \phi_m^n + S u_\phi + M p_\phi \phi p_\phi \right) \quad (7-10)$$

Results of the error test conducted on the solution code are discussed in Chapter 8.

TABLE 7-1 $*R_{anal\phi}$ for various ϕ 's.

ϕ	$\nabla\phi$	S_ϕ
u	$\frac{1}{R} (x^2 r + \frac{4}{3} t^2 x^3 r^2) - (a + b(x+r)^2)(2tr + t \frac{x^2}{r})$ $- b(x+r)(4xr + 2x^2)t$	$- \frac{\partial P}{\partial x} + 2b(x+r)(2xr - \frac{2}{3} r^2)t$ $- \frac{2}{3} \frac{C_6}{R} (2xr + r^2)t$
v	$\frac{1}{R} (-\frac{2}{3} xr^2 + \frac{2}{9} t^2 x^2 r^3) + (a + b(x+r)^2)(\frac{8}{3} tx)$ $+ b(x+r)(\frac{4}{3} r^2 + \frac{8}{3} xr)t$	$- \frac{\partial P}{\partial r} + (a + b(x+r)^2)(\frac{2}{3} tx) +$ $2b(x+r)(x^2 - \frac{4}{3} xr)t - \frac{2}{3} \frac{C_6}{R} (x^2 + 2xr)t$
k	$\frac{C_6}{R} (xr(x+r) + t^2 x^2 r^2 (\frac{4}{3} x - \frac{1}{3} r))$ $- (a_1 + b_1(x+r)^2)(4x + \frac{x^2}{r} + 2r) C_6 t$ $- 2b_1(x+r)(x^2 + 4xr + r^2) C_6 t$	$- \frac{C_D}{R} C_6^2 x^2 r^2 t C_7 + \bar{G}^{**}$ $**\bar{G} = 2(a + b(x+r)^2)(\frac{1}{2} x^4 + \frac{50}{9} x^2 r^2 + \frac{2}{3} r^2)t^2$
e	$[\frac{1}{R} (x^2 r^2 + \frac{2}{3} t^2 x^3 r^3)$ $- (a_2 + b_2(x+r)^2)(r^2 + 2x^2)2t$ $- 2b_2(x+r)(xr^2 + x^2 r)2t] C_6^2 C_7$	$\frac{C_6 x r C_7}{x+r} (C_1 \bar{G} - \frac{C_2}{R} C_6^2 x^2 r^2 t C_7)$
T	$\frac{1}{R} (x^2 r^2 + \frac{2}{3} t^2 x^3 r^3)$ $- \frac{1}{C_p} (a_3 + b_3(x+r)^2)(r^2 + 2x^2)2t$ $- \frac{2}{C_p} b_3(x+r)(xr^2 + x^2 r)2t$	$\frac{1}{C_p} [\frac{\partial P}{\partial t} + v \frac{dP}{dr} + \frac{u}{\delta p} \frac{\partial P}{\partial x} + \bar{G}]$

where

$$a = \frac{\mu \ell}{RC_7} t$$

$$a_1 = \frac{\mu \ell}{\sigma_k} \quad b_1 = \frac{C_\mu t}{RC_7 \sigma_k}$$

$$a_2 = \frac{\mu \ell}{\sigma_e} \quad b_2 = \frac{C_\mu t}{RC_7 \sigma_e}$$

$$a_3 = \frac{\mu \ell}{Pr \ell} \quad b_3 = \frac{C_\mu t}{RPr t C_7}$$

$$*R_{anal\phi} = \nabla\phi - \bar{S}_\phi$$

CHAPTER 8

DISCUSSION OF RESULTS

In its development, the solution code was configured to handle five specific engine cases: (1) the open orifice case, (2) the continuously closed valve case, (3) the open fixed valve case, (4) the fully operating valve case, and (5) the fully operating valve with combustion case. The present chapter will report on the results obtained from the code for cases (3) and (5) only along with results obtained from the application of the error analysis formulation of Chapter 7 to the code.

8.1 Error Analysis Results

Several series of error test runs were conducted during the development of the solution code as a means of checking for mistakes both in the discretization of the governing equations and in the actual programming of the code. The first set of tests was made on the code representation of the untransformed equations for u , v , k , ϵ and T . In these tests the spacing was uniform for both the z and r coordinate systems. Afterwards, the code representation of the transformed equations for these same five primitive variables was tested with non-uniform spacing in the z direction but with uniform spacing in the r direction. The error tests reported on in this section are for a series of runs made much later, in the weeks just prior to the final data runs for engine cases 3 and 5. The rationale for conducting this final round of tests was to ensure that no bugs had been inadvertently inserted into the program in the interim.

The geometric values used in the formulation of the boundary conditions for these runs (see figure 7-1) are as follows:

$$r_{\text{small}} = 1.0144 \text{ m},$$

$$r_{\text{large}} = 1.06424 \text{ m},$$

$$\text{dist1} = .04 \text{ m}$$

and

$$\text{dist2} = .0033333 \text{ m}.$$

Values used in the solutions of equations (B-1) and (B-2) for z_p and u_p respectively are as follows:

$$\ell = .01 \text{ m},$$

$$L = .06 \text{ m},$$

$$C = 1.0 \text{ m} \quad (\text{Clearance})$$

and

$$\text{RPM} = 1900.$$

The values of δ_p (obtained from z_p - see equation (2-12)) and u_p define the transformation [see equations (2-13) through (2-15)].

The time domain boundary conditions corresponding to the previous time step were specified for $\phi(x, r, t - \Delta t)$ using a time step of

$$\Delta t = \frac{1}{\text{RPM}}.$$

The value of time used in the analysis was

$$t = \frac{3000}{\text{RPM}} = 1.57895 \text{ sec}.$$

As mentioned in Chapter 7 the error analysis scheme was programmed in such a way as to facilitate the testing of the code representation of one primitive variable at a time, as well as any combination of primitive variables at a time. Obviously, those variables not being tested had to be specified analytically due to the fact that the governing equations are coupled.

In Appendix E, results of seven of these runs are listed. Tables E-1 through E-5 represent individual variable runs for the primitive variables u , v , k , ϵ and T respectively. Table E-6 represents a combined run for all five of these variables. For the runs depicted in Tables E-1 through E-6 the r spacing is uniform while the z spacing is non-uniform. The last run, given in Table E-7, was for the combination of primitive variables u , v and k . During this run, the spacing in both the r and z directions is non-uniform. As can be seen from data contained in these seven tables the comparison between the numerically computed values of the various ϕ 's with the actual (analytic) values is excellent for all five primitive variables both when they are computed individually and in combination.

8.2 Case 3 Results

A computation was conducted for a dense mesh of 23×29 for the up stroke of a two stroke engine with its valve in a fixed position (open orifice). The purpose of the computation was to compare the ability of the code to compute the u -component of velocity with the code of another researcher, Ramos⁶⁹ whose valve model is similar to the model used herein. Ramos' work for the case of a 2-stroke engine gave fair agreement with recent experimental data. The objective of the run was the comparison of the u -velocity profile along a specific z position ($z = .003350$ m) between the valve and the top of the cylinder.

The engine along with the valve model was configured in a manner identical to that used in reference [69]. The mesh size and nodal point spacing of the two computations were similar (22×30 mesh used in [69]). In Ramos' calculation, the engine was run through several

complete cycles until periodic solutions of the flow field variables were obtained. Then using the final values of the previous cycle as initial conditions, he made his data computations. His work utilized a UNIVAC 1100/40 and a CDC 6600, and required 35 and 10 minutes of CPU time respectively. The present computations were made on a VAX 11780 and required approximately two days of on line time to complete the computations for a single stroke for the 23 x 29 mesh size. Because, obtaining warm up conditions for this calculation was not possible, it was decided best to compare only the up stroke calculations for the u-velocity at the z location approximately halfway between the fixed valve and the top of the cylinder. The comparison was made at a crankshaft angle of 300°. Part of the rationale for this choice of comparison was the expectation that the valve would dominate the flow in this region and the lack of start-up conditions would have little effect on the computation of the u-velocity at this axial location.

The following are characteristics of the engine configuration used in this run:

$$a = .0381 \text{ m (semi-stroke length),}$$

$$L = .2032 \text{ m (connecting rod length),}$$

$$\text{valve radius} = .00785 \text{ m,}$$

$$\text{cylinder radius} = .03835 \text{ m,}$$

$$C = .0127 \text{ m (clearance),}$$

and

$$z_v = .00793 \text{ m (valve position).}$$

Additional values included:

$$\theta = 300^\circ \text{ (crank shaft angle),}$$

$$\text{RPM} = 31.25,$$

$$\Delta t = \frac{1}{\text{RPM}} = .032 \text{ sec.}$$

$$\text{dist1} = .0085 \text{ m}$$

and

$$\text{dist2} = .001 \text{ m.}$$

The run was started at $\theta = 180^\circ$ with the values u , v , k and ϵ set equal to zero. The air temperature was specified at 300 K throughout and the initial pressure set at atmospheric pressure. The wall temperature boundary conditions were set at 350 K for the cylinder head, cylinder side and piston surface.

There are only several real differences in the solution formulation of reference [69] and the present analysis. Ramos' code, based on the Teach-T code [78], used a hybrid central/upwind spacial differencing scheme in computing the total flux terms while as explained in Chapter 4, the present code uses a power law spacial differencing scheme [76]. The present work specifies the turbulent kinetic energy boundary conditions in a manner identical to Teach-T while Ramos assumed the flux of zero for this primitive variable between the wall and the near wall nodal points. Also, the present run used a fixed value for the specific heat throughout. In Appendix E, figure E-1 gives a vector plot of the velocities computed in the case 3 run. A recirculation zone is visible behind the valve. Figure E-2 shows a comparison of the u -velocity profiles for the $z = .003350$ positions of the two runs. For completeness, profile comparisons are given near the $z = .017037$ and at the $z = .026695$ positions also. As can be seen, there is excellent comparison for the two profiles at the $z = .003350$ position. The profiles at the other positions do not compare well, as expected. This is due to the fact that during the intake stroke, a strong recirculation zone is formed

below the valve. During the up-stroke, the effects of this zone are still present causing the irregular patterns shown for Ramos' profiles near the $z = .017037$ and at the $.026695$ positions. Because the present analysis assumed the velocities to be zero, throughout the flow field at the $\theta = 180^\circ$ position the effects of this recirculation are not present. Thus the profiles at these z locations are much flatter.

Figure E-3 shows the isotherms for this computation. As can be seen the temperature gradient near the walls are much greater.

8.3 Case 5 Results

Two computations (runs 1 and 2) were conducted for the compression stroke and fuel ignition portion of the strokes to test the nozzle model. One computation of the first 56° of the exhaust stroke (run 3) was conducted to test the valve model. The computational mesh for Run number 1 was 20×27 from the viewpoint of the energy equation (including both the blow and non-flow regions) and 17×21 from the viewpoint of the other flow field equations. The engine geometry used in this run is identical to that utilized in case 3 with the exception of the use of a valve radius of $.0086$ m and the use of an RPM of 1900. Note that the corresponding time step for this RPM was $.0005263$ seconds. The engine was started at a crank case angle of 180° corresponding to the beginning of the compression stroke. The values of u , v , k and ϵ were initialized at zero. The temperature and pressure specified throughout were standard atmospheric values. The temperature of the valve was set at 400 K throughout. Constant values of specific heat were used during the compression stroke, and then computed as per equation (3-10) during combustion. ks_1' was set at zero at the symmetry axis boundary nodal points (equation 4-18). Just as the piston reached TDC ($\theta = 360^\circ$), the fuel injector was instantly inserted into the engine

and sprayed in fuel in a gaseous state ($T = 805 \text{ K}$, $P = 821,000 \text{ N/m}^2$) for 5 time steps. During the compression stroke the mass fractions of the working substance were fixed at their atmospheric values, and the equations for f and m_f were not solved. At and after $\theta = 360^\circ$ these additional equations are utilized for the power stroke calculations.

Run 2 was identical to run 1 with several exceptions. The mesh size used was 17×20 and 20×26 for the flow field and extended energy equation solution realms. The value of $k_{S1'}$ was specified at the symmetry axis nodal points as per equation (4-18) during compression and set at zero during combustion. The values of specific heats were spatially computed during the entire run. The temperature boundary conditions used were as specified in figure (2-4). For run 1 the 7 nodal points corresponding to the upper left hand corner of the cylinder configuration given in figure (2-4) had values of 325° during much of the calculation instead of the values shown. Fuel was injected for 12 degrees (two time steps). The value of Pr_t for run 2 was set at 1.0 while for run 1 it was specified at 0.9. Also the valve radius was changed to 7.5 cm. For the exhaust stroke calculations (run 3), the dependent variables were initialized identically to run 2 and the same mesh spacing and engine dimensions were used. Piston motion was begun at $\theta = 534^\circ$ and continued for 10 time steps. The valve was operated as per equation (5-16). Results for these 3 runs are given in Appendix E. Values displayed in the Appendix are in SI units.

Run 1 results are given in figures E-5,6,7,11,12,13 and 14. Prior to combustion the temperature of the flow field is essentially uniform as shown in figure E-4 and the flow is in the axial direction only (figure E-11). The duration of the fuel injection for this run was 30° of crankshaft angle movement. The iteration limit per time step was

specified as 650 which was sufficient for all but the time step corresponding to $\theta = 360^\circ$. Figure E-5 through E-7 show in succession, the growth and expansion of high temperature regions to the right and left of the path of the fuel spray for $\theta = 360, 372$ and 384 respectively. These figures are given in a modified x coordinate system in order to show the details of the profiles in the expanding and contracting portion of the solution scheme more clearly. The corresponding velocity vector plots for these values of θ are given in figure E-12 through 14. As can be seen in figure E-12, there is a fairly strong flow along the side of the cylinder in the direction of the piston even though the piston velocity is zero. Also, two recirculation zones are created above and below the path of the fuel spray.

Run 2 results are shown in figures E-4,8,9, 15, 16 and 18-25. For this run, the iteration limit per time step was increased and the source term convergence criteria was obtained for all values of θ . Though the value of \bar{P}' did not go below .01 for $\theta = 360^\circ$, it attained acceptably low levels. The additional iterations allowed, account for the difference in the isotherm plot for this run at $\theta = 360^\circ$ (figure E-8) and the isotherm plot for run 1 at the same crankshaft angle (figure E-5). In figure E-16 one can see that, even though the piston velocity is small, there is a relatively large velocity component at the side of the cylinder wall in the direction of the piston. This is due largely to the influence of the fuel stream as well as the fact that the off centeredness of the fuel injector in the flow field at $\theta = 360^\circ$ coupled with the upward momentum of the flow due to the piston motion of the compression stroke caused the flow to turn downward in the upper corner of the side wall at that time (see figure E-15). This high velocity value near the wall accounts in part for the high values of the

$\theta = 366^\circ$ as shown in figures E-21 and E-23 respectively. In figure E-20 an isobar plot of the specific heats for the flow field at $\theta = 366^\circ$ is given. As shown, the highest values are located in the vicinity of high fuel mass fractions (see figure E-19) and higher flow field temperatures. The mass fractions of the products at $\theta = 366^\circ$ shown in figure E-18 are high in the vicinity of the recirculation areas depicted in figure E-16 and conform also to the high temperature regions shown in figure E-9. The maximum values of both turbulent kinetic energy and turbulent energy dissipation rate for $\theta = 366^\circ$ are located in the vicinity of the fuel injector as expected (see figures E-21 and E-23). This is due primarily to the high values specified at the nodal point adjacent to the injector orifice opening in the modeling of the fuel injector. Another factor accounting for the high values of turbulent kinetic energy at the side wall of the cylinder shown in figure E-21 may be the inadequacy of the wall boundary condition assumption made in Chapter 2 in the discretization of the k source term (see equation 2-38). Plots of pressure versus crankshaft angle and the rate of heat transfer between the surface of the piston and the engine gases per crankshaft angle are given in figures E-24 and E-25.

The results of run 3 are given in figures E-10 and 17. The influence of the valve on the temperature of the flow field is obvious in figure E-10. The velocity of the flow field is essentially axial between the piston and the area below the the valve (see figure E-17) and is dominated in the upper portion of the engine cylinder by valve motion and the valve orifice.

8.4 Concluding Remarks

The model described in Chapters 1 through 6 brings to a focus on a potentially significant engine configuration an assortment of recent

developments in the areas of fluid mechanics, combustion and heat transfer. The results outlined in sections 8.1 through 8.3 demonstrate the accuracy and utility of this model. It is now a viable tool for use in the study of low heat rejection engines. Though in its present configuration, it is designed specifically for the study of heat transfer in an engine with a weak heat barrier in the piston and using hypergolic combustion, it was developed in such a way as to facilitate its use in other engine configurations. Engines with geometries of greater complexity, with different combustion conditions, with barriers in other locations in the engine, etc. could be solved by it without major modifications. In the future the code may prove valuable for cross comparison purposes in the evaluation of other codes.

The code represents a compromise between accuracy and computational efficiency. In order to obtain more precise wall heat transfer calculations, a low Reynolds number model with a refined mesh (such as Jones and Launder's in [93]) is needed for the near wall calculations. Real engines are not axisymmetric and require three-dimensional calculations which include swirl to simulate them. Though hypergolic combustion shows promise in future engine applications, most engines use other combustion techniques which require more sophisticated combustion models to adequately simulate. Also, a more accurate specification of the specific heat, more sophisticated equations of state, higher order closure models for turbulence, etc. could be incorporated - all increasing the required computational time.

The code assumes the adequacy of the $k-\epsilon$ model in the rapid compression and expansion situations occurring in IC engines which is not the case. Turbulence in the engine flow field is not isotropic as the $k-\epsilon$

model assumes. Reference [94] points to the need for modifying the $k-\epsilon$ model under these circumstances and postulates such a modification. As conclusive improvements are made in the $k-\epsilon$ model for engine applications the code presented herein should be updated. Also, as alluded to in section 8.3, further study of the boundary conditions for k at the near wall nodal point is in order.

In its present state, the code should hopefully serve as a baseline for the analysis of the engine processes involved in internal regeneration and be of aid in the development of the heat barrier piston engine. It may also be of assistance in the evaluation and design of engines using hypergolic combustion.

Follow on research should be conducted to make the model usable in the study of stronger heat barriers. In such conditions, radiation becomes a significant factor and can not be neglected. Future work to extend such developments as Shih's two-dimensional radiative flux model [94,95] to the axisymmetric case is needed in order, to facilitate meaningful calculations for these conditions. However, before such modifications to the code are attempted, it should first be used to in the analysis of heat transfer in engines configured with weak piston barriers and using hypergolic combustion. As the code finds use in conjunction with experimental work, it should become possible to calibrate the code to give better results. At the same time, it is expected that the code will serve to help give direction to follow on experimental research in heat barrier piston engines and in other low heat rejection engine configurations. When used hand in hand with an experimental effort it anticipated that the code will serve to reduce time spent in analysis while helping to accelerate the rate of progress in these important areas of study.

APPENDIX A
ENERGY EQUATION

A general expression for the energy equation is given by [91]

$$\frac{D}{Dt} (\rho h) = \frac{D}{Dt} (P) + \frac{\partial Q}{\partial t} + \phi + \nabla \cdot \left(\frac{\mu}{\sigma} \nabla \cdot h \right) - \nabla \cdot q_r , \quad (A-1)$$

where

Q = internal heat generation,

q_r = radiation heat flux vector,

and

ϕ = viscous dissipation function.

For no radiation or internal heat generation this reduces to:

$$\frac{D}{Dt} (\rho h) = \frac{D}{Dt} (P) + \phi + \nabla \cdot \left(\frac{\mu}{\sigma} \nabla \cdot h \right) , \quad (A-2)$$

which Ramos modeled for turbulent flow [66,69] as -

$$\frac{D}{Dt} (\rho T) = \frac{1}{C_p} \left[\frac{D}{Dt} (P) + G \right] + \nabla \cdot \left(\frac{K_{eff}}{C_p} \nabla \cdot T \right) , \quad (A-3)$$

by assuming that

$$h = C_p(T) T.$$

In this formulation:

$$\frac{K_{eff}}{C_p} = \gamma_{eff}$$

Equation A-2 was used by Ramos⁶⁹ using a 22 x 30 mesh to give results with fair agreement to recent experimental data for two stroke calculations in a motored IC engine with a valve arrangement very similar to that used in the present analysis.

However, the present analysis is for a combustng engine, not a motored one. Most researchers at this point, shift to the use of an energy equation which is derived in terms of total enthalpy instead of temperature. However, because the ultimate objective of this analysis is a study of heat transfer, and for greater ease in keeping track of temperature throughout the solution process, it was decided best to develop an expression for the energy equation in terms of temperature. To facilitate this it was assumed that:

$$h = \bar{C}_p T + \sum_{i=1}^n m_i h_i^0,$$

where

$$\bar{C}_p = \sum_{i=1}^n m_i C_{p_i}(T),$$

m_i = mass fraction of species i ,

h_i^0 = heat of formulation of species i ,

$C_{p_i}(T)$ = the specific heat at constant pressure of species i at temperature T .

Substitution of h into equation A-2 yields:

$$\begin{aligned} \frac{D}{Dt} (\rho \bar{C}_p T) + \frac{D}{Dt} \left(\rho \sum_{i=1}^n m_i h_i^0 \right) = \frac{D}{Dt} (P) + \Phi + \nabla \cdot (K \nabla T) \\ + \nabla \cdot \left[\frac{u}{\sigma} \nabla \cdot \sum_{i=1}^n m_i h_i^0 \right]. \end{aligned} \quad (A-4)$$

Note that the equation for the conservation of an individual species is given by [92]

$$\frac{D}{Dt} (\rho m_i) = \nabla \cdot (\rho D \nabla m_i) + \rho \dot{m}_i, \quad (A-5)$$

where

\dot{m}_i = rate of formulation of species i per unit volume.

Note that we can multiply each expression in equation (A-5) by h_i^0 because the heat of formation for species i is a scalar constant. Summing the sets of resulting equations and solving for $\sum_{i=1}^n \dot{m}_i h_i^0$ we obtain

$$\rho \sum_{i=1}^n \dot{m}_i h_i^0 = \frac{D}{Dt} \left(\rho \sum_{i=1}^n m_i h_i^0 \right) - \nabla \cdot \left(\rho D \nabla \cdot \sum_{i=1}^n m_i h_i^0 \right).$$

With the Prandtl and Schmidt numbers equal to one (and thus a Lewis number of one), the above expression can be substituted into equation (A-4) with the following result:

$$\frac{D}{Dt} (\rho T) = \frac{1}{C_p} \left[\frac{D}{Dt} (P) + \Phi + \nabla \cdot (K \nabla \cdot T) - \rho \sum_{i=1}^n \dot{m}_i h_i^0 \right]. \quad (A-6)$$

It follows for the case of turbulent reacting flow that the above expression would take the form of equation (2-6) with

$$\dot{q}_c''' = -\rho \sum_{i=1}^n \dot{m}_i h_i^0$$

and

$$\dot{q}_r''' = 0$$

APPENDIX 8

PISTON DISPLACEMENT AND VELOCITY [65]

The equations for piston displacement z_p and piston velocity u_p are expressed below in terms of engine geometry.

$$z_p = C + \ell (1 - \cos(\omega t)) + L \left(1 - \sqrt{1 - \left(\frac{\ell}{L} \sin(\omega t) \right)^2} \right) \quad (B-1)$$

$$u_p = \omega \ell \left[\sin(\omega t) + \frac{\ell}{2} \frac{\sin(2\omega t)}{\sqrt{L^2 - (\ell \sin(\omega t))^2}} \right] \quad (B-2)$$

where

C = clearance (i.e., distance between TDC of the piston and top of cylinder). (value of 1.27 cm used)

$\omega = \text{RPM} \frac{\pi}{30}$ (angular velocity in radians per second)

ℓ = semi-stroke length (value of 3.81 cm used)

L = connecting rod length (value of 20.32 cm used)

RPM = revolutions per minute (value of 1900 used)

APPENDIX C

Non-Flow Region Temperature Transformation Technique

The relative geometric positions of the near wall nodal points for the energy equation in the flow region are invariant in relation to the adjacent cylinder-piston wall nodal points in regions 1 and along the piston surface of region 3. As can be seen from figure C-1, this is not the case for the nodal points in the vicinity of the wall along the side of the cylinder of regions 2 and 3 as well as in the area between the cylinder and the side of the piston. It is desirable to be able to continuously match boundary conditions between the flow and non-flow portions of these areas of the solution scheme even though they are moving in relation to one another. It was considered optimum to redefine the x positions of the temperature nodal points in this portion of region 4 for each new time step so that they always match the x positions of the corresponding flow field nodal points. If the nodal points in the portion of region 4 corresponding to an i indicy value greater than or equal to izstep are allowed to move in the x direction with piston motion, a means of accounting for the "old" values of temperature corresponding to the new nodal points of the new temperature control volumes is necessary.

Adequate for the present analysis is the simple linear technique given below for downward piston motion:

If $z(i) < zold(i+1)$ -

$$T_{pnew}^{old} = \frac{T_{pold}^{old} (z(i) - zold(i+1)) + T_{Eold}^{old} (zold(i) - z(i))}{zold(i) - zold(i+1)} \quad (C-1)$$

If $z(i) > zold(i+1)$ -

$$T_{pnew}^{old} = \frac{T_{Eold}^{old} (z(i) - zold(i+2)) + T_{Eold}^{old} (zold(i+1) - z(i))}{zold(i+1) - zold(i+2)} \quad (C-2)$$

where

T_{Eold}^{old} = the old temperature corresponding to the nodal point directly east of T_{Eold}^{old} .

Similarly for upward piston motion:

If $z(i) > zold(i-1)$ -

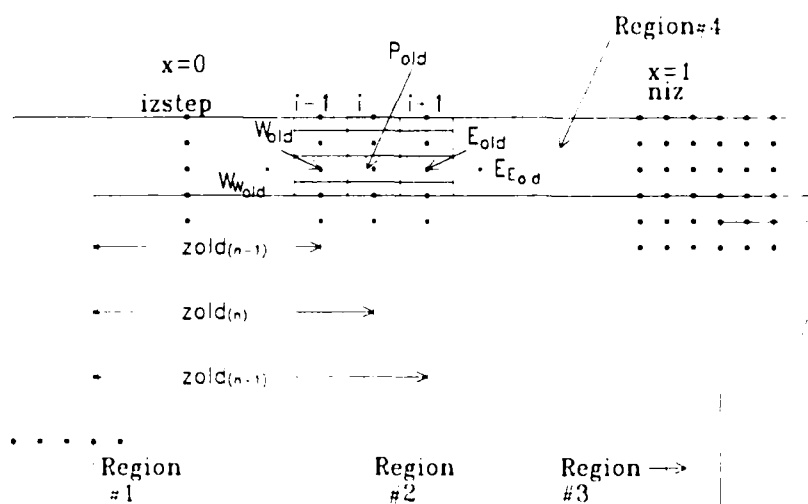
$$T_{pnew}^{old} = \frac{T_{pold}^{old} (z(i) - zold(i-1)) + T_{Wold}^{old} (zold(i) - z(i))}{zold(i) - zold(i-1)} \quad (C-3)$$

If $z(i) < zold(i-1)$ -

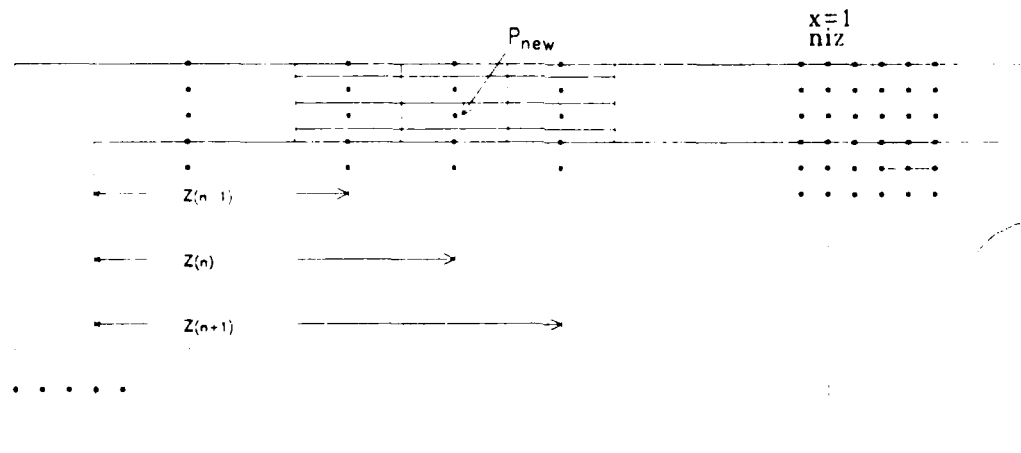
$$T_{pnew}^{old} = \frac{T_{Wold}^{old} (z(i) - zold(i-2)) + T_{Wold}^{old} (zold(i-1) - z(i))}{zold(i-1) - zold(i-2)} \quad (C-4)$$

where

T_{Wold}^{old} = the old temperature corresponding to the nodal point directly west of T_{Wold}^{old} .



a. Region 4 energy equation nodal points at time $= (n-1)/rpm$.



b. Region 4 Energy equation nodal points at time $= n/rpm$.

Figure C-1. Comparison of Region 4 nodal points at times $(n-1)/rpm$ and n/rpm

APPENDIX D

Solution Region Interface Code Modifications

As can be seen in Figure D-1, the east boundary of the control volume for each of the u-velocity nodal points corresponding to the indicy $i=izstep$ can be in either region 1 or region 2 depending on the piston position and can actually move back and forth between regions with piston motion. Similarly, the west boundaries of the u-velocity nodal points corresponding to $i=niz+1$ is also slaved to piston motion and can move back and forth from region 2 and region 3. For these two situations, the values for the expressions of $x \cdot u_p$ corresponding to the moving boundaries are specified as follows:

For the east boundary of a u-velocity nodal point control volume corresponding to $i=izstep$ -

$$x_{e_{i=izstep}} \cdot u_p = \frac{[.5(zu(izstep+1) + zu(izstep)) - z(istep)]}{\delta_p} u_p \quad (D-1)$$

For the west boundary of a u-velocity nodal point control volume corresponding to $i = niz + 1$ -

$$x_{w_{i=niz+1}} \cdot u_p = \frac{[.5(zu(niz+1) + zu(niz)) - z(istep)]}{\delta_p} u_p \quad (D-2)$$

Note that for the west boundary of the control volume of the u-velocity nodal point corresponding to the $i=izstep+1$, $x \cdot u_p$ is identical to that given for D-1. Also, for the east boundary of the control volume for the u-velocity nodal point for $i=niz$, D-2 applies. Obviously, these two boundaries also migrate between regions. Thus, for completeness the $x \cdot u_p$ values for these boundaries follow:

$$x_{w_{uj}=izstep+1} \cdot u_p = x_{e_{uj}=izstep} \cdot u_p \quad (D-3)$$

$$x_{e_{uj}=niz} \cdot u_p = x_{w_{uj}=niz+1} \cdot u_p \quad (D-4)$$

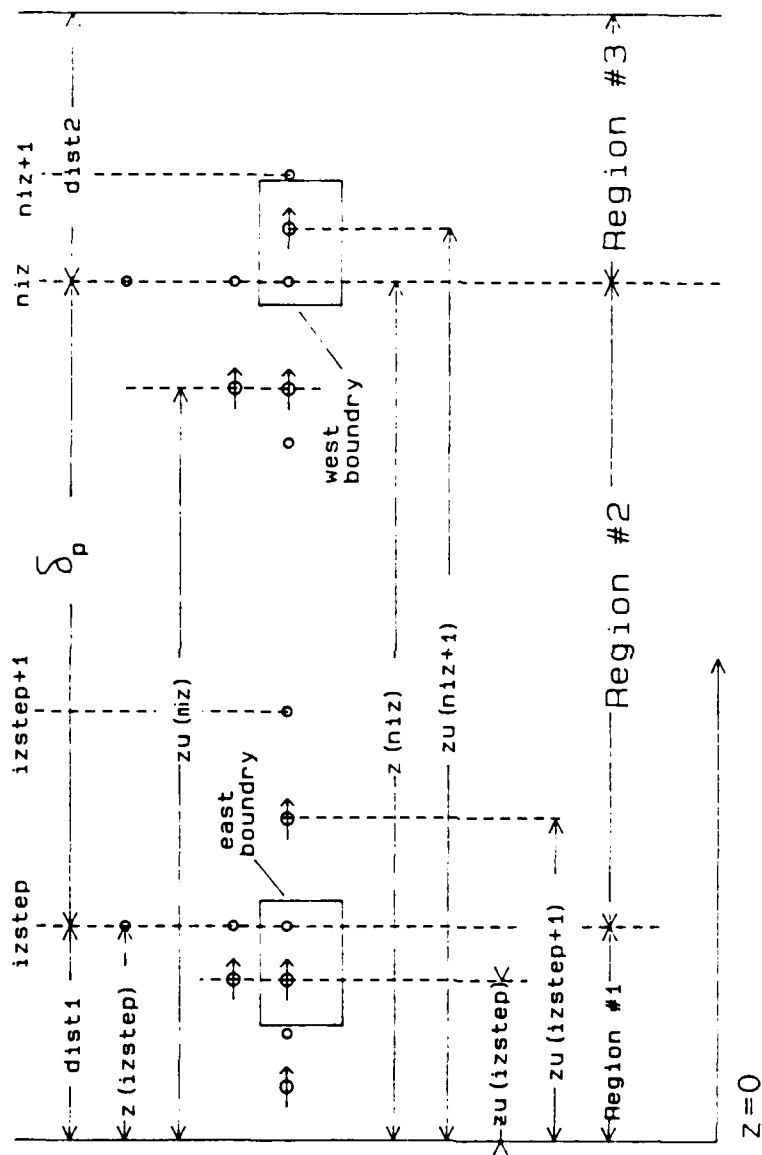


Figure D-1 Solution region interfaces

APPENDIX E

RESULTS

This Appendix contains the following Tables and Figures:

Table E-1	u-velocity equation error analysis
Table E-2	v-velocity equation error analysis
Table E-3	Turbulent kinetic energy equation error analysis
Table E-4	Turbulent kinetic energy dissipation rate equation error analysis
Table E-5	Flow energy equation error analysis
Table E-6	Error analysis for combined u, v, k, ϵ , T equations
Table E-7	Error analysis for combined u, v and k equations
Figure E-1	Case 3 velocity vector plot for a crank shaft angle
Figure E-1	Comparison of u-velocity profiles for case 3 run with an identical run performed by Ramos and Sirignano
Figure E-3	Case 3 temperature profile for a crank shaft angle of 300°
Figure E-4	Case 5 temperature profile for $\theta = 300^\circ$, run 1
Figure E-5	Case 5 temperature profile for $\theta = 360^\circ$, run 1
Figure E-6	Case 5 temperature profile for $\theta = 372^\circ$, run 1
Figure E-7	Case 5 temperature profile for $\theta = 384^\circ$, run 1
Figure E-8	Case 5 temperature profile for $\theta = 360^\circ$, run 2
Figure E-9	Case 5 temperature profile for $\theta = 366^\circ$, run 2
Figure E-10	Case 5 temperature profile for $\theta = 570^\circ$, run 3
Figure E-11	Case 5 velocity vector plot for $\theta = 300^\circ$, run 1
Figure E-12	Case 5 velocity vector plot for $\theta = 360^\circ$, run 1
Figure E-13	Case 5 velocity vector plot for $\theta = 372^\circ$, run 1

- Figure E-14 Case 5 velocity vector plot for $\theta = 384^\circ$, run 1
- Figure E-15 Case 5 velocity vector plot for $\theta = 360^\circ$, run 2
- Figure E-16 Case 5 velocity vector plot for $\theta = 366^\circ$, run 2
- Figure E-17 Case 5 velocity vector plot for $\theta = 570^\circ$, run 3
- Figure E-18 Case 5 product mass fraction distribution for $\theta = 372^\circ$
- Figure E-19 Case 5 specific heat values at $\theta = 366^\circ$, run 2
- Figure E-20 Case 5 fuel mass fraction distribution for $\theta = 366^\circ$, run 2
- Figure E-21 Case 5 turbulent kinetic energy distribution at $\theta = 366^\circ$, run 2
- Figure E-22 Case 5 turbulent kinetic energy dissipation rate distribution at $\theta = 366^\circ$, run 2
- Figure E-23 Case 5 effective viscosity (μ_{eff}) profile for $\theta = 366^\circ$, run 2
- Figure E-24 Case 5 pressure (P) versus crankshaft angle (θ), run 2
- Figure E-25 Case 5 piston surface heat transfer rate versus crankshaft angle (θ), run 2

TABLE E-1 u-velocity equation error analysis

u velocity time = 1.57895

i	j	num	anal	rnum	ranal
4	2	0.042979	0.042993	-0.001225	-0.001225
4	3	0.044346	0.044400	-0.001214	-0.001235
4	4	0.044732	0.044807	-0.001218	-0.001246
4	5	0.044199	0.044214	-0.001249	-0.001256
4	6	0.044636	0.044621	-0.001267	-0.001266
5	2	0.143667	0.143714	-0.002145	-0.002160
5	3	0.143449	0.143436	-0.002142	-0.002176
5	4	0.142311	0.142358	-0.002164	-0.002203
5	5	0.143633	0.143680	-0.002196	-0.002230
5	6	0.144354	0.144303	-0.002190	-0.002257
6	2	0.423889	0.424030	-0.003822	-0.003822
6	3	0.427900	0.428043	-0.003863	-0.003863
6	4	0.431911	0.432055	-0.003805	-0.003804
6	5	0.435923	0.436068	-0.003650	-0.003646
6	6	0.439936	0.440081	-0.003788	-0.003783
7	2	0.968029	0.968347	-0.005286	-0.005509
7	3	0.977187	0.977512	-0.005086	-0.005528
7	4	0.986347	0.986676	-0.005329	-0.005548
7	5	0.995508	0.995840	-0.005351	-0.005568
7	6	1.004673	1.005004	-0.005445	-0.005588
8	2	1.453868	1.454340	-0.005637	-0.006127
8	3	1.467612	1.468104	-0.005660	-0.006096
8	4	1.481372	1.481867	-0.005632	-0.006064
8	5	1.495132	1.495631	-0.006033	-0.006033
8	6	1.508896	1.509394	-0.006001	-0.006001

numerical values u velocity time = 1.57895

i =	3	4	5	6	7	8	9	y =
j								
7	1.07e-02	4.50e-02	1.46e-01	4.44e-01	1.01e+00	1.52e+00	1.68e+00	1.06e+00
6	1.36e-02	4.46e-02	1.45e-01	4.40e-01	1.00e+00	1.51e+00	1.66e+00	1.05e+00
5	1.05e-02	4.42e-02	1.44e-01	4.36e-01	9.96e-01	1.50e+00	1.65e+00	1.04e+00
4	1.34e-02	4.38e-02	1.42e-01	4.32e-01	9.86e-01	1.48e+00	1.63e+00	1.03e+00
3	1.03e-02	4.34e-02	1.41e-01	4.28e-01	9.77e-01	1.47e+00	1.62e+00	1.02e+00
2	1.33e-02	4.30e-02	1.40e-01	4.24e-01	9.68e-01	1.45e+00	1.60e+00	1.01e+00
1	1.02e-02	4.26e-02	1.38e-01	4.20e-01	9.59e-01	1.44e+00	1.59e+00	1.00e+00
0x =	-0.04000	0.05000	0.20000	0.45000	0.75000	0.95000	1.00333	
0z =	0.08000	0.16384	0.29535	0.51453	0.77755	0.95289	1.00006	

analytic values u velocity time = 1.57895

i =	3	4	5	6	7	8	9	y =
j								
7	1.07e-02	4.50e-02	1.46e-01	4.44e-01	1.01e+00	1.52e+00	1.68e+00	1.06e+00
6	1.06e-02	4.46e-02	1.45e-01	4.40e-01	1.01e+00	1.51e+00	1.66e+00	1.05e+00
5	1.05e-02	4.42e-02	1.44e-01	4.36e-01	9.96e-01	1.50e+00	1.65e+00	1.04e+00
4	1.04e-02	4.38e-02	1.42e-01	4.32e-01	9.87e-01	1.48e+00	1.63e+00	1.03e+00
3	1.03e-02	4.34e-02	1.41e-01	4.28e-01	9.78e-01	1.47e+00	1.62e+00	1.02e+00
2	1.03e-02	4.30e-02	1.40e-01	4.24e-01	9.68e-01	1.45e+00	1.60e+00	1.01e+00
1	1.02e-02	4.26e-02	1.38e-01	4.20e-01	9.59e-01	1.44e+00	1.59e+00	1.00e+00
0x =	-0.04000	0.05000	0.20000	0.45000	0.75000	0.95000	1.00333	
0z =	0.08000	0.16384	0.29535	0.51453	0.77755	0.95289	1.00006	

TABLE E-2 v-velocity equation error analysis

		v velocity		time= 1.57895	
i	j	v num	v anal	rnum	ranal
3	3	-0.13117	-0.13121	0.00301	0.00304
3	4	-0.13365	-0.13370	0.00306	0.00310
3	5	-0.13616	-0.13620	0.00312	0.00315
3	6	-0.13869	-0.13873	0.00321	0.00321
4	3	-0.22701	-0.22708	0.00456	0.00456
4	4	-0.23130	-0.23138	0.00459	0.00464
4	5	-0.23564	-0.23571	0.00467	0.00471
4	6	-0.24002	-0.24009	0.00475	0.00479
5	3	-0.41868	-0.41881	0.00813	0.00813
5	4	-0.42660	-0.42674	0.00814	0.00825
5	5	-0.43460	-0.43474	0.00803	0.00836
5	6	-0.44267	-0.44281	0.00839	0.00848
6	3	-0.70617	-0.70640	0.01480	0.01480
6	4	-0.71953	-0.71977	0.01499	0.01499
6	5	-0.73302	-0.73327	0.01481	0.01517
6	6	-0.74664	-0.74689	0.01536	0.01536
7	3	-0.99365	-0.99400	0.02304	0.02304
7	4	-1.01245	-1.01281	0.02331	0.02331
7	5	-1.03143	-1.03180	0.02305	0.02359
7	6	-1.05061	-1.05097	0.02366	0.02388
8	3	-1.08951	-1.08987	0.02587	0.02613
8	4	-1.11012	-1.11049	0.02644	0.02644
8	5	-1.13094	-1.13132	0.02676	0.02676
8	6	-1.15196	-1.15233	0.02687	0.02707

		numerical values v velocity		time= 1.57895						
i	j	2	3	4	5	6	7	8	9	y =
7	7	-7.50e-02	-1.43e-01	-2.47e-01	-4.55e-01	-7.68e-01	-1.08e+00	-1.18e+00	-1.19e+00	1.06e+00
6	6	-9.25e-02	-1.39e-01	-2.40e-01	-4.43e-01	-7.47e-01	-1.05e+00	-1.15e+00	-1.16e+00	1.05e+00
5	5	-9.08e-02	-1.36e-01	-2.36e-01	-4.35e-01	-7.33e-01	-1.03e+00	-1.13e+00	-1.14e+00	1.04e+00
4	4	-8.91e-02	-1.34e-01	-2.31e-01	-4.27e-01	-7.20e-01	-1.01e+00	-1.11e+00	-1.11e+00	1.03e+00
3	3	-8.75e-02	-1.31e-01	-2.27e-01	-4.19e-01	-7.06e-01	-9.94e-01	-1.09e+00	-1.09e+00	1.02e+00
2	2	-8.53e-02	-1.29e-01	-2.23e-01	-4.11e-01	-6.93e-01	-9.75e-01	-1.07e+00	-1.07e+00	1.01e+00
1	1	-8.50e-02	0. e+00	0. e+00	0. e+00	0. e+00	0. e+00	0. e+00	-1.06e+00	1.00e+00
0x =		-0.04000	0.	0.10000	0.30000	0.60000	0.90000	1.00000	1.00333	
0z =		0.08000	0.12000	0.20767	0.38302	0.64604	0.90906	0.99673	1.00006	

		analytic values v velocity		time= 1.57895						
i	j	2	3	4	5	6	7	8	9	y =
7	7	-7.50e-02	-1.43e-01	-2.47e-01	-4.55e-01	-7.68e-01	-1.08e+00	-1.18e+00	-1.19e+00	1.06e+00
6	6	-9.25e-02	-1.39e-01	-2.40e-01	-4.43e-01	-7.47e-01	-1.05e+00	-1.15e+00	-1.16e+00	1.05e+00
5	5	-9.08e-02	-1.36e-01	-2.36e-01	-4.35e-01	-7.33e-01	-1.03e+00	-1.13e+00	-1.14e+00	1.04e+00
4	4	-8.91e-02	-1.34e-01	-2.31e-01	-4.27e-01	-7.20e-01	-1.01e+00	-1.11e+00	-1.11e+00	1.03e+00
3	3	-8.75e-02	-1.31e-01	-2.27e-01	-4.19e-01	-7.06e-01	-9.94e-01	-1.09e+00	-1.09e+00	1.02e+00
2	2	-8.53e-02	-1.29e-01	-2.23e-01	-4.11e-01	-6.93e-01	-9.75e-01	-1.07e+00	-1.07e+00	1.01e+00
1	1	-8.50e-02	0. e+00	0. e+00	0. e+00	0. e+00	0. e+00	0. e+00	-1.06e+00	1.00e+00
0x =		-0.04000	0.	0.10000	0.30000	0.60000	0.90000	1.00000	1.00333	
0z =		0.08000	0.12000	0.20767	0.38302	0.64604	0.90906	0.99673	1.00006	

TABLE E-3 Turbulent kinetic energy equation error analysis

turbulence energy time= 1.57875

i	j	k num	k anal	rnum	ranal
3	2	0.163471	0.163526	-.008841	-.008841
3	3	0.166414	0.166470	-.009025	-.009062
3	4	0.169383	0.169441	-.009251	-.009287
3	5	0.172379	0.172438	-.009518	-.009519
3	6	0.175401	0.175461	-.009755	-.009755
4	2	0.304770	0.304871	-.011801	-.011847
4	3	0.310070	0.310173	-.012130	-.012133
4	4	0.315416	0.315522	-.012372	-.012413
4	5	0.320808	0.320915	-.012759	-.012713
4	6	0.326246	0.326354	-.012955	-.013015
5	2	0.642750	0.642962	-.021413	-.021521
5	3	0.653288	0.653506	-.021905	-.022016
5	4	0.663912	0.664133	-.022627	-.022517
5	5	0.674619	0.674844	-.023029	-.023029
5	6	0.685411	0.685639	-.023552	-.023552
6	2	1.288175	1.288603	-.048866	-.048866
6	3	1.307881	1.308319	-.049590	-.049959
6	4	1.327731	1.328176	-.051073	-.051073
6	5	1.347721	1.348173	-.052028	-.052209
6	6	1.367862	1.368312	-.053368	-.053368
7	2	2.099759	2.100449	-.099271	-.099829
7	3	2.130200	2.130909	-.102570	-.102016
7	4	2.160851	2.161569	-.103697	-.104245
7	5	2.191700	2.192426	-.105973	-.106516
7	6	2.222744	2.223482	-.109188	-.108830
8	2	2.407219	2.407999	-.124223	-.124223
8	3	2.441588	2.442390	-.126405	-.126919
8	4	2.476178	2.477000	-.129666	-.129666
8	5	2.510998	2.511827	-.132465	-.132465
8	6	2.546032	2.546872	-.135981	-.135316

numerical values turbulence energy time= 1.57895

i =	2	3	4	5	6	7	8	9	y =
7	1.15e-01	1.79e-01	3.32e-01	6.97e-01	1.39e+00	2.25e+00	2.58e+00	2.59e+00	1.06e+00
6	1.13e-01	1.75e-01	3.26e-01	6.85e-01	1.37e+00	2.22e+00	2.55e+00	2.56e+00	1.05e+00
5	1.11e-01	1.72e-01	3.21e-01	6.75e-01	1.35e+00	2.19e+00	2.51e+00	2.52e+00	1.04e+00
4	1.09e-01	1.69e-01	3.15e-01	6.64e-01	1.33e+00	2.16e+00	2.48e+00	2.49e+00	1.03e+00
3	1.07e-01	1.66e-01	3.10e-01	6.53e-01	1.31e+00	2.13e+00	2.44e+00	2.45e+00	1.02e+00
2	1.05e-01	1.63e-01	3.05e-01	6.43e-01	1.29e+00	2.10e+00	2.41e+00	2.42e+00	1.01e+00
1	1.03e-01	1.61e-01	3.00e-01	6.33e-01	1.27e+00	2.07e+00	2.37e+00	2.39e+00	1.00e+00
0y =	-.04000	0.	0.10000	0.30000	0.60000	0.90000	1.00000	1.00333	
0x =	0.08000	0.12000	0.20767	0.38302	0.64604	0.90906	0.99673	1.00006	

analytic values turbulence energy time= 1.57895

i =	2	3	4	5	6	7	8	9	y =
7	1.15e-01	1.79e-01	3.32e-01	6.97e-01	1.39e+00	2.25e+00	2.58e+00	2.59e+00	1.06e+00
6	1.13e-01	1.75e-01	3.26e-01	6.86e-01	1.37e+00	2.22e+00	2.55e+00	2.56e+00	1.05e+00
5	1.11e-01	1.72e-01	3.21e-01	6.75e-01	1.35e+00	2.19e+00	2.51e+00	2.52e+00	1.04e+00
4	1.09e-01	1.69e-01	3.16e-01	6.64e-01	1.33e+00	2.16e+00	2.48e+00	2.49e+00	1.03e+00
3	1.07e-01	1.66e-01	3.10e-01	6.54e-01	1.31e+00	2.13e+00	2.44e+00	2.45e+00	1.02e+00
2	1.05e-01	1.64e-01	3.05e-01	6.43e-01	1.29e+00	2.10e+00	2.41e+00	2.42e+00	1.01e+00
1	1.03e-01	1.61e-01	3.00e-01	6.33e-01	1.27e+00	2.07e+00	2.37e+00	2.39e+00	1.00e+00
0y =	-.04000	0.	0.10000	0.30000	0.60000	0.90000	1.00000	1.00333	
0x =	0.08000	0.12000	0.20767	0.38302	0.64604	0.90906	0.99673	1.00006	

TABLE E-4 Turbulent kinetic energy dissipation
rate equation error analysis

energy dissipation					time= 1.57895	
i	j	e num	e anal	rnum	ranal	
3	2	0.011693	0.011697	-.002516	-.002518	
3	3	0.011915	0.011919	-.002592	-.002589	
3	4	0.012140	0.012144	-.002662	-.002662	
3	5	0.012366	0.012371	-.002737	-.002737	
3	6	0.012595	0.012599	-.002810	-.002813	
4	2	0.035021	0.035033	-.003334	-.003334	
4	3	0.035687	0.035699	-.003434	-.003428	
4	4	0.046359	0.046371	-.003525	-.003525	
4	5	0.037037	0.037050	-.003618	-.003623	
4	6	0.037722	0.037735	-.003732	-.003725	
5	2	0.119126	0.119166	-.006478	-.006478	
5	3	0.121391	0.121433	-.006630	-.006657	
5	4	0.123678	0.123720	-.006813	-.006840	
5	5	0.125986	0.126029	-.007027	-.007027	
5	6	0.128315	0.128359	-.007219	-.007219	
6	2	0.338906	0.339023	-.017955	-.018048	
6	3	0.345350	0.345470	-.018625	-.018533	
6	4	0.351855	0.351978	-.019028	-.019028	
6	5	0.358421	0.358547	-.019535	-.019535	
6	6	0.365049	0.365176	-.020114	-.020054	
7	2	0.671031	0.671267	-.044494	-.044494	
7	3	0.683790	0.684033	-.045672	-.045672	
7	4	0.696670	0.696918	-.046875	-.046875	
7	5	0.709672	0.709924	-.048106	-.048106	
7	6	0.722794	0.723051	-.049184	-.049363	
8	2	0.806706	0.806990	-.058347	-.058347	
8	3	0.822044	0.822337	-.059884	-.059884	
8	4	0.837529	0.837829	-.061199	-.061454	
8	5	0.853159	0.853464	-.062932	-.063058	
8	6	0.868934	0.869244	-.064697	-.064697	

numerical values energy dissipation					time= 1.57895				
i =	2	3	4	5	6	7	8	9	y =
J									
7	5.70e-03	1.28e-02	3.84e-02	1.31e-01	3.72e-01	7.36e-01	8.85e-01	8.91e-01	1.06e+00
6	5.60e-03	1.26e-02	3.77e-02	1.28e-01	3.65e-01	7.23e-01	8.69e-01	8.75e-01	1.05e+00
5	5.50e-03	1.24e-02	3.70e-02	1.26e-01	3.58e-01	7.10e-01	8.53e-01	8.59e-01	1.04e+00
4	5.40e-03	1.21e-02	3.64e-02	1.24e-01	3.52e-01	6.97e-01	8.38e-01	8.43e-01	1.03e+00
3	5.30e-03	1.19e-02	3.57e-02	1.21e-01	3.45e-01	6.84e-01	8.22e-01	8.28e-01	1.02e+00
2	5.20e-03	1.17e-02	3.50e-02	1.19e-01	3.39e-01	6.71e-01	8.07e-01	8.12e-01	1.01e+00
1	5.10e-03	1.15e-02	3.44e-02	1.17e-01	3.33e-01	6.59e-01	7.92e-01	7.97e-01	1.00e+00
0x =	-0.04000	0.	0.10000	0.30000	0.60000	0.90000	1.00000	1.00333	
0z =	0.08000	0.12000	0.20767	0.38302	0.64604	0.90906	0.99673	1.00006	

analytic values energy dissipation					time= 1.57895				
i =	2	3	4	5	6	7	8	9	y =
J									
7	5.70e-03	1.28e-02	3.84e-02	1.31e-01	3.72e-01	7.36e-01	8.85e-01	8.91e-01	1.06e+00
6	5.60e-03	1.26e-02	3.77e-02	1.28e-01	3.65e-01	7.23e-01	8.69e-01	8.75e-01	1.05e+00
5	5.50e-03	1.24e-02	3.71e-02	1.26e-01	3.59e-01	7.10e-01	8.53e-01	8.59e-01	1.04e+00
4	5.40e-03	1.21e-02	3.64e-02	1.24e-01	3.52e-01	6.97e-01	8.38e-01	8.43e-01	1.03e+00
3	5.30e-03	1.19e-02	3.57e-02	1.21e-01	3.45e-01	6.84e-01	8.22e-01	8.28e-01	1.02e+00
2	5.20e-03	1.17e-02	3.50e-02	1.19e-01	3.39e-01	6.71e-01	8.07e-01	8.12e-01	1.01e+00
1	5.10e-03	1.15e-02	3.44e-02	1.17e-01	3.33e-01	6.59e-01	7.92e-01	7.97e-01	1.00e+00
0x =	-0.04000	0.	0.10000	0.30000	0.60000	0.90000	1.00000	1.00333	
0z =	0.08000	0.12000	0.20767	0.38302	0.64604	0.90906	0.99673	1.00006	

TABLE E-5 Flow energy Equation error analysis

temperature						time= 1.57895			
i	j	t num	t anal	rnum	ranal				
3	2	0.023389	0.023396	-.002394	-.002403				
3	3	0.023834	0.023841	-.002499	-.002503				
3	4	0.024283	0.024290	-.002607	-.002607				
3	5	0.024736	0.024744	-.002710	-.002714				
3	6	0.025193	0.025201	-.002814	-.002825				
4	2	0.070049	0.070072	-.003917	-.003929				
4	3	0.071391	0.071405	-.004050	-.004073				
4	4	0.072726	0.072750	-.004187	-.004221				
4	5	0.074083	0.074108	-.004352	-.004375				
4	6	0.075453	0.075479	-.004533	-.004533				
5	2	0.238276	0.238357	-.010099	-.010211				
5	3	0.242807	0.242889	-.010474	-.010529				
5	4	0.247381	0.247465	-.010800	-.010855				
5	5	0.251998	0.252083	-.011136	-.011190				
5	6	0.256657	0.256744	-.011426	-.011533				
6	2	0.677883	0.678114	-.031359	-.031545				
6	3	0.690772	0.691010	-.032424	-.032424				
6	4	0.703784	0.704027	-.033505	-.033322				
6	5	0.716919	0.717166	-.033878	-.034240				
6	6	0.730174	0.730426	-.034939	-.035173				
7	2	1.342205	1.342668	-.075901	-.075622				
7	3	1.367725	1.368202	-.077311	-.077587				
7	4	1.393490	1.393976	-.079044	-.079592				
7	5	1.419495	1.419991	-.081637	-.081637				
7	6	1.445742	1.446246	-.083006	-.083722				
8	2	1.613586	1.614141	-.097298	-.097557				
8	3	1.644264	1.644838	-.100298	-.100041				
8	4	1.675239	1.675823	-.102317	-.102572				
8	5	1.706502	1.707098	-.104900	-.105153				
8	6	1.738055	1.738661	-.107450	-.107783				

numerical values temperature						time= 1.57895			
i =	2	3	4	5	6	7	8	9	y =
J									
7	1.14e-02	2.57e-02	7.69e-02	2.61e-01	7.44e-01	1.47e+00	1.77e+00	1.78e+00	1.06e+00
6	1.12e-02	2.52e-02	7.55e-02	2.57e-01	7.30e-01	1.45e+00	1.74e+00	1.75e+00	1.05e+00
5	1.10e-02	2.47e-02	7.41e-02	2.52e-01	7.17e-01	1.42e+00	1.71e+00	1.72e+00	1.04e+00
4	1.08e-02	2.43e-02	7.27e-02	2.47e-01	7.04e-01	1.39e+00	1.68e+00	1.69e+00	1.03e+00
3	1.06e-02	2.38e-02	7.14e-02	2.43e-01	6.91e-01	1.37e+00	1.64e+00	1.66e+00	1.02e+00
2	1.04e-02	2.34e-02	7.00e-02	2.38e-01	6.78e-01	1.34e+00	1.61e+00	1.62e+00	1.01e+00
1	1.02e-02	2.30e-02	6.88e-02	2.34e-01	6.65e-01	1.32e+00	1.58e+00	1.59e+00	1.00e+00
0x =	-.04000	0.	0.10000	0.30000	0.60000	0.90000	1.00000	1.00333	
0z =	0.08000	0.12000	0.20767	0.38302	0.64604	0.90906	0.99673	1.00006	

analytic values temperature						time= 1.57895			
i =	2	3	4	5	6	7	8	9	y =
J									
7	1.14e-02	2.57e-02	7.69e-02	2.61e-01	7.44e-01	1.47e+00	1.77e+00	1.78e+00	1.06e+00
6	1.12e-02	2.52e-02	7.55e-02	2.57e-01	7.30e-01	1.45e+00	1.74e+00	1.75e+00	1.05e+00
5	1.10e-02	2.47e-02	7.41e-02	2.52e-01	7.17e-01	1.42e+00	1.71e+00	1.72e+00	1.04e+00
4	1.08e-02	2.43e-02	7.27e-02	2.47e-01	7.04e-01	1.39e+00	1.68e+00	1.69e+00	1.03e+00
3	1.06e-02	2.38e-02	7.14e-02	2.43e-01	6.91e-01	1.37e+00	1.64e+00	1.66e+00	1.02e+00
2	1.04e-02	2.34e-02	7.01e-02	2.38e-01	6.78e-01	1.34e+00	1.61e+00	1.62e+00	1.01e+00
1	1.02e-02	2.30e-02	6.88e-02	2.34e-01	6.65e-01	1.32e+00	1.58e+00	1.59e+00	1.00e+00
0x =	-.04000	0.	0.10000	0.30000	0.60000	0.90000	1.00000	1.00333	
0z =	0.08000	0.12000	0.20767	0.38302	0.64604	0.90906	0.99673	1.00006	

TABLE E-6 Error analysis for combined
u, v, k, ε, T equations

u velocity						v velocity						turbulence energy					
time= 1.57895						time= 1.57895						time= 1.57895					
i	j	u num	u anal	rnum	ranal	i	j	v num	v anal	rnum	ranal	i	j	k num	k anal	rnum	ranal
4	2	0.042179	0.042993	-.001225	-.001225	3	3	-0.13117	-0.13121	0.00101	0.00104	3	2	0.161871	0.163526	-.008841	-.008841
4	3	0.041195	0.041400	-.001228	-.001235	3	4	-0.13365	-0.13370	0.00101	0.00110	3	3	0.166414	0.166470	-.009062	-.009062
4	4	0.043792	0.043807	-.001246	-.001246	3	5	-0.13616	-0.13620	0.00115	0.00115	3	4	0.169383	0.169441	-.009287	-.009287
4	5	0.044199	0.044214	-.001249	-.001256	3	6	-0.13869	-0.13873	0.00116	0.00121	3	5	0.172379	0.172438	-.009518	-.009518
4	6	0.044606	0.044621	-.001257	-.001266	4	3	-0.22701	-0.22708	0.00447	0.00456	3	6	0.175401	0.175461	-.009848	-.009848
5	2	0.139667	0.139714	-.002150	-.002150	4	4	-0.23130	-0.23138	0.00459	0.00464	4	2	0.304770	0.304871	-.011801	-.011847
5	3	0.140989	0.141036	-.002176	-.002176	4	5	-0.23564	-0.23571	0.00467	0.00471	4	3	0.310707	0.310773	-.012083	-.012130
5	4	0.142311	0.142358	-.002203	-.002203	4	6	-0.24002	-0.24009	0.00471	0.00479	4	4	0.315416	0.315521	-.012418	-.012418
5	5	0.143633	0.143680	-.002230	-.002230	5	3	-0.41868	-0.41881	0.00802	0.00813	4	5	0.320808	0.320915	-.012623	-.012713
5	6	0.144954	0.145001	-.002257	-.002257	5	4	-0.42660	-0.42674	0.00814	0.00825	4	6	0.326246	0.326354	-.013075	-.013075
6	2	0.423889	0.424030	-.003822	-.003822	5	5	-0.43460	-0.43474	0.00814	0.00816	5	2	0.642750	0.642762	-.021524	-.021524
6	3	0.427900	0.428043	-.003863	-.003863	5	6	-0.44267	-0.44281	0.00839	0.00848	5	3	0.653288	0.653506	-.021905	-.022015
6	4	0.431911	0.432055	-.003905	-.003904	6	3	-0.70617	-0.70640	0.01443	0.01480	5	4	0.663712	0.664133	-.022408	-.022515
6	5	0.435923	0.436068	-.003949	-.003946	6	4	-0.71953	-0.71977	0.01499	0.01499	5	5	0.674619	0.674844	-.023138	-.023207
6	6	0.439936	0.440081	-.003993	-.003988	6	5	-0.73302	-0.73327	0.01499	0.01517	5	6	0.685411	0.685638	-.023552	-.023552
7	2	0.768029	0.768347	-.005042	-.005509	6	6	-0.74664	-0.74689	0.01538	0.01538	6	2	1.249175	1.248803	-.048640	-.048640
7	3	0.772187	0.772512	-.005086	-.005528	7	3	-0.99365	-0.99400	0.02100	0.02100	6	3	1.307481	1.308319	-.048959	-.048959
7	4	0.786398	0.786676	-.005103	-.005548	7	4	-1.01245	-1.01281	0.02345	0.02331	6	4	1.327130	1.328176	-.051013	-.051073
7	5	0.795508	0.795840	-.005568	-.005568	7	5	-1.03143	-1.03180	0.02359	0.02359	6	5	1.347721	1.348173	-.052390	-.052209
7	6	1.004673	1.005004	-.005588	-.005588	7	6	-1.05061	-1.05097	0.02388	0.02388	6	6	1.367862	1.368312	-.053368	-.053368
8	2	1.453868	1.454340	-.005687	-.006127	8	3	-1.08951	-1.08987	0.02613	0.02613	7	2	2.097759	2.100449	-.099271	-.099829
8	3	1.467512	1.468104	-.005660	-.006096	8	4	-1.11012	-1.11049	0.02619	0.02644	7	3	2.130200	2.130909	-.102570	-.102016
8	4	1.481372	1.481867	-.005848	-.006064	8	5	-1.13094	-1.13132	0.02574	0.02676	7	4	2.160851	2.161568	-.103697	-.104245
8	5	1.495132	1.495631	-.005819	-.006033	8	6	-1.15196	-1.15233	0.02687	0.02707	7	5	2.191700	2.192426	-.106516	-.106516
8	6	1.508896	1.509394	-.005437	-.006001							7	6	2.222744	2.223482	-.109188	-.108830
												8	2	2.407218	2.407998	-.123704	-.124223
												8	3	2.441588	2.442390	-.126405	-.126919
												8	4	2.476178	2.477000	-.130176	-.129666
												8	5	2.510998	2.511827	-.133960	-.132465
												8	6	2.546033	2.546872	-.135316	-.135316

energy dissipation						temperature					
time= 1.57895						time= 1.57895					
i	j	e num	e anal	rnum	ranal	i	j	t num	t anal	rnum	ranal
3	2	0.011693	0.011697	-.002516	-.002518	3	2	0.023389	0.023396	-.002403	-.002403
3	3	0.011915	0.011919	-.002592	-.002589	3	3	0.023834	0.023841	-.002503	-.002503
3	4	0.012140	0.012144	-.002660	-.002662	3	4	0.024283	0.024290	-.002598	-.002607
3	5	0.012366	0.012371	-.002737	-.002737	3	5	0.024736	0.024744	-.002714	-.002714
3	6	0.012595	0.012599	-.002813	-.002813	3	6	0.025193	0.025201	-.002819	-.002825
4	2	0.035021	0.035033	-.003328	-.003334	4	2	0.070049	0.070072	-.003894	-.003929
4	3	0.035687	0.035699	-.003422	-.003428	4	3	0.071381	0.071405	-.004038	-.004073
4	4	0.036359	0.036371	-.003519	-.003525	4	4	0.072726	0.072750	-.004187	-.004221
4	5	0.037038	0.037050	-.003629	-.003633	4	5	0.074083	0.074108	-.004364	-.004375
4	6	0.037723	0.037735	-.003725	-.003725	4	6	0.075453	0.075478	-.004503	-.004533
5	2	0.119127	0.119166	-.006451	-.006478	5	2	0.238276	0.238357	-.010267	-.010211
5	3	0.121392	0.121433	-.006657	-.006657	5	3	0.242807	0.242889	-.010474	-.010529
5	4	0.123679	0.123720	-.006813	-.006840	5	4	0.247381	0.247465	-.010800	-.010855
5	5	0.125987	0.126029	-.007027	-.007027	5	5	0.251998	0.252083	-.011190	-.011190
5	6	0.128316	0.128359	-.007219	-.007219	5	6	0.256657	0.256744	-.011408	-.011533
6	2	0.338911	0.339023	-.018094	-.018048	6	2	0.677882	0.678114	-.031545	-.031545
6	3	0.345355	0.345470	-.018533	-.018533	6	3	0.690772	0.691010	-.032424	-.032424
6	4	0.351881	0.351978	-.018937	-.019028	6	4	0.703784	0.704027	-.033322	-.033322
6	5	0.358427	0.358541	-.019535	-.019535	6	5	0.716919	0.717166	-.033878	-.034240
6	6	0.365055	0.365176	-.020054	-.020054	6	6	0.730174	0.730426	-.035058	-.035178
7	2	0.671045	0.671267	-.044354	-.044494	7	2	1.342205	1.342668	-.075342	-.075622
7	3	0.683805	0.684033	-.045533	-.045672	7	3	1.367725	1.368202	-.077587	-.077587
7	4	0.696686	0.696918	-.046875	-.046875	7	4	1.393490	1.393976	-.079044	-.079592
7	5	0.709688	0.709924	-.047970	-.048106	7	5	1.419495	1.419991	-.080822	-.081637
7	6	0.722810	0.723051	-.049542	-.049363	7	6	1.445741	1.446246	-.083722	-.083722
8	2	0.806726	0.806990	-.058477	-.058347	8	2	1.613586	1.614141	-.097298	-.097557
8	3	0.822065	0.822337	-.059755	-.059884	8	3	1.644265	1.644838	-.100041	-.100041
8	4	0.837550	0.837828	-.061454	-.061454	8	4	1.675239	1.675823	-.102317	-.102572
8	5	0.853181	0.853464	-.063058	-.063058	8	5	1.706502	1.707098	-.104900	-.105153
8	6	0.868957	0.869244	-.064531	-.064697	8	6	1.738056	1.738661	-.107117	-.107783

TABLE E-6 Error analysis for combined
u, v, k, ε, T equations (cont.)

numerical values time= 1.57395

u velocity									
i =	3	4	5	6	7	8	9	y =	
j									
7	1.07e-02	4.50e-02	1.46e-01	4.44e-01	1.01e+00	1.52e+00	1.68e+00	1.06e+00	
6	1.06e-02	4.46e-02	1.45e-01	4.40e-01	1.00e+00	1.51e+00	1.66e+00	1.05e+00	
5	1.05e-02	4.42e-02	1.44e-01	4.36e-01	9.96e-01	1.50e+00	1.65e+00	1.04e+00	
4	1.04e-02	4.38e-02	1.42e-01	4.32e-01	9.86e-01	1.48e+00	1.63e+00	1.03e+00	
3	1.03e-02	4.34e-02	1.41e-01	4.28e-01	9.77e-01	1.47e+00	1.62e+00	1.02e+00	
2	1.03e-02	4.30e-02	1.40e-01	4.24e-01	9.68e-01	1.45e+00	1.60e+00	1.01e+00	
1	1.02e-02	4.26e-02	1.38e-01	4.20e-01	9.59e-01	1.44e+00	1.59e+00	1.00e+00	
0x =	-0.04000	0.05000	0.20000	0.45000	0.75000	0.95000	1.00333		
0z =	0.08000	0.16384	0.29535	0.51453	0.77755	0.95289	1.00006		

v velocity									
i =	2	3	4	5	6	7	8	9	y =
j									
7	-9.50e-02	-1.43e-01	-2.47e-01	-4.55e-01	-7.68e-01	-1.08e+00	-1.18e+00	-1.19e+00	1.06e+00
6	-9.25e-02	-1.39e-01	-2.40e-01	-4.43e-01	-7.47e-01	-1.05e+00	-1.15e+00	-1.16e+00	1.05e+00
5	-9.08e-02	-1.36e-01	-2.36e-01	-4.35e-01	-7.33e-01	-1.03e+00	-1.13e+00	-1.14e+00	1.04e+00
4	-8.91e-02	-1.34e-01	-2.31e-01	-4.27e-01	-7.20e-01	-1.01e+00	-1.11e+00	-1.11e+00	1.03e+00
3	-8.75e-02	-1.31e-01	-2.27e-01	-4.19e-01	-7.06e-01	-9.94e-01	-1.09e+00	-1.09e+00	1.02e+00
2	-8.58e-02	-1.29e-01	-2.23e-01	-4.11e-01	-6.93e-01	-9.75e-01	-1.07e+00	-1.07e+00	1.01e+00
1	-8.50e-02	0. e+00	0. e+00	0. e+00	0. e+00	0. e+00	0. e+00	-1.06e+00	1.00e+00
0x =	-0.04000	0.	0.10000	0.30000	0.60000	0.90000	1.00000	1.00333	
0z =	0.08000	0.12000	0.20767	0.38302	0.64604	0.90906	0.99673	1.00006	

turbulence energy									
i =	2	3	4	5	6	7	8	9	y =
j									
7	1.15e-01	1.79e-01	3.32e-01	6.97e-01	1.39e+00	2.25e+00	2.58e+00	2.59e+00	1.06e+00
6	1.13e-01	1.75e-01	3.26e-01	6.85e-01	1.37e+00	2.22e+00	2.55e+00	2.56e+00	1.05e+00
5	1.11e-01	1.72e-01	3.21e-01	6.75e-01	1.35e+00	2.19e+00	2.51e+00	2.52e+00	1.04e+00
4	1.09e-01	1.69e-01	3.15e-01	6.64e-01	1.33e+00	2.16e+00	2.48e+00	2.49e+00	1.03e+00
3	1.07e-01	1.66e-01	3.10e-01	6.53e-01	1.31e+00	2.13e+00	2.44e+00	2.45e+00	1.02e+00
2	1.05e-01	1.63e-01	3.05e-01	6.43e-01	1.29e+00	2.10e+00	2.41e+00	2.42e+00	1.01e+00
1	1.03e-01	1.61e-01	3.00e-01	6.33e-01	1.27e+00	2.07e+00	2.37e+00	2.39e+00	1.00e+00
0x =	-0.04000	0.	0.10000	0.30000	0.60000	0.90000	1.00000	1.00333	
0z =	0.08000	0.12000	0.20767	0.38302	0.64604	0.90906	0.99673	1.00006	

energy dissipation									
i =	2	3	4	5	6	7	8	9	y =
j									
7	5.70e-03	1.28e-02	3.84e-02	1.31e-01	3.72e-01	7.36e-01	8.85e-01	8.91e-01	1.06e+00
6	5.60e-03	1.26e-02	3.77e-02	1.28e-01	3.65e-01	7.23e-01	8.69e-01	8.75e-01	1.05e+00
5	5.50e-03	1.24e-02	3.70e-02	1.26e-01	3.58e-01	7.10e-01	8.53e-01	8.59e-01	1.04e+00
4	5.40e-03	1.21e-02	3.64e-02	1.24e-01	3.52e-01	6.97e-01	8.38e-01	8.43e-01	1.03e+00
3	5.30e-03	1.19e-02	3.57e-02	1.21e-01	3.45e-01	6.84e-01	8.22e-01	8.28e-01	1.02e+00
2	5.20e-03	1.17e-02	3.50e-02	1.19e-01	3.39e-01	6.71e-01	8.07e-01	8.12e-01	1.01e+00
1	5.10e-03	1.15e-02	3.44e-02	1.17e-01	3.33e-01	6.59e-01	7.92e-01	7.97e-01	1.00e+00
0x =	-0.04000	0.	0.10000	0.30000	0.60000	0.90000	1.00000	1.00333	
0z =	0.08000	0.12000	0.20767	0.38302	0.64604	0.90906	0.99673	1.00006	

temperature									
i =	2	3	4	5	6	7	8	9	y =
j									
7	1.14e-02	2.57e-02	7.69e-02	2.61e-01	7.44e-01	1.47e+00	1.77e+00	1.78e+00	1.06e+00
6	1.12e-02	2.52e-02	7.55e-02	2.57e-01	7.30e-01	1.45e+00	1.74e+00	1.75e+00	1.05e+00
5	1.10e-02	2.47e-02	7.41e-02	2.52e-01	7.17e-01	1.42e+00	1.71e+00	1.72e+00	1.04e+00
4	1.08e-02	2.43e-02	7.27e-02	2.47e-01	7.04e-01	1.39e+00	1.68e+00	1.69e+00	1.03e+00
3	1.06e-02	2.38e-02	7.14e-02	2.43e-01	6.91e-01	1.37e+00	1.64e+00	1.66e+00	1.02e+00
2	1.04e-02	2.34e-02	7.00e-02	2.38e-01	6.78e-01	1.34e+00	1.61e+00	1.62e+00	1.01e+00
1	1.02e-02	2.30e-02	6.88e-02	2.34e-01	6.65e-01	1.32e+00	1.58e+00	1.59e+00	1.00e+00
0x =	-0.04000	0.	0.10000	0.30000	0.60000	0.90000	1.00000	1.00333	
0z =	0.08000	0.12000	0.20767	0.38302	0.64604	0.90906	0.99673	1.00006	

TABLE E-6 Error analysis for combined
u, v, k, ϵ , T equations (cont.)

analytic values time= 1.57895

u velocity									
i =	3	4	5	6	7	8	9	y =	
j									
7	1.07e-02	4.50e-02	1.46e-01	4.44e-01	1.01e+00	1.52e+00	1.68e+00	1.06e+00	
6	1.36e-02	4.46e-02	1.45e-01	4.40e-01	1.01e+00	1.51e+00	1.66e+00	1.05e+00	
5	1.05e-02	4.42e-02	1.44e-01	4.36e-01	9.96e-01	1.50e+00	1.65e+00	1.04e+00	
4	1.04e-02	4.38e-02	1.42e-01	4.32e-01	9.87e-01	1.48e+00	1.63e+00	1.03e+00	
3	1.03e-02	4.34e-02	1.41e-01	4.28e-01	9.78e-01	1.47e+00	1.62e+00	1.02e+00	
2	1.03e-02	4.30e-02	1.40e-01	4.24e-01	9.68e-01	1.45e+00	1.60e+00	1.01e+00	
1	1.02e-02	4.26e-02	1.38e-01	4.20e-01	9.59e-01	1.44e+00	1.59e+00	1.00e+00	
0x =	-0.04000	0.05000	0.20000	0.45000	0.75000	0.95000	1.00333		
0z =	0.08000	0.16384	0.29535	0.51453	0.77755	0.95289	1.00006		

v velocity									
i =	2	3	4	5	6	7	8	9	y =
j									
7	-9.50e-02	-1.43e-01	-2.47e-01	-4.55e-01	-7.68e-01	-1.08e+00	-1.18e+00	-1.19e+00	1.06e+00
6	-9.25e-02	-1.39e-01	-2.40e-01	-4.43e-01	-7.47e-01	-1.05e+00	-1.15e+00	-1.16e+00	1.05e+00
5	-9.08e-02	-1.36e-01	-2.36e-01	-4.35e-01	-7.33e-01	-1.03e+00	-1.13e+00	-1.14e+00	1.04e+00
4	-8.91e-02	-1.34e-01	-2.31e-01	-4.27e-01	-7.20e-01	-1.01e+00	-1.11e+00	-1.11e+00	1.03e+00
3	-8.75e-02	-1.31e-01	-2.27e-01	-4.19e-01	-7.06e-01	-9.94e-01	-1.09e+00	-1.09e+00	1.02e+00
2	-8.58e-02	-1.29e-01	-2.23e-01	-4.11e-01	-6.93e-01	-9.75e-01	-1.07e+00	-1.07e+00	1.01e+00
1	-8.50e-02	0. e+00	0. e+00	0. e+00	0. e+00	0. e+00	0. e+00	-1.00e+00	1.00e+00
0x =	-0.04000	0.	0.10000	0.30000	0.60000	0.90000	1.00000	1.00333	
0z =	0.08000	0.12000	0.20767	0.38302	0.64604	0.90906	0.99673	1.00006	

turbulence energy									
i =	2	3	4	5	6	7	8	9	y =
j									
7	1.15e-01	1.79e-01	3.32e-01	6.97e-01	1.39e+00	2.25e+00	2.58e+00	2.59e+00	1.06e+00
6	1.13e-01	1.75e-01	3.26e-01	6.86e-01	1.37e+00	2.22e+00	2.55e+00	2.56e+00	1.05e+00
5	1.11e-01	1.72e-01	3.21e-01	6.75e-01	1.35e+00	2.19e+00	2.51e+00	2.52e+00	1.04e+00
4	1.09e-01	1.69e-01	3.16e-01	6.64e-01	1.33e+00	2.16e+00	2.48e+00	2.49e+00	1.03e+00
3	1.07e-01	1.66e-01	3.10e-01	6.54e-01	1.31e+00	2.13e+00	2.44e+00	2.45e+00	1.02e+00
2	1.05e-01	1.64e-01	3.05e-01	6.43e-01	1.29e+00	2.10e+00	2.41e+00	2.42e+00	1.01e+00
1	1.03e-01	1.61e-01	3.00e-01	6.33e-01	1.27e+00	2.07e+00	2.37e+00	2.39e+00	1.00e+00
0x =	-0.04000	0.	0.10000	0.30000	0.60000	0.90000	1.00000	1.00333	
0z =	0.08000	0.12000	0.20767	0.38302	0.64604	0.90906	0.99673	1.00006	

energy dissipation									
i =	2	3	4	5	6	7	8	9	y =
j									
7	5.70e-03	1.28e-02	3.84e-02	1.31e-01	3.72e-01	7.36e-01	8.85e-01	8.91e-01	1.06e+00
6	5.60e-03	1.26e-02	3.77e-02	1.28e-01	3.65e-01	7.23e-01	8.69e-01	8.75e-01	1.05e+00
5	5.50e-03	1.24e-02	3.71e-02	1.26e-01	3.59e-01	7.10e-01	8.53e-01	8.59e-01	1.04e+00
4	5.40e-03	1.21e-02	3.64e-02	1.24e-01	3.52e-01	6.97e-01	8.38e-01	8.43e-01	1.03e+00
3	5.30e-03	1.19e-02	3.57e-02	1.21e-01	3.45e-01	6.84e-01	8.22e-01	8.28e-01	1.02e+00
2	5.20e-03	1.17e-02	3.50e-02	1.19e-01	3.39e-01	6.71e-01	8.07e-01	8.12e-01	1.01e+00
1	5.10e-03	1.15e-02	3.44e-02	1.17e-01	3.33e-01	6.59e-01	7.92e-01	7.97e-01	1.00e+00
0x =	-0.04000	0.	0.10000	0.30000	0.60000	0.90000	1.00000	1.00333	
0z =	0.08000	0.12000	0.20767	0.38302	0.64604	0.90906	0.99673	1.00006	

temperature									
i =	2	3	4	5	6	7	8	9	y =
j									
7	1.14e-02	2.57e-02	7.69e-02	2.61e-01	7.44e-01	1.47e+00	1.77e+00	1.78e+00	1.06e+00
6	1.12e-02	2.52e-02	7.55e-02	2.57e-01	7.30e-01	1.45e+00	1.74e+00	1.75e+00	1.05e+00
5	1.10e-02	2.47e-02	7.41e-02	2.52e-01	7.17e-01	1.42e+00	1.71e+00	1.72e+00	1.04e+00
4	1.09e-02	2.43e-02	7.27e-02	2.47e-01	7.04e-01	1.39e+00	1.68e+00	1.69e+00	1.03e+00
3	1.06e-02	2.38e-02	7.14e-02	2.43e-01	6.91e-01	1.37e+00	1.64e+00	1.66e+00	1.02e+00
2	1.04e-02	2.34e-02	7.01e-02	2.38e-01	6.78e-01	1.34e+00	1.61e+00	1.62e+00	1.01e+00
1	1.02e-02	2.30e-02	6.88e-02	2.34e-01	6.65e-01	1.32e+00	1.58e+00	1.59e+00	1.00e+00
0x =	-0.04000	0.	0.10000	0.30000	0.60000	0.90000	1.00000	1.00333	
0z =	0.08000	0.12000	0.20767	0.38302	0.64604	0.90906	0.99673	1.00006	

TABLE E-7 Error analysis for combined u , v and k equations

u velocity			time= 1.57895			v velocity			time= 1.57895			turbulence energy			time= 1.57899		
i	j	u num	u anal	rnum	ranal	i	j	v num	v anal	rnum	ranal	i	j	k num	k anal	rnum	ranal
4	2	0.042979	0.042993	-0.001211	-0.001225	3	3	-0.13117	-0.13121	0.00297	0.00304	3	2	0.163471	0.163526	-0.008805	-0.008841
4	3	0.043388	0.043400	-0.001229	-0.001235	3	4	-0.13404	-0.13409	0.00314	0.00311	3	3	0.166414	0.166470	-0.009093	-0.009062
4	4	0.043922	0.043934	-0.001249	-0.001259	3	5	-0.13655	-0.13660	0.00314	0.00316	3	4	0.170317	0.170375	-0.009323	-0.009359
4	5	0.044201	0.044214	-0.001240	-0.001256	3	6	-0.13869	-0.13873	0.00318	0.00321	3	5	0.172379	0.172438	-0.009476	-0.009518
4	6	0.044608	0.044621	-0.001248	-0.001266	4	3	-0.22701	-0.22708	0.00452	0.00456	3	6	0.175401	0.175461	-0.009755	-0.009755
5	2	0.139667	0.139714	-0.002150	-0.002150	4	4	-0.23198	-0.23205	0.00456	0.00465	3	2	0.304770	0.304871	-0.011801	-0.011847
5	3	0.140591	0.141036	-0.002146	-0.002176	4	5	-0.23632	-0.23640	0.00467	0.00472	4	3	0.310070	0.310173	-0.012130	-0.012130
5	4	0.142726	0.142771	-0.002211	-0.002211	4	6	-0.24002	-0.24009	0.00475	0.00479	4	3	0.310796	0.31202	-0.012595	-0.012510
5	5	0.143635	0.143680	-0.002189	-0.002230	5	3	-0.41868	-0.41881	0.00803	0.00813	4	4	0.320808	0.320915	-0.012606	-0.012713
5	6	0.144957	0.145003	-0.002235	-0.002257	5	4	-0.42798	-0.42798	0.00816	0.00826	4	5	0.326246	0.326354	-0.012954	-0.013015
6	2	0.423889	0.424030	-0.003720	-0.003822	5	5	-0.43585	-0.43599	0.00838	0.00838	5	2	0.642750	0.642962	-0.021413	-0.021524
6	3	0.427900	0.428043	-0.003776	-0.003863	5	6	-0.44267	-0.44281	0.00838	0.00848	5	3	0.653288	0.653506	-0.022016	-0.022016
6	4	0.433165	0.433310	-0.003818	-0.003917	6	3	-0.70617	-0.70640	0.01497	0.01480	5	5	0.667249	0.667471	-0.022567	-0.022676
6	5	0.435923	0.436068	-0.003712	-0.003946	6	4	-0.72163	-0.72188	0.01484	0.01501	5	6	0.674844	0.674944	-0.022901	-0.023029
6	6	0.439536	0.440081	-0.003793	-0.003988	6	5	-0.73514	-0.73539	0.01501	0.01520	5	6	0.685411	0.685638	-0.023552	-0.023552
7	2	0.968029	0.968347	-0.005509	-0.005509	7	3	-0.74664	-0.74689	0.01536	0.01536	6	2	1.288175	1.288603	-0.048866	-0.048866
7	3	0.977187	0.977512	-0.005146	-0.005258	7	4	-0.99365	-0.99400	0.02304	0.02304	6	3	1.307681	1.308319	-0.049640	-0.049959
7	4	0.989210	0.989540	-0.005544	-0.005554	7	5	-1.01541	-1.01577	0.02285	0.02326	6	4	1.333970	1.334410	-0.051426	-0.051426
7	5	0.995508	0.995840	-0.005311	-0.005568	7	6	-1.03441	-1.03479	0.02334	0.02364	6	5	1.347721	1.348173	-0.051995	-0.052209
7	6	1.004673	1.005004	-0.005302	-0.005588	7	6	-1.05060	-1.05097	0.02365	0.02388	6	6	1.367863	1.368312	-0.053368	-0.053368
8	2	1.453868	1.454340	-0.005687	-0.006127	8	3	-1.08951	-1.08987	0.02637	0.02613	7	2	2.099759	2.100449	-0.100388	-0.099829
8	3	1.467612	1.468104	-0.005344	-0.006096	8	4	-1.11337	-1.11373	0.02625	0.02649	7	3	2.130201	2.130309	-0.101538	-0.102016
8	4	1.485672	1.486168	-0.005623	-0.006054	8	5	-1.13421	-1.13459	0.02653	0.02681	7	4	2.170470	2.171190	-0.104403	-0.104950
8	5	1.495132	1.495631	-0.005272	-0.006033	8	6	-1.15196	-1.15233	0.02665	0.02707	7	5	2.191700	2.192426	-0.106516	-0.106516
8	6	1.508896	1.509394	-0.006001	-0.006001							7	6	2.222744	2.223482	-0.108830	-0.108830
												8	2	2.407218	2.407496	-0.124223	-0.124223
												8	3	2.441588	2.442390	-0.127808	-0.126919
												8	4	2.467036	2.467860	-0.130027	-0.130535
												8	5	2.510998	2.511827	-0.133063	-0.132465
												8	6	2.546872	2.546872	-0.135316	-0.135316

TABLE E-7 Error analysis for combined u, v and k equations (cont.)

numerical values times 1.57895									
u velocity									
i =	3	4	5	6	7	8	9	y =	
7	1.07e-02	4.50e-02	1.46e-01	4.44e-01	1.01e+00	1.52e+00	1.68e+00	1.06e+00	
6	1.06e-02	4.46e-02	1.45e-01	4.40e-01	1.00e+00	1.51e+00	1.66e+00	1.05e+00	
5	1.05e-02	4.42e-02	1.44e-01	4.36e-01	9.96e-01	1.50e+00	1.65e+00	1.04e+00	
4	1.05e-02	4.39e-02	1.43e-01	4.33e-01	9.89e-01	1.49e+00	1.64e+00	1.04e+00	
3	1.01e-02	4.34e-02	1.41e-01	4.28e-01	9.77e-01	1.47e+00	1.62e+00	1.02e+00	
2	1.03e-02	4.30e-02	1.40e-01	4.24e-01	9.68e-01	1.45e+00	1.60e+00	1.01e+00	
1	1.02e-02	4.26e-02	1.38e-01	4.20e-01	9.59e-01	1.44e+00	1.59e+00	1.00e+00	
0x =	-0.04000	0.05000	0.20000	0.45000	0.75000	0.95000	1.00333		
0z =	0.08000	0.16384	0.29535	0.51453	0.77755	0.95289	1.00006		
v velocity									
i =	2	3	4	5	6	7	8	9	y =
7	-9.50e-02	-1.43e-01	-2.47e-01	-4.55e-01	-7.68e-01	-1.08e+00	-1.18e+00	-1.19e+00	1.06e+00
6	-9.25e-02	-1.39e-01	-2.40e-01	-4.43e-01	-7.47e-01	-1.05e+00	-1.15e+00	-1.16e+00	1.05e+00
5	-9.11e-02	-1.37e-01	-2.36e-01	-4.36e-01	-7.35e-01	-1.03e+00	-1.13e+00	-1.14e+00	1.04e+00
4	-8.94e-02	-1.34e-01	-2.32e-01	-4.28e-01	-7.22e-01	-1.02e+00	-1.11e+00	-1.12e+00	1.03e+00
3	-8.75e-02	-1.31e-01	-2.27e-01	-4.19e-01	-7.06e-01	-9.94e-01	-1.09e+00	-1.09e+00	1.02e+00
2	-8.58e-02	-1.29e-01	-2.23e-01	-4.11e-01	-6.93e-01	-9.75e-01	-1.07e+00	-1.07e+00	1.01e+00
1	-8.50e-02	0. e+00	0. e+00	0. e+00	0. e+00	0. e+00	0. e+00	-1.06e+00	1.00e+00
0x =	-0.04000	0.	0.10000	0.30000	0.60000	0.90000	1.00000	1.00333	
0z =	0.08000	0.12000	0.20767	0.38302	0.64604	0.90906	0.99673	1.00006	
turbulence energy									
i =	2	3	4	5	6	7	8	9	y =
7	1.15e-01	1.79e-01	3.32e-01	6.97e-01	1.39e+00	2.25e+00	2.58e+00	2.59e+00	1.06e+00
6	1.13e-01	1.75e-01	3.26e-01	6.86e-01	1.37e+00	2.22e+00	2.55e+00	2.56e+00	1.05e+00
5	1.11e-01	1.72e-01	3.21e-01	6.75e-01	1.35e+00	2.19e+00	2.51e+00	2.52e+00	1.04e+00
4	1.10e-01	1.70e-01	3.17e-01	6.67e-01	1.33e+00	2.17e+00	2.49e+00	2.50e+00	1.04e+00
3	1.07e-01	1.66e-01	3.10e-01	6.54e-01	1.31e+00	2.13e+00	2.44e+00	2.45e+00	1.02e+00
2	1.05e-01	1.64e-01	3.05e-01	6.43e-01	1.29e+00	2.10e+00	2.41e+00	2.42e+00	1.01e+00
1	1.03e-01	1.61e-01	3.00e-01	6.33e-01	1.27e+00	2.07e+00	2.37e+00	2.39e+00	1.00e+00
0x =	-0.04000	0.	0.10000	0.30000	0.60000	0.90000	1.00000	1.00333	
0z =	0.08000	0.12000	0.20767	0.38302	0.64604	0.90906	0.99673	1.00006	
analytic values for times 1.57895									
u velocity									
i =	3	4	5	6	7	8	9	y =	
7	1.07e-02	4.50e-02	1.46e-01	4.44e-01	1.01e+00	1.52e+00	1.68e+00	1.06e+00	
6	1.06e-02	4.46e-02	1.45e-01	4.40e-01	1.01e+00	1.51e+00	1.66e+00	1.05e+00	
5	1.05e-02	4.42e-02	1.44e-01	4.36e-01	9.96e-01	1.50e+00	1.65e+00	1.04e+00	
4	1.05e-02	4.39e-02	1.43e-01	4.33e-01	9.90e-01	1.49e+00	1.64e+00	1.04e+00	
3	1.03e-02	4.34e-02	1.41e-01	4.28e-01	9.78e-01	1.47e+00	1.62e+00	1.02e+00	
2	1.03e-02	4.30e-02	1.40e-01	4.24e-01	9.68e-01	1.45e+00	1.60e+00	1.01e+00	
1	1.02e-02	4.26e-02	1.38e-01	4.20e-01	9.59e-01	1.44e+00	1.59e+00	1.00e+00	
0x =	-0.04000	0.05000	0.20000	0.45000	0.75000	0.95000	1.00333		
0z =	0.08000	0.16384	0.29535	0.51453	0.77755	0.95289	1.00006		
v velocity									
i =	2	3	4	5	6	7	8	9	y =
7	-9.50e-02	-1.43e-01	-2.47e-01	-4.55e-01	-7.68e-01	-1.08e+00	-1.18e+00	-1.19e+00	1.06e+00
6	-9.25e-02	-1.39e-01	-2.40e-01	-4.43e-01	-7.47e-01	-1.05e+00	-1.15e+00	-1.16e+00	1.05e+00
5	-9.11e-02	-1.37e-01	-2.36e-01	-4.36e-01	-7.35e-01	-1.03e+00	-1.13e+00	-1.14e+00	1.04e+00
4	-8.94e-02	-1.34e-01	-2.32e-01	-4.28e-01	-7.22e-01	-1.02e+00	-1.11e+00	-1.12e+00	1.03e+00
3	-8.75e-02	-1.31e-01	-2.27e-01	-4.19e-01	-7.06e-01	-9.94e-01	-1.09e+00	-1.09e+00	1.02e+00
2	-8.58e-02	-1.29e-01	-2.23e-01	-4.11e-01	-6.93e-01	-9.75e-01	-1.07e+00	-1.07e+00	1.01e+00
1	-8.50e-02	0. e+00	0. e+00	0. e+00	0. e+00	0. e+00	0. e+00	-1.06e+00	1.00e+00
0x =	-0.04000	0.	0.10000	0.30000	0.60000	0.90000	1.00000	1.00333	
0z =	0.08000	0.12000	0.20767	0.38302	0.64604	0.90906	0.99673	1.00006	
turbulence energy									
i =	2	3	4	5	6	7	8	9	y =
7	1.15e-01	1.79e-01	3.32e-01	6.97e-01	1.39e+00	2.25e+00	2.58e+00	2.59e+00	1.06e+00
6	1.13e-01	1.75e-01	3.26e-01	6.86e-01	1.37e+00	2.22e+00	2.55e+00	2.56e+00	1.05e+00
5	1.11e-01	1.72e-01	3.21e-01	6.75e-01	1.35e+00	2.19e+00	2.51e+00	2.52e+00	1.04e+00
4	1.10e-01	1.70e-01	3.17e-01	6.67e-01	1.33e+00	2.17e+00	2.49e+00	2.50e+00	1.04e+00
3	1.07e-01	1.66e-01	3.10e-01	6.54e-01	1.31e+00	2.13e+00	2.44e+00	2.45e+00	1.02e+00
2	1.05e-01	1.64e-01	3.05e-01	6.43e-01	1.29e+00	2.10e+00	2.41e+00	2.42e+00	1.01e+00
1	1.03e-01	1.61e-01	3.00e-01	6.33e-01	1.27e+00	2.07e+00	2.37e+00	2.39e+00	1.00e+00
0x =	-0.04000	0.	0.10000	0.30000	0.60000	0.90000	1.00000	1.00333	
0z =	0.08000	0.12000	0.20767	0.38302	0.64604	0.90906	0.99673	1.00006	

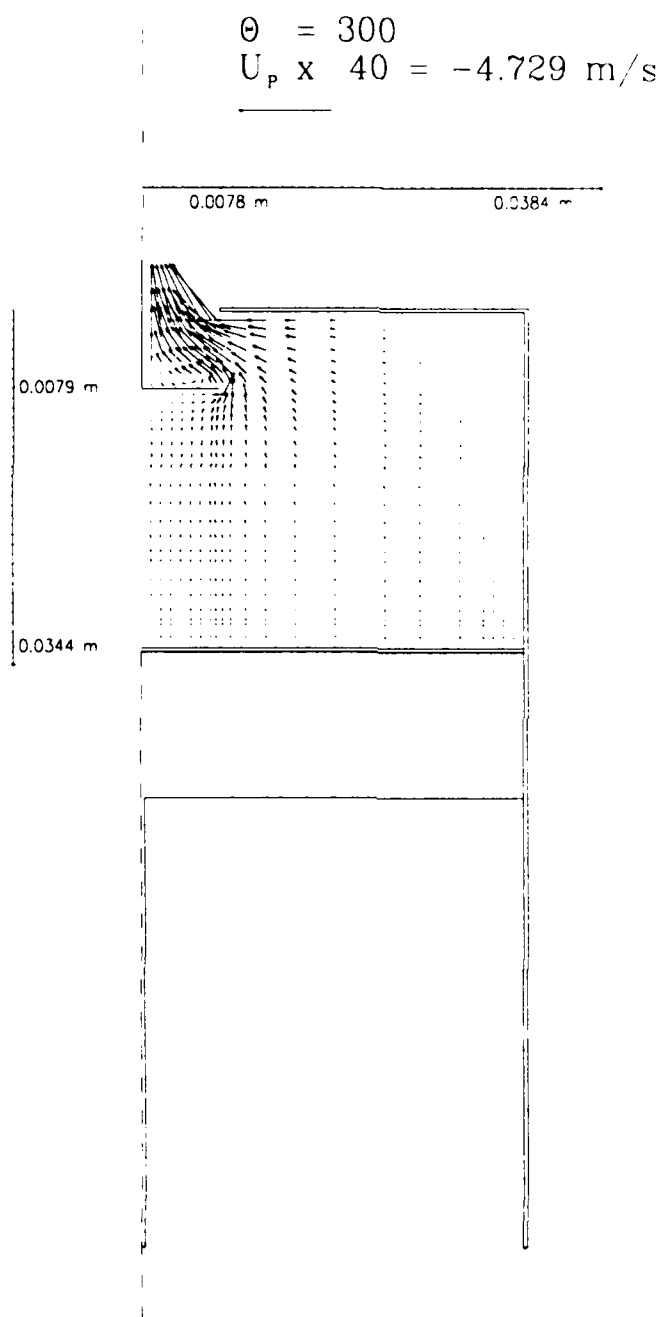


Figure E-1 Case 3 velocity vector plot for a crank shaft angle of 300°

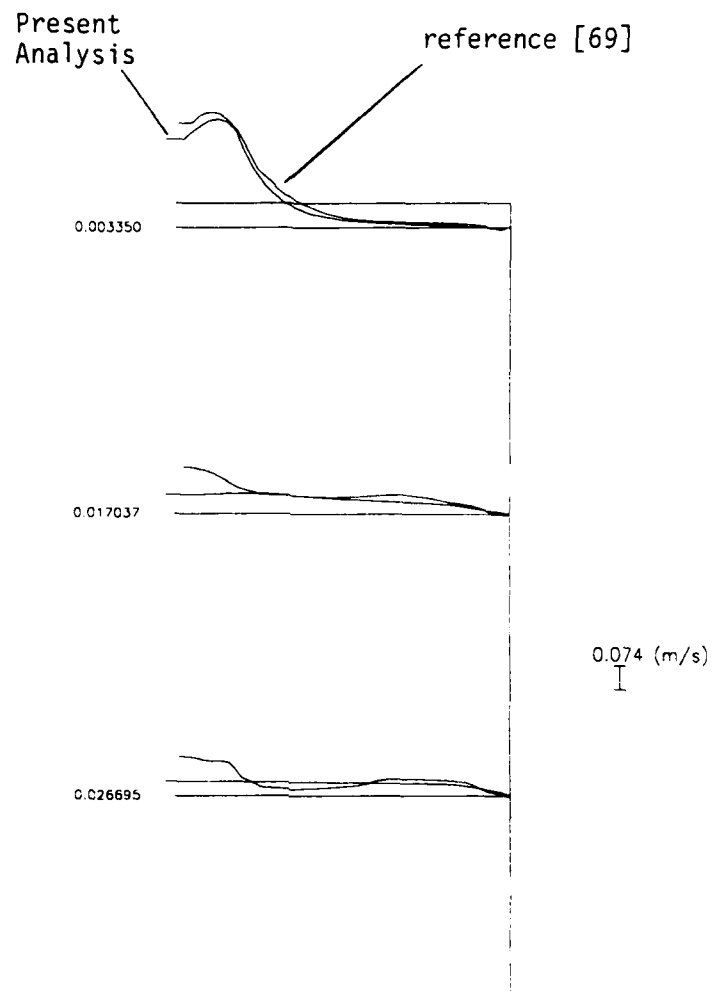


Figure E-2 Comparison of u-velocity profiles for case 3 run with an identical run performed by Ramos and Sirignano^{6,9}

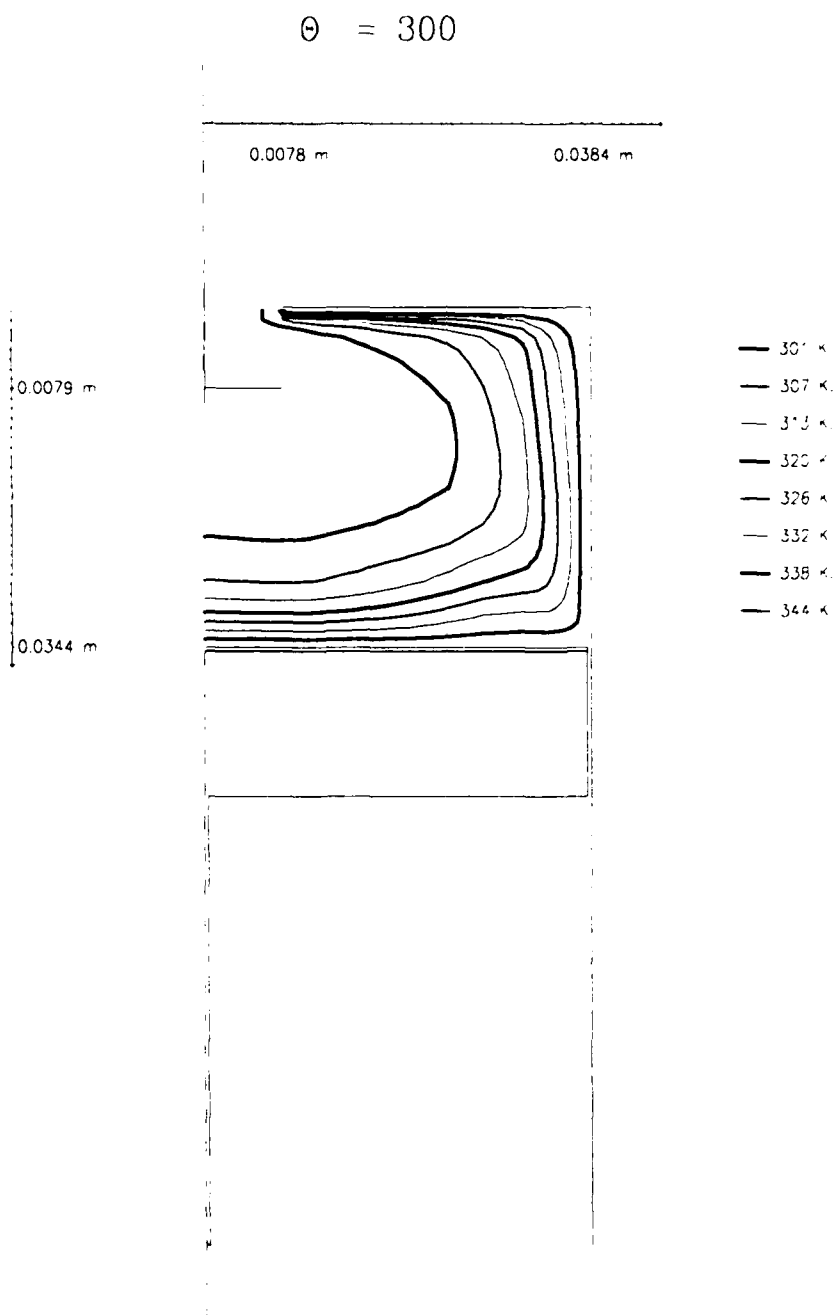


Figure E-3 Case 3 temperature profile for a crank shaft angle of 300°

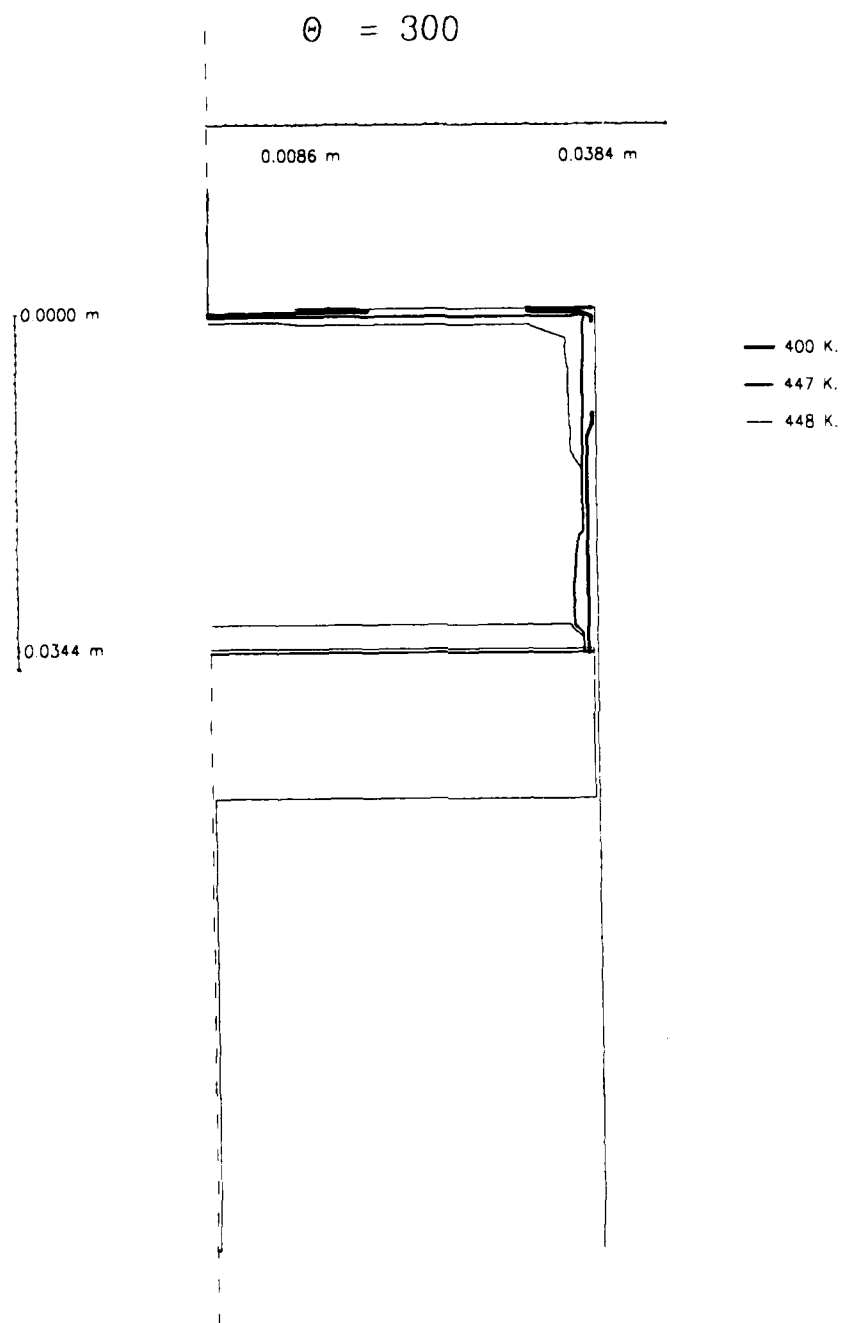


Figure E-4 Case 5 temperature profile for $\theta = 300^\circ$, run 1

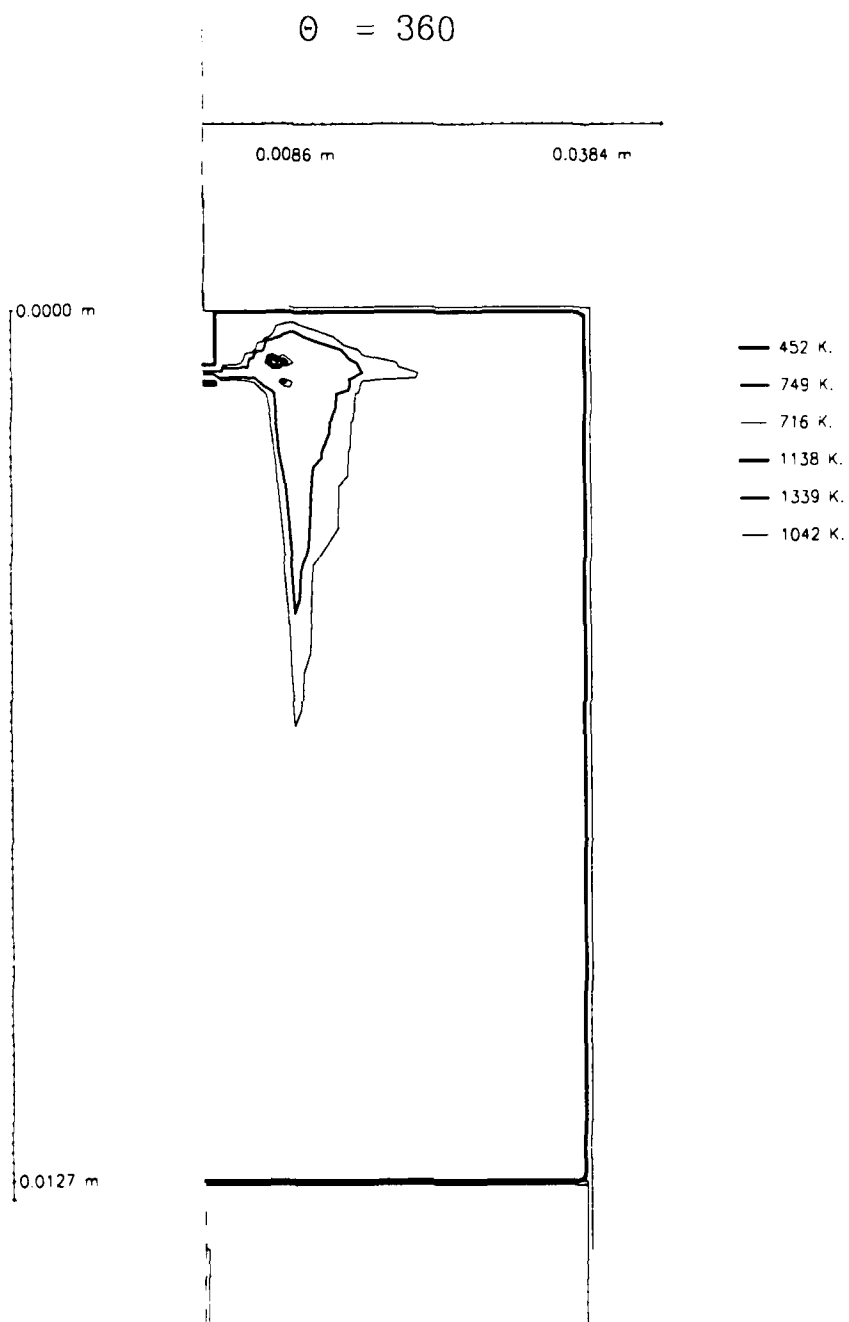


Figure E-5 Case 5 temperature profile for $\theta = 360^\circ$, run 1
(using x coordinate spacing (modified))

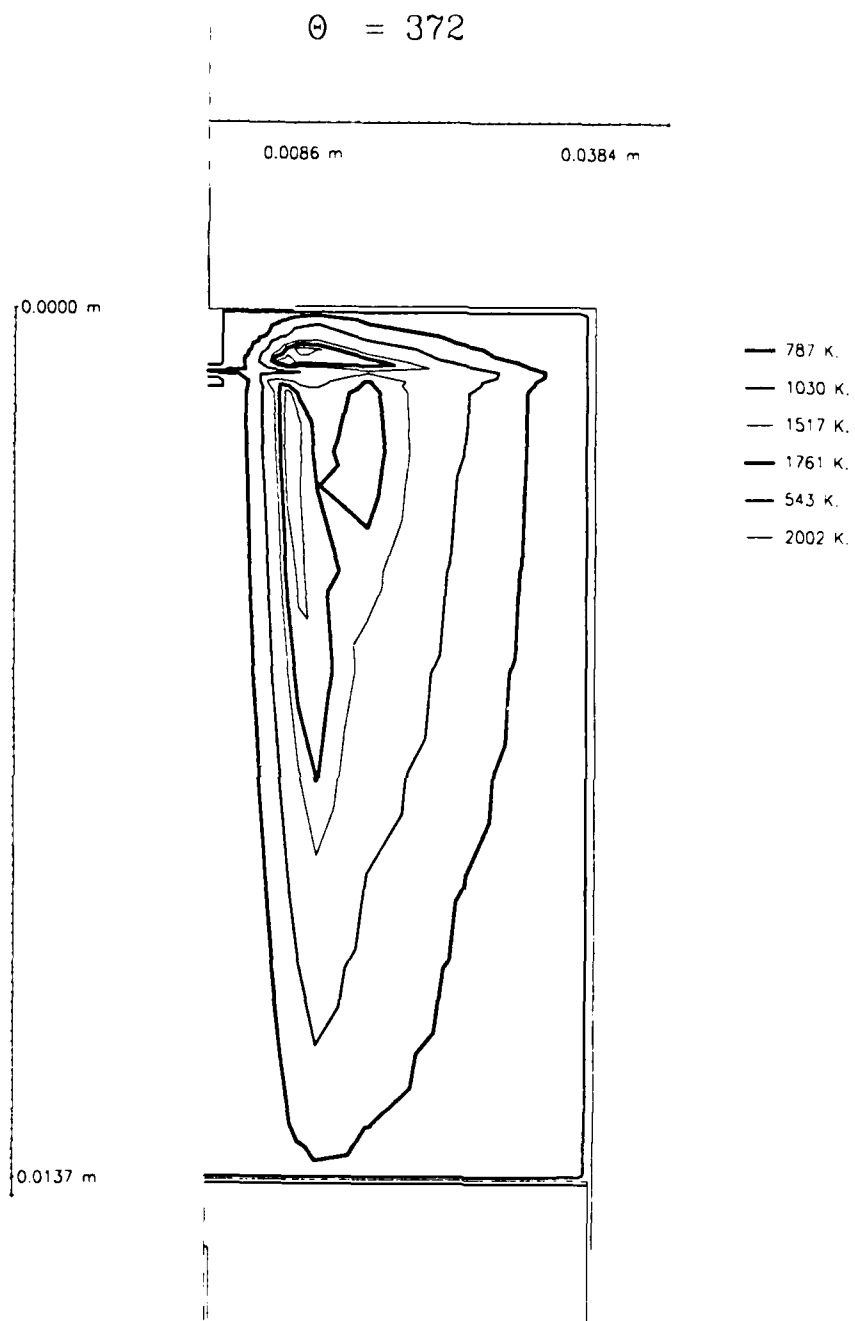


Figure E-6 Case 5 temperature profile for $\theta = 372^\circ$, run 1
(using x coordinate spacing (modified))

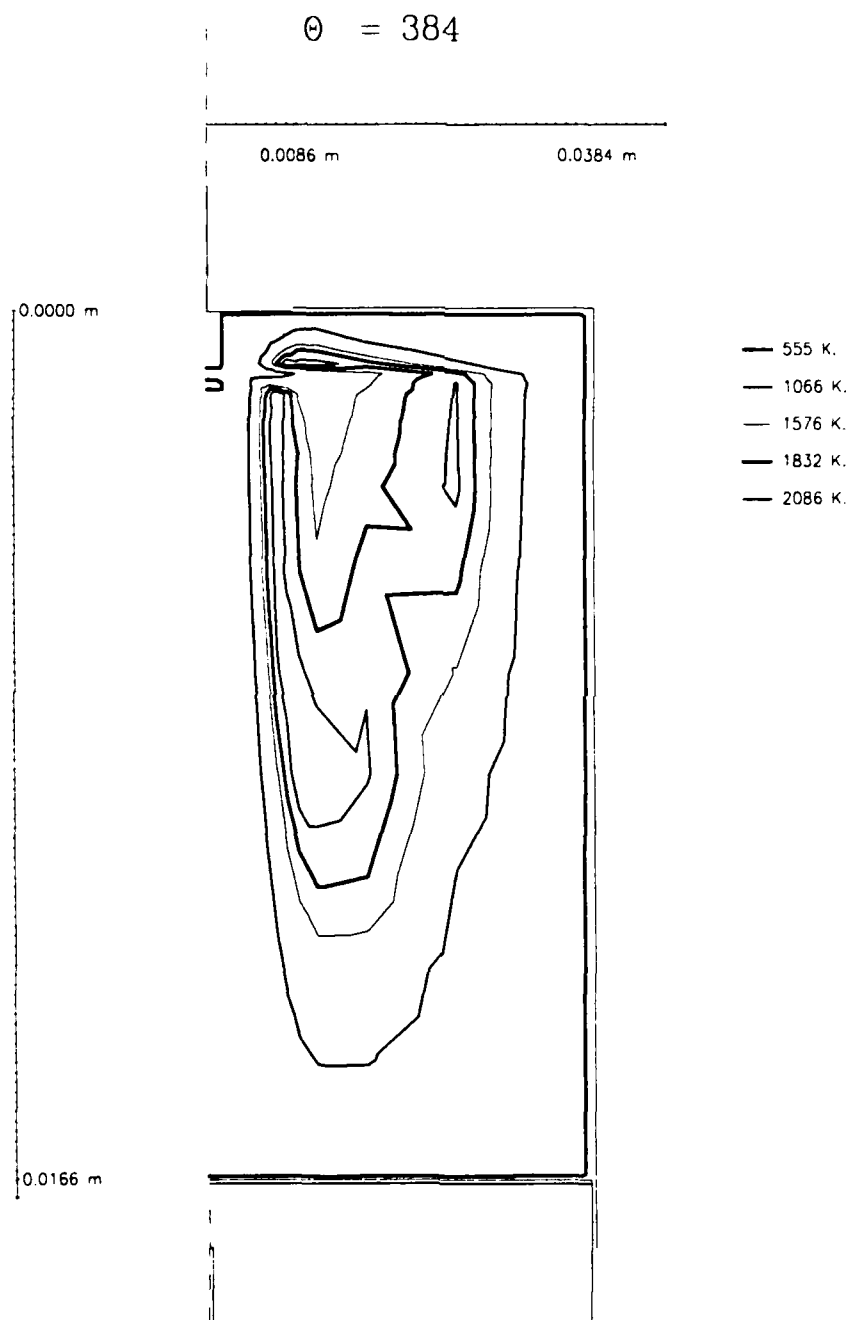


Figure E-7 Case 5 temperature profile for $\theta = 384^\circ$, run 1
(using x coordinate spacing(modified))

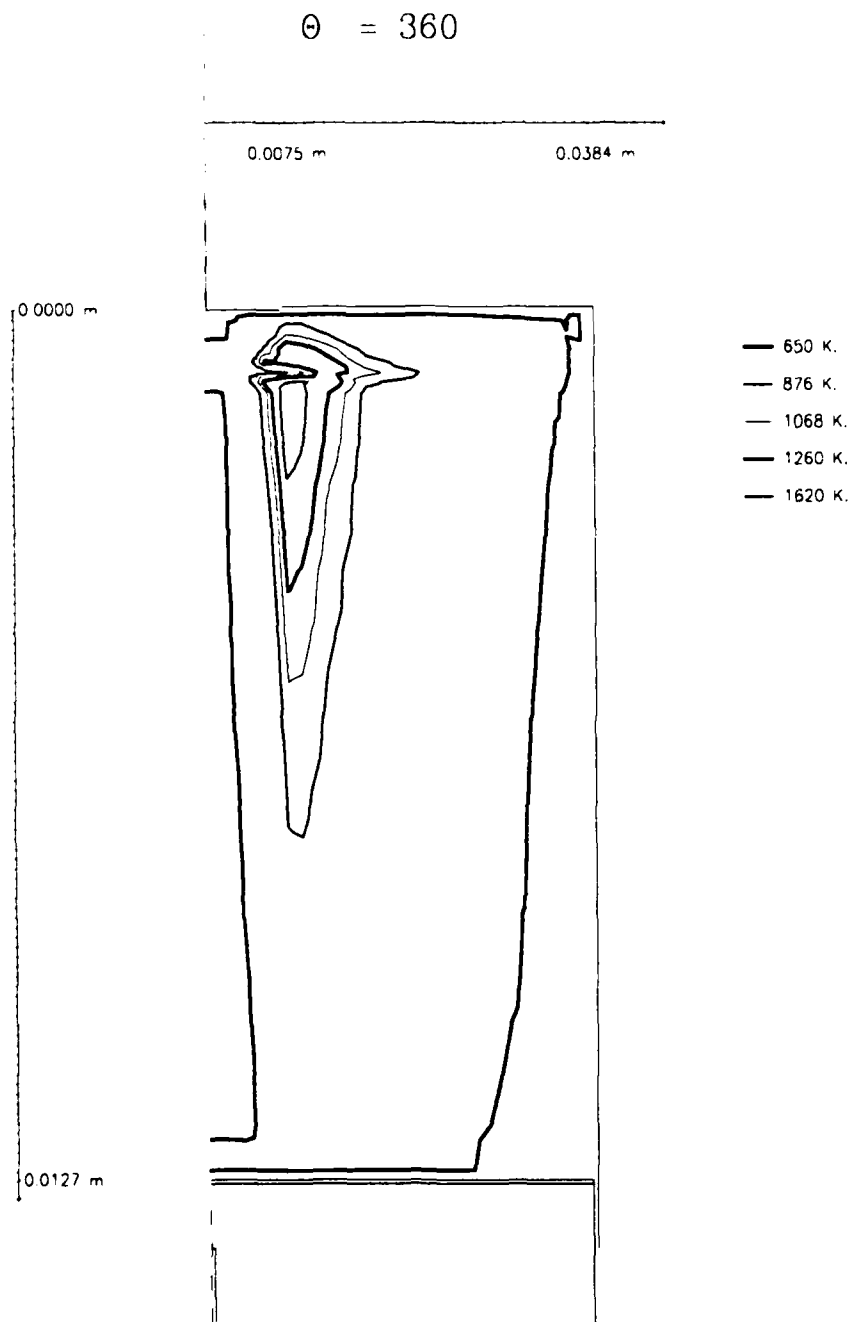


Figure E-8 Case 5 temperature profile for $\theta = 360^\circ$, run 2
(using x coordinate spacing (modified))

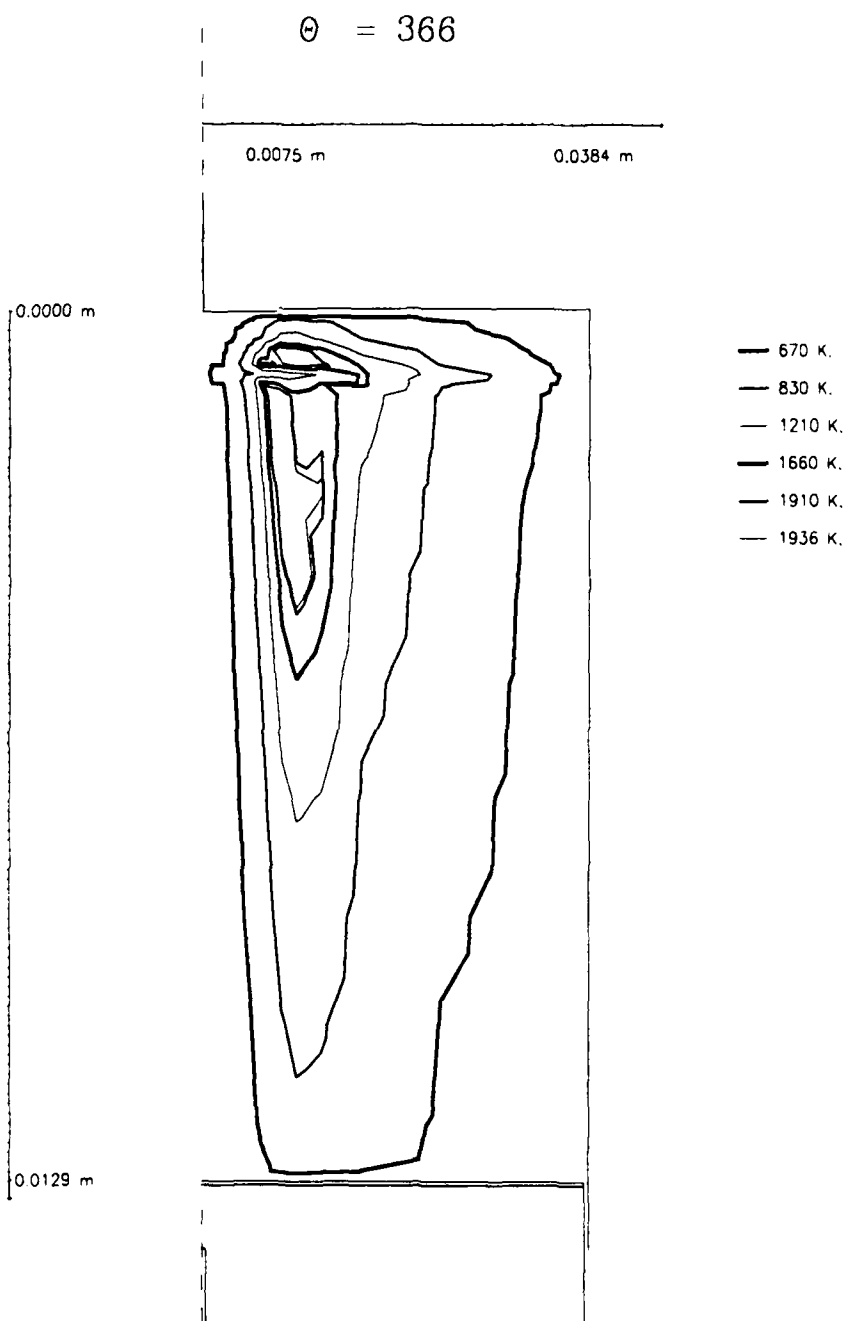


Figure E-9 Case 5 temperature profile for $\theta = 366^\circ$, run 2
(using x coordinate spacing (modified))

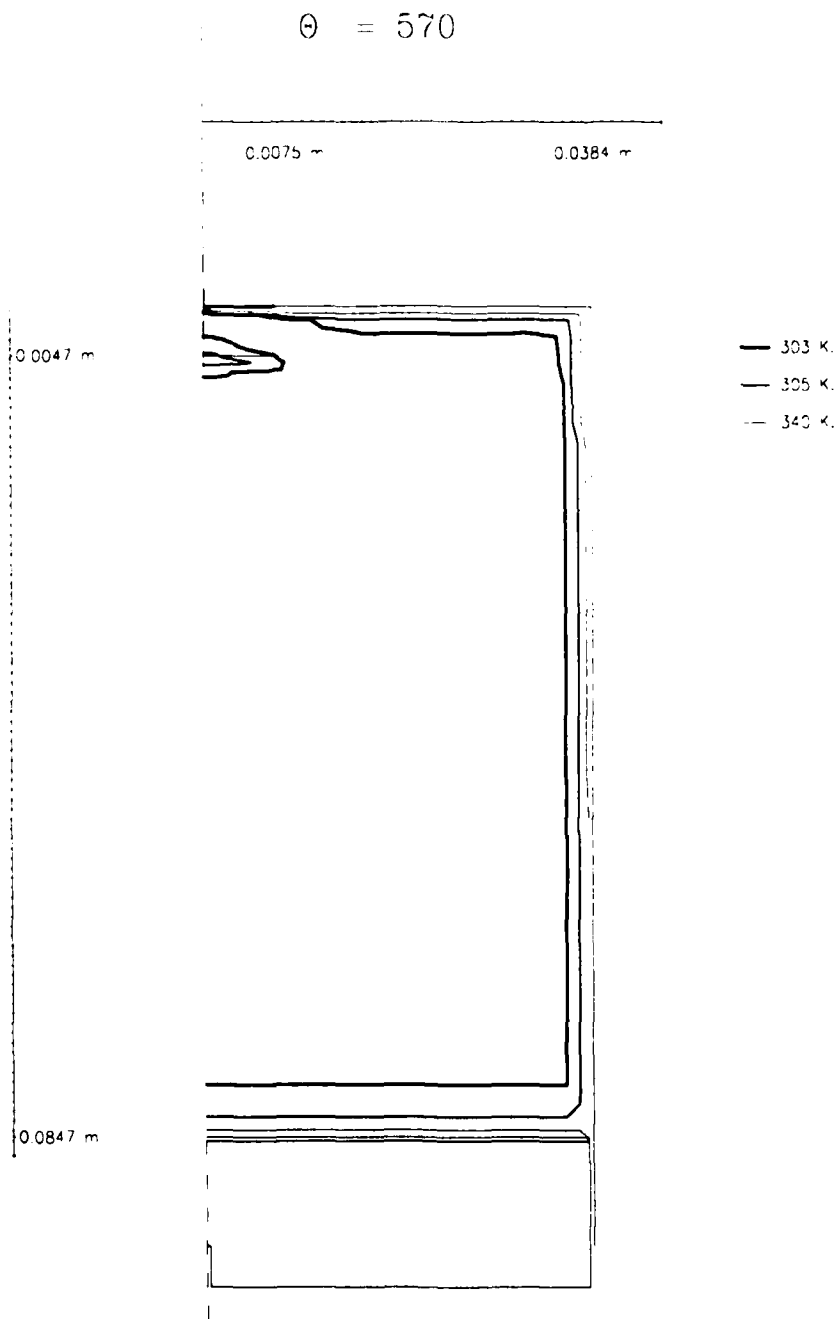


Figure E-10 Case 5 temperature profile for $\theta = 570^\circ$, run 3

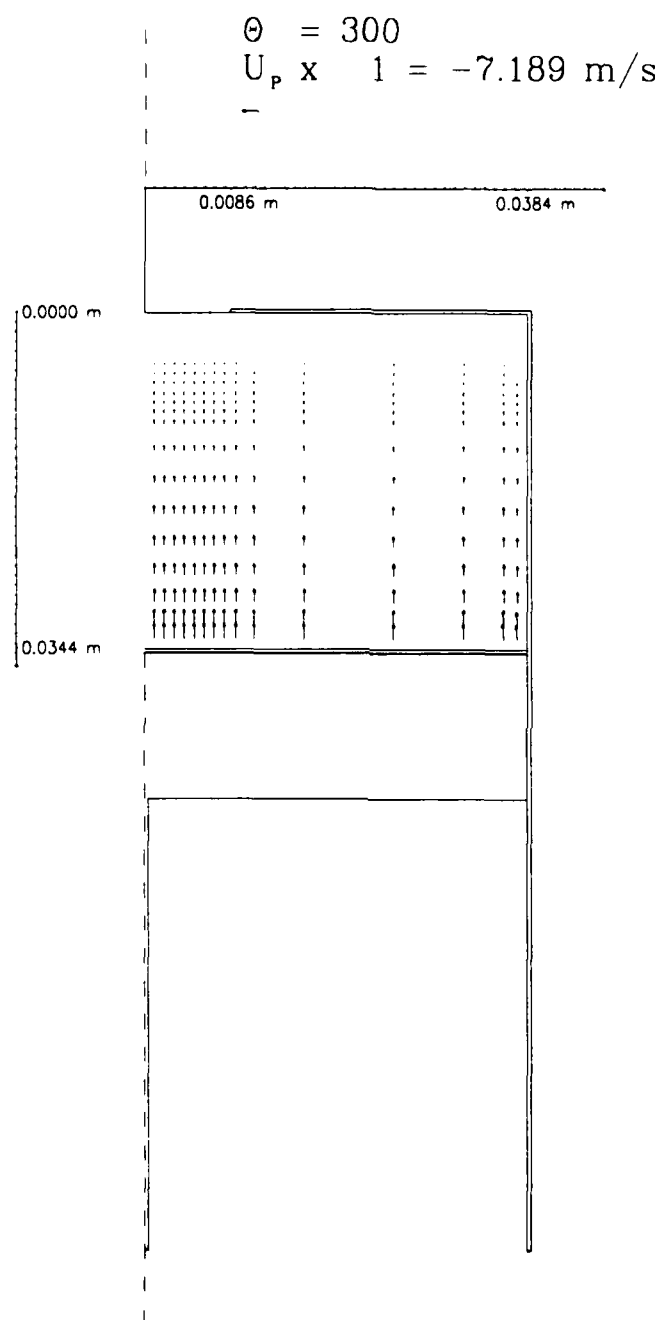


Figure E-11 Case 5 velocity vector plot for $\theta = 300^\circ$, run 1

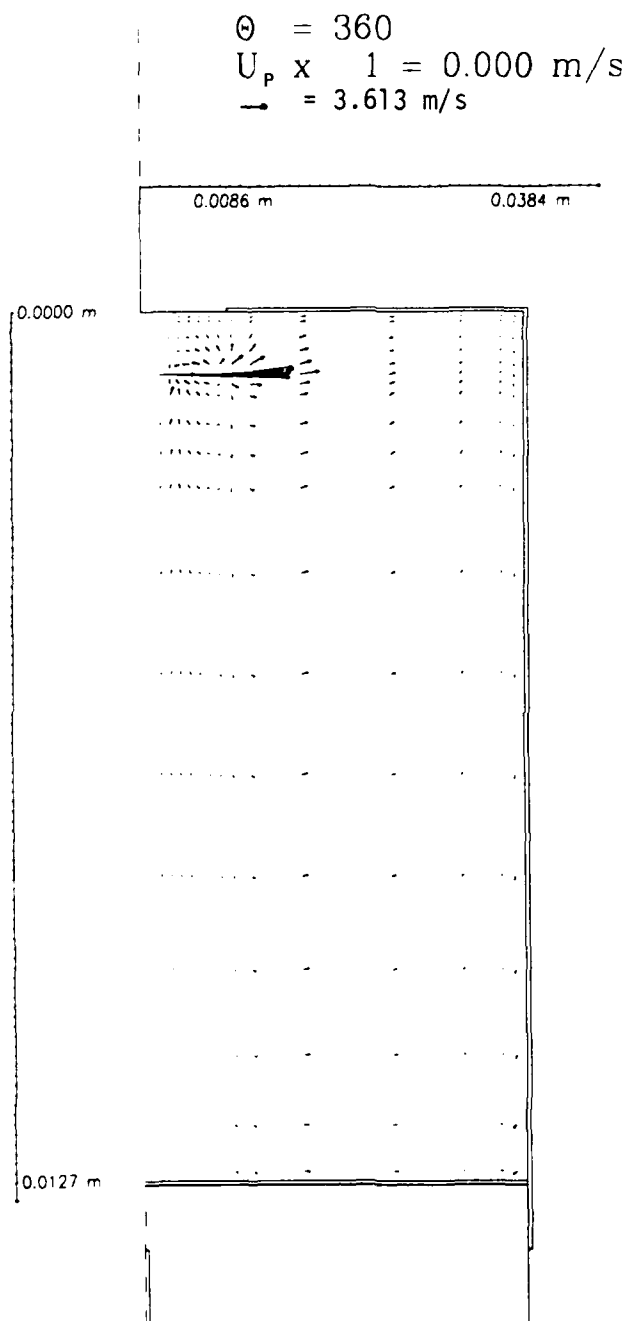


Figure E-12 Case 5 velocity vector plot for $\theta = 360^\circ$, run 1
(using x coordinate spacing (modified))

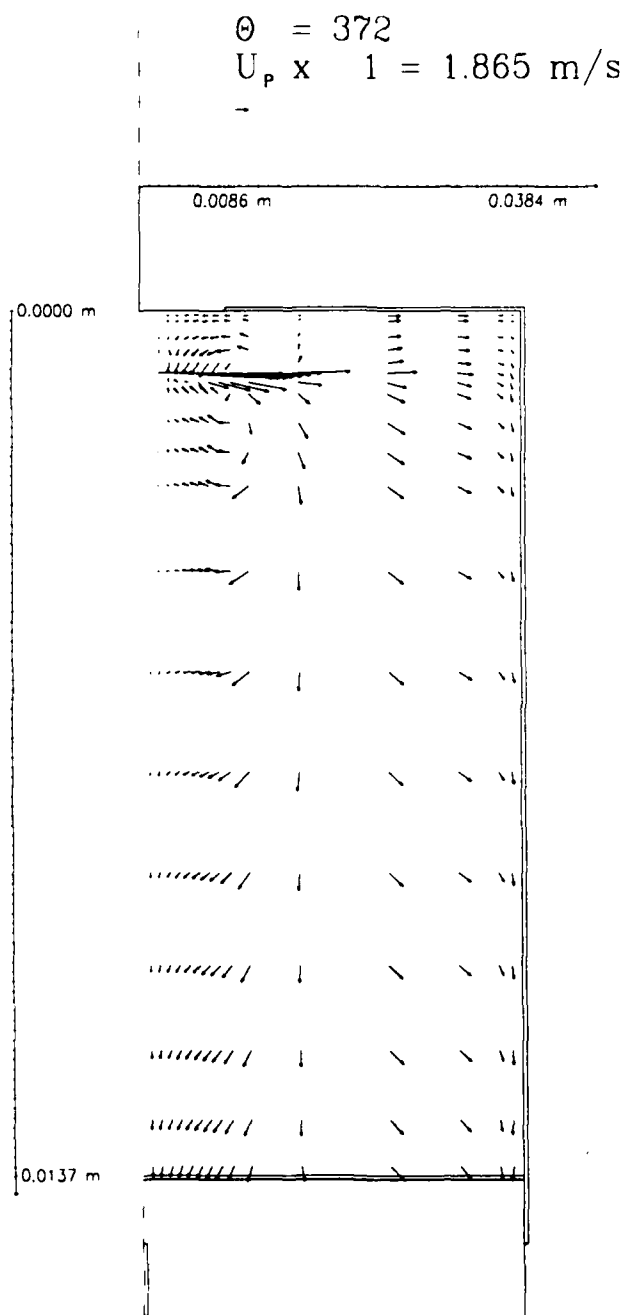


Figure E-13 Case 5 velocity vector plot for $\theta = 372^\circ$, run 1
(using x coordinate spacing(modified))

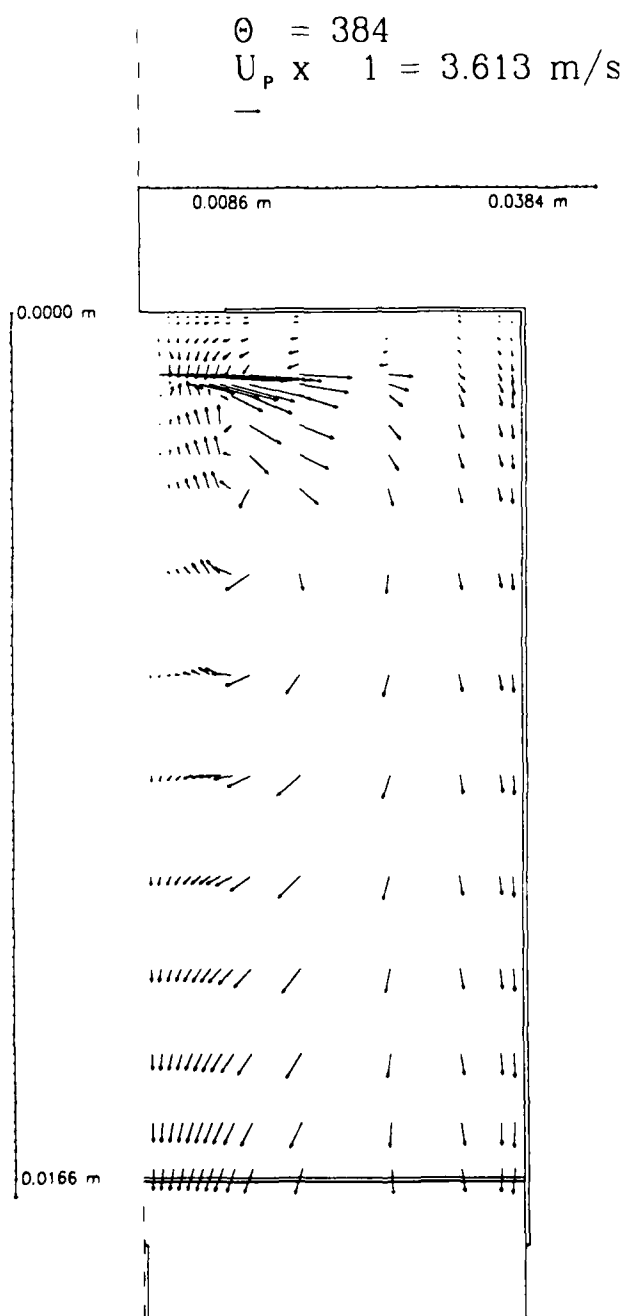


Figure E-14 Case 5 velocity vector plot for $\theta = 384^\circ$, run 1
 (using x coordinate spacing (modified))

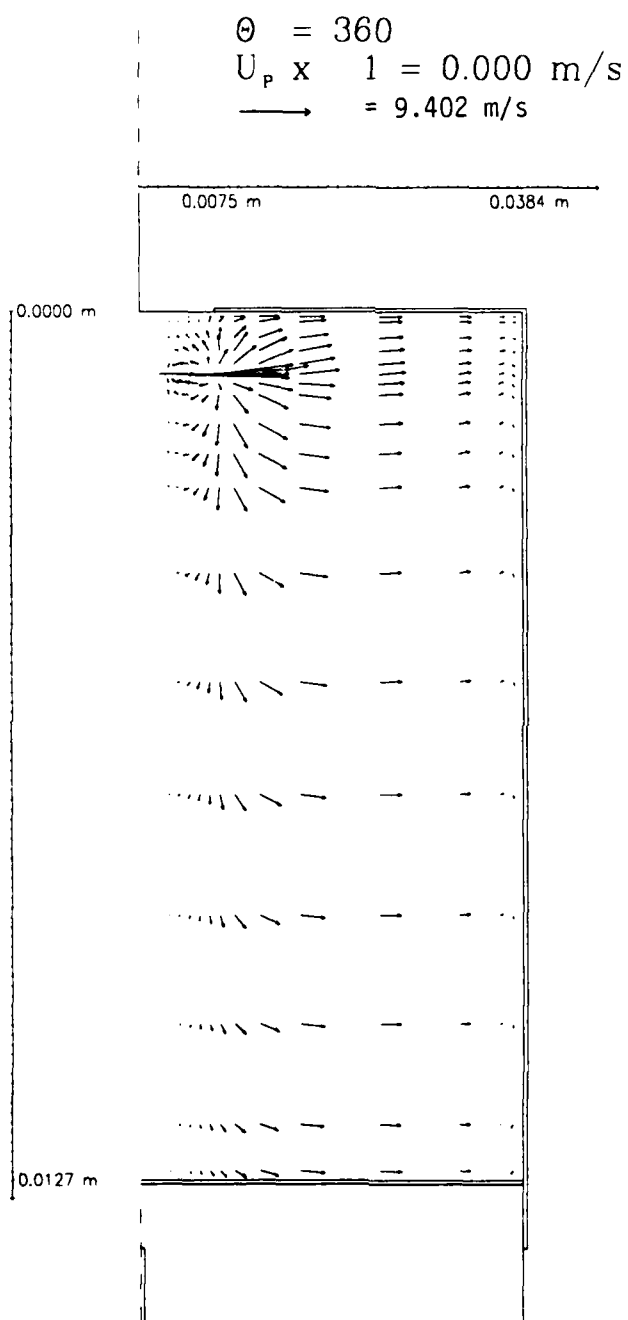


Figure E-15 Case 5 velocity vector plot for $\theta = 360^\circ$, run 2
(using x coordinate spacing (modified))

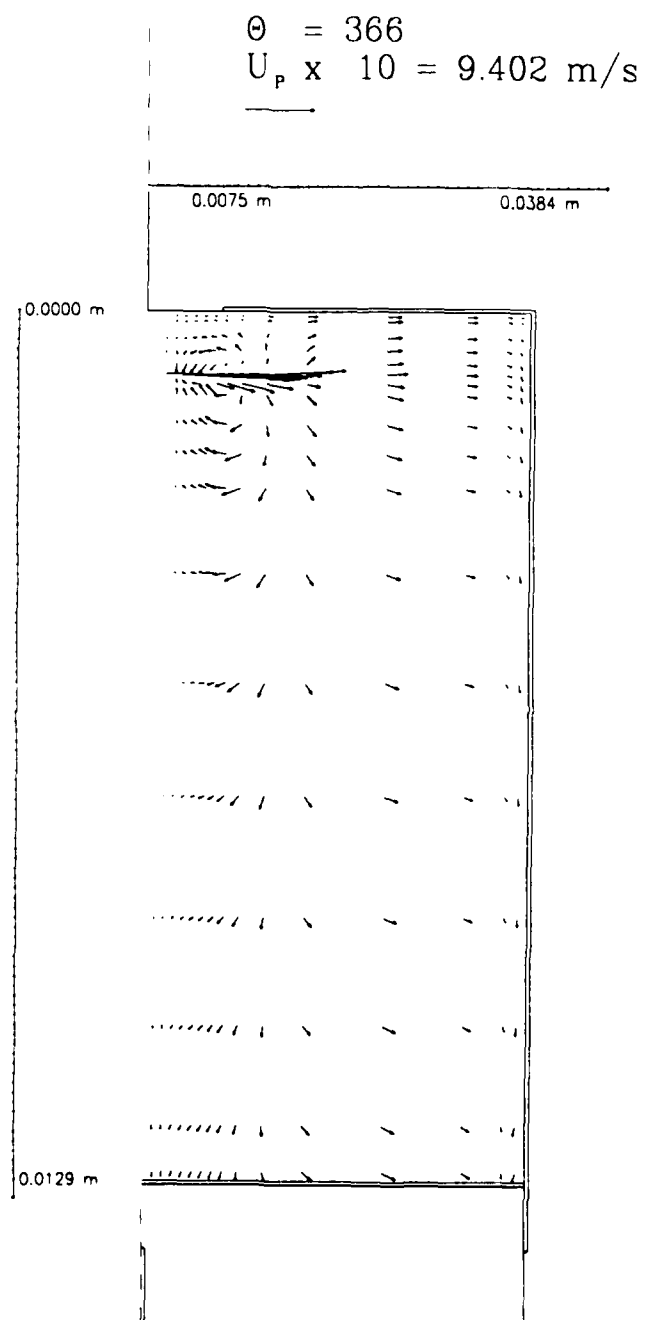


Figure E-16 Case 5 velocity vector plot for $\theta = 366^\circ$, run 2
(using x coordinate spacing (modified))

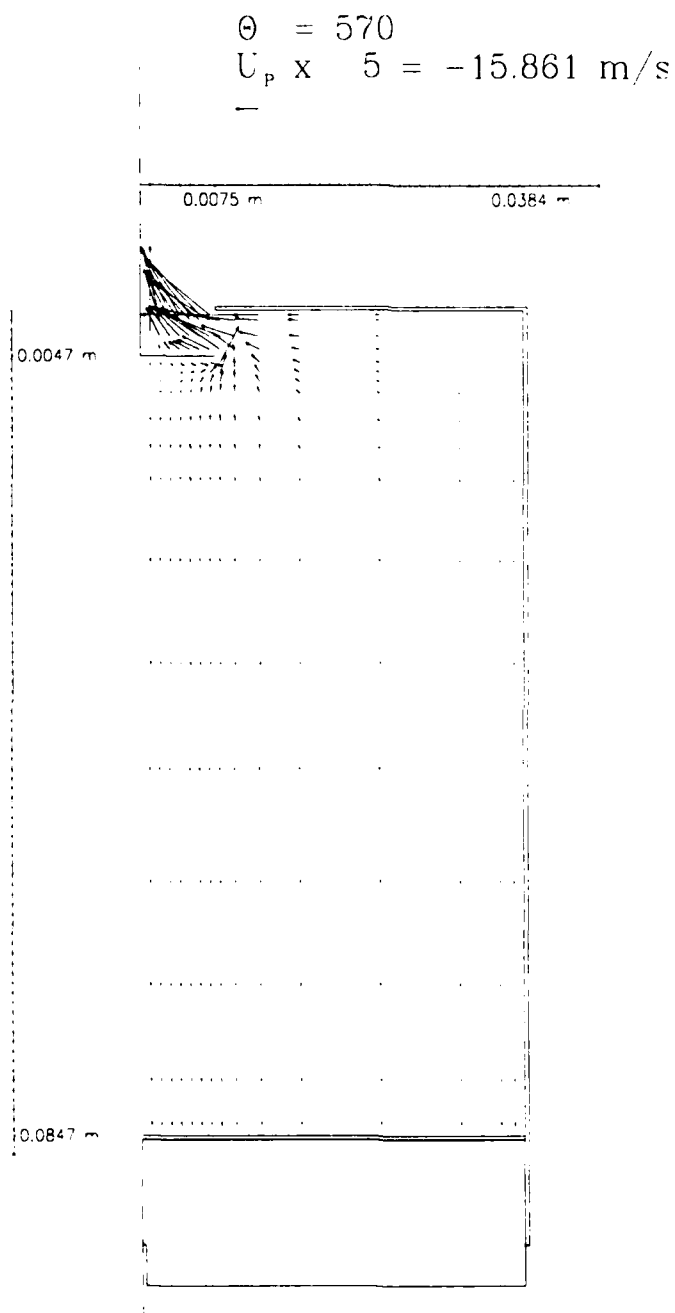


Figure E-17 Case 5 velocity vector plot for $\theta = 570^\circ$, run 3

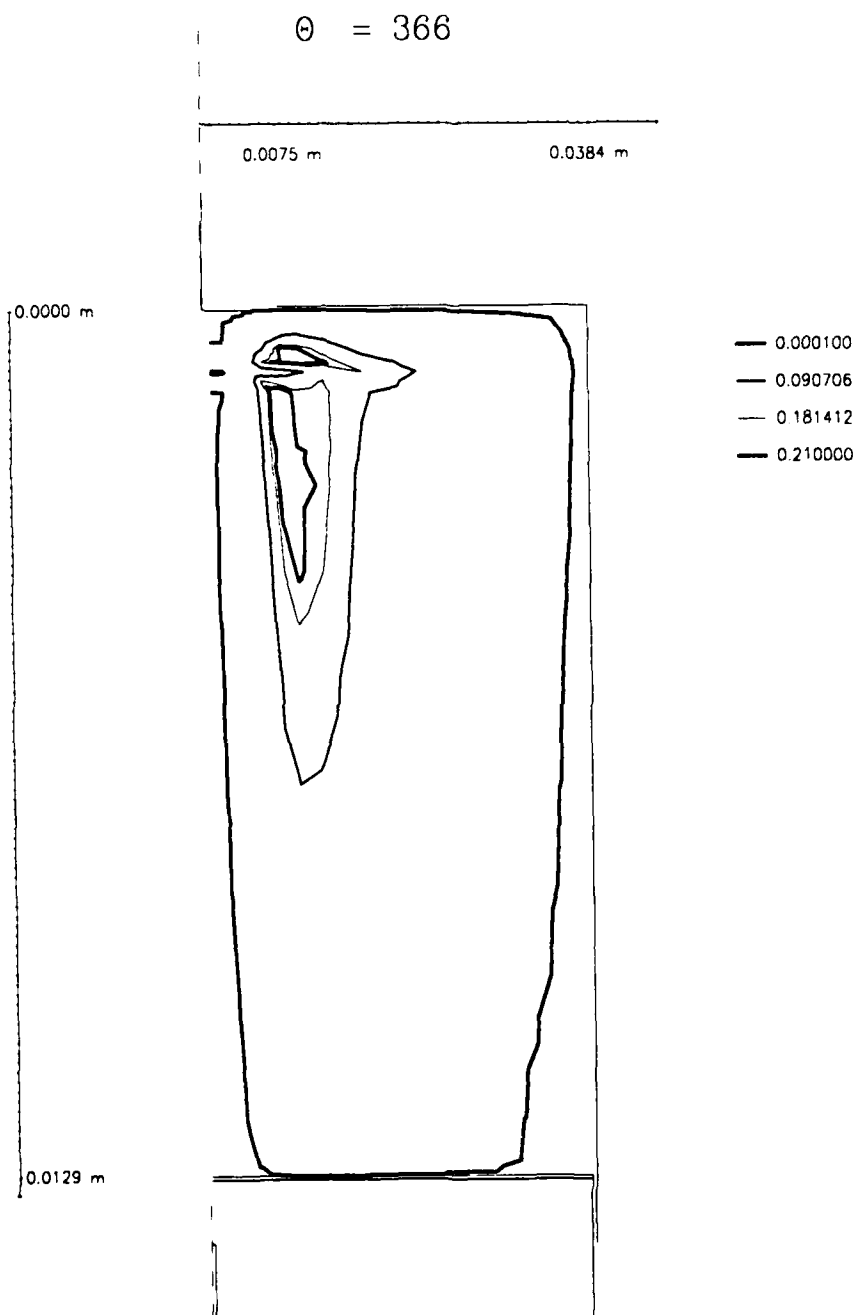


Figure E-18 Case 5 product mass fraction distribution for $\theta = 366^\circ$, run 2 (using x coordinate spacing (modified))

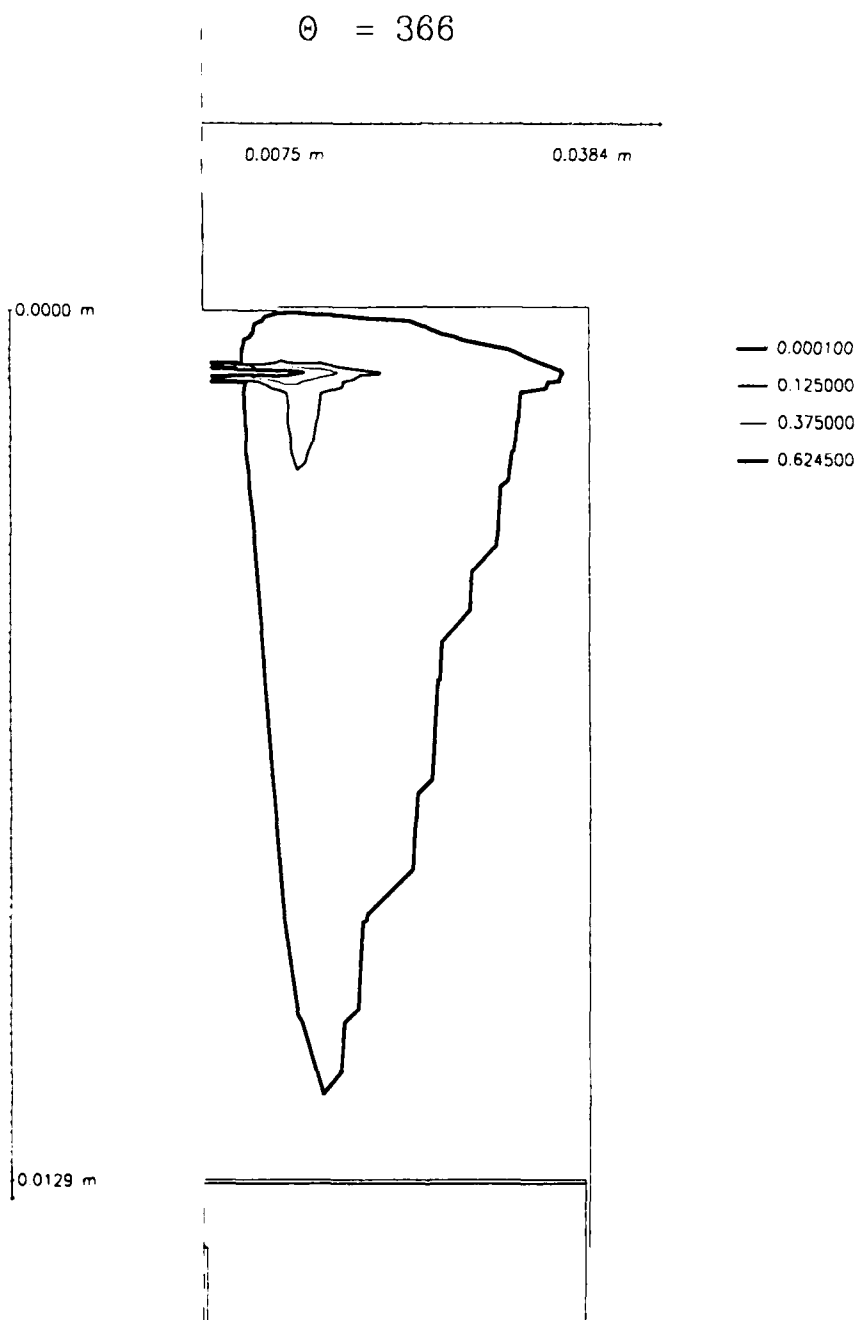


Figure E-19 Case 5 fuel mass fraction distribution at $\theta = 366^\circ$, run 2
(using x coordinate spacing (modified))

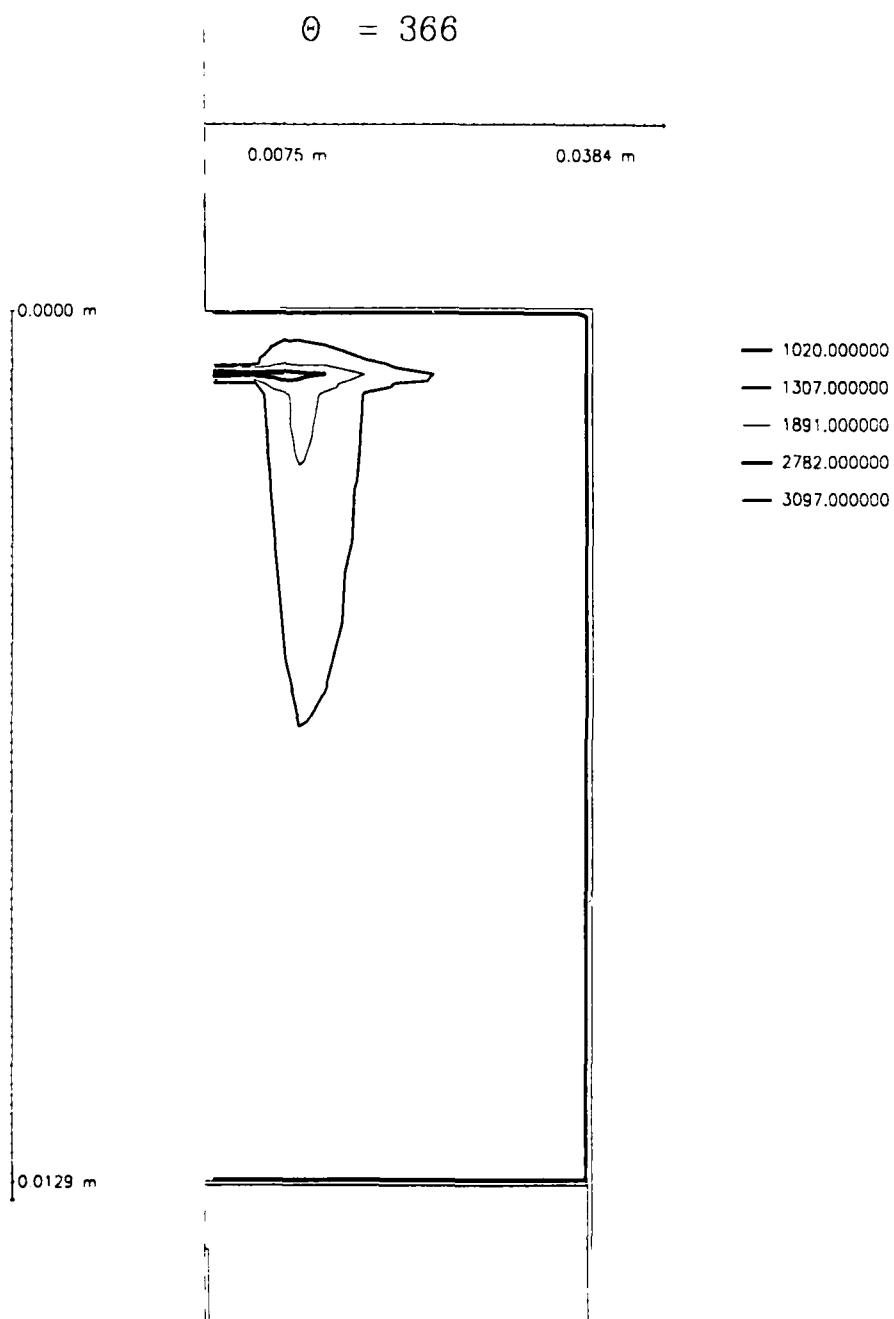


Figure E-20 Case 5 specific heat values at $\theta = 372^\circ$, run 2
(using x coordinate spacing (modified))

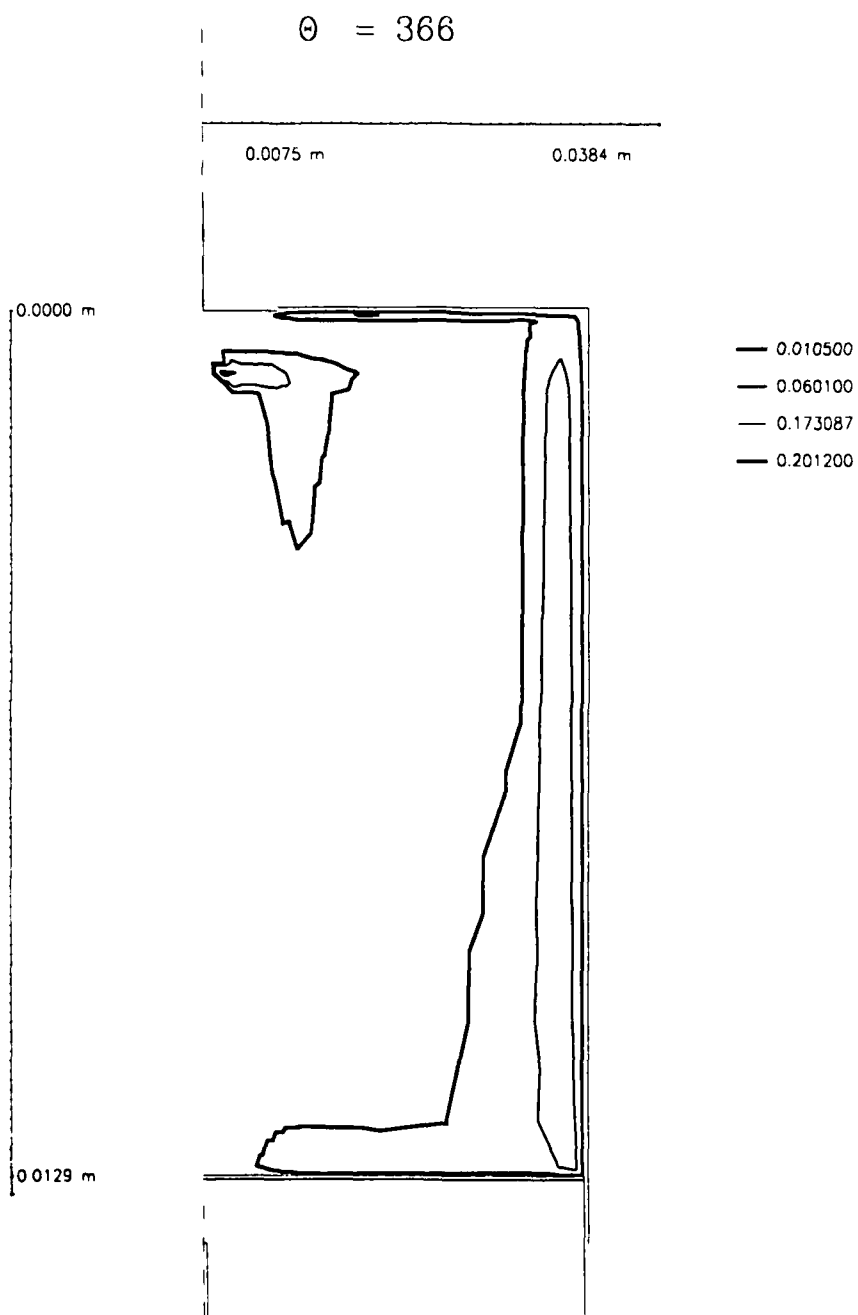


Figure E-21 Case 5 turbulent kinetic energy distribution at $\theta = 366^\circ$, run 2 (using x coordinate spacing (modified))

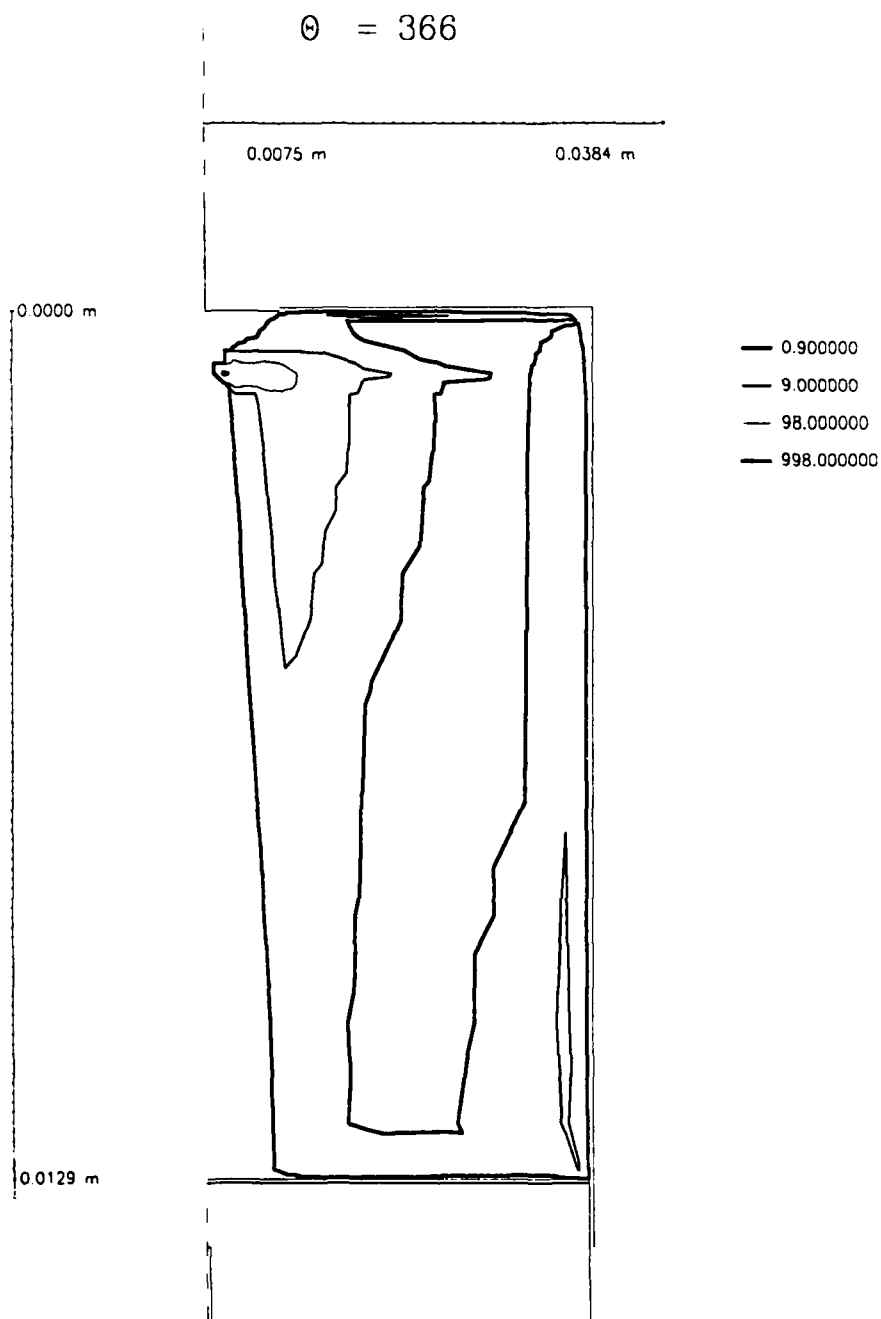


Figure E-22 Case 5 turbulent kinetic energy dissipation rate distribution at $\theta = 366^\circ$, run 2 (using x coordinate spacing (modified))

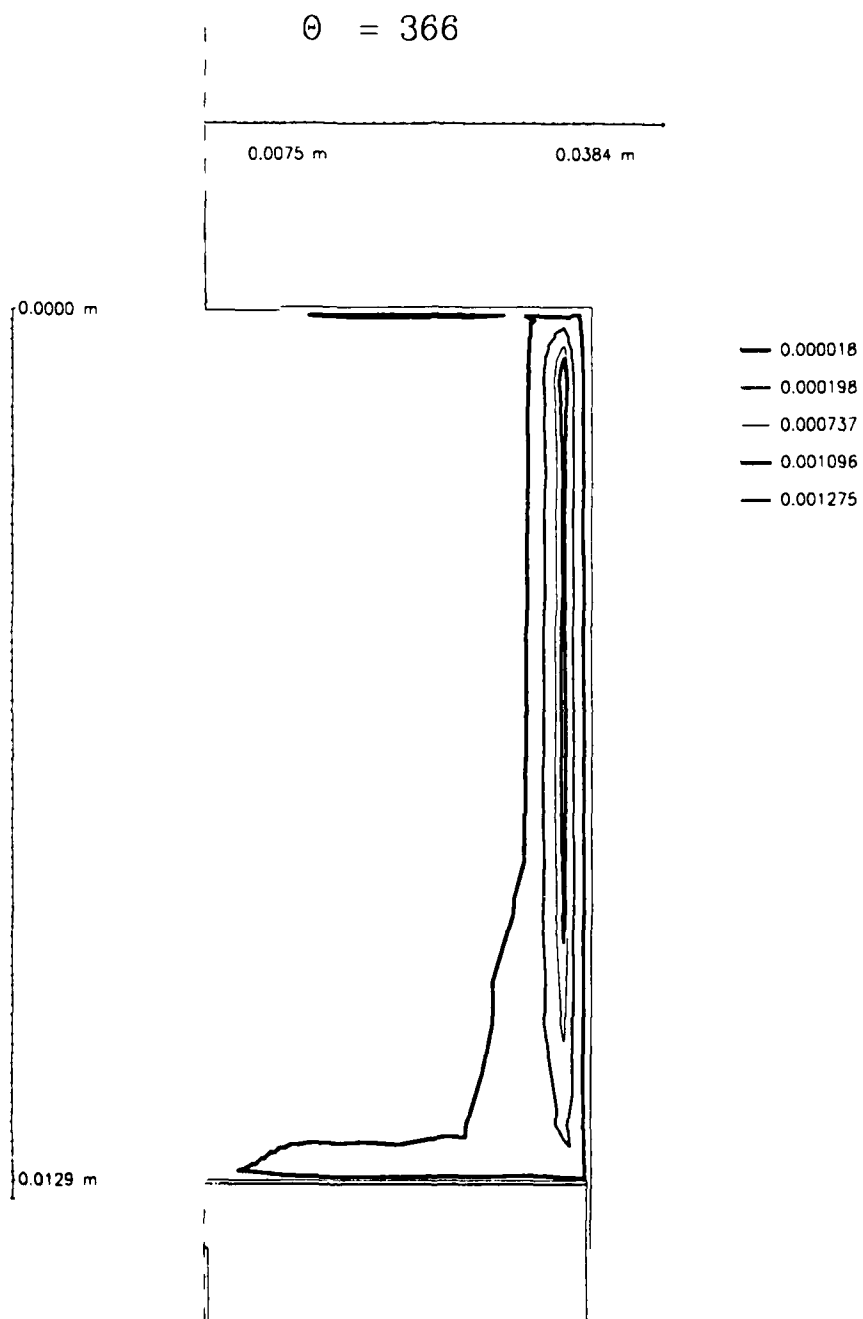


Figure E-23 Case 5 effective viscosity (μ_{eff}) profile for $\theta = 366^\circ$, run 2 (using x coordinate spacing (modified))

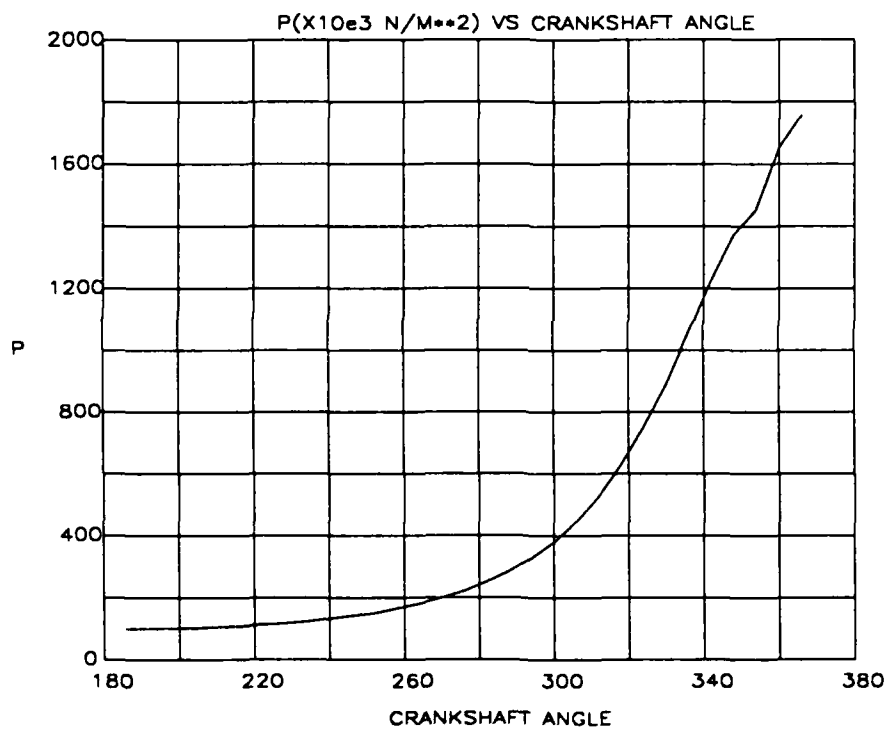


Figure E-24 Case 5 pressure (P) versus crankshaft angle (θ), run 2

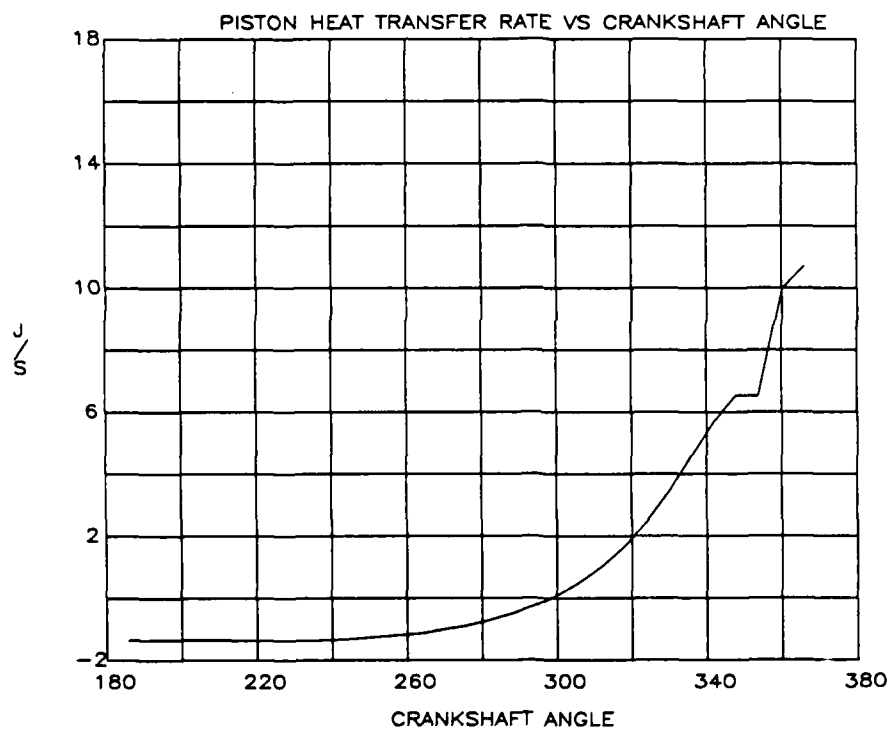


Figure E-25 Case 5 piston surface heat transfer rate versus crankshaft angle (θ), run 2 (rate through 1 radian of the piston's surface area)

REFERENCES

1. Scharnweber, D. H., "Hypergolic Combustion Demonstration in a Reciprocating Internal Combustion Engine," Eaton Corporation Report No. 84033, Warren, Michigan: U.S. Army Tank-Automotive Command Research and Development Center, May 1984.
2. Pouring, A. A., Blaser, R. F., Keating, E. L., and Rankin, B. H., "The Influence of Combustion with Pressure Exchange on the Performance of Heat Balanced Internal Combustion Engines," Presented at the International Automotive Engineering Congress and Exposition, February-March 1977, SAE Paper No. 770120.
3. Keating, E. L., Blaser, R. F., and Pouring, A. A., "Quasi-Equilibrium Air Standard Heat Balanced Cycle Analysis," SAE Paper No. 789036, August 1978.
4. Failla, C. C., Keating, E. L., Pouring, A. A., Rankin, B. H., and Riddell, F., "Parametric Variations of a Heat Balanced Engine," Fluid Mechanics of Combustion Systems Symposium, ASME, June 1981.
5. Pouring, A. A. and Rankin, B. H., "Time Dependent Analytical and Optical Studies of Heat Balanced Internal Combustion Engine Flow Fields," U.S. Naval Academy Engineering and Weapons Report, EW-13-80, November 1980, Joint ASME, SAE, AIAA Propulsion Conference, June 1982.
6. Adams, J. A., "Heat Transfer Analysis of the NAHBE Piston Cap," U.S. Naval Academy Engineering and Weapons Report, EW-11-77, September 1977.
7. Adams, J. A., "Heat Transfer Analysis of NAHBE Piston Cap, Part II - An Extension," U.S. Naval Academy Engineering and Weapons Report, EW-6-79, February 1979.
8. Keating, E. L. and Pouring, A. A., "Internal Regenerative Air Standard I.C. Engine Cycle Performance," AIAA-82-1281, AIAA/SAE/ASME 18th Joint Propulsion Conference, June 1982.
9. Keating, E. L., Pouring, A. A., and Chute, R., "Internally Regenerative Engine Cycle Analysis; A Parametric Study," Presented at the ASME Winter Annual Meeting, November 1983, ASME Paper No. 83-WA-AERO-3, November 1983.
10. Kamo, R., and Bryzik, W., "Adiabatic Turbocompound Engine Performance Prediction," Presented at the Congress and Exposition, Cobo Hall, Detroit, February-March 1978, SAE Paper No. 780068, February 1978.
11. Murray, Richard G., "Improved Engine Performance Through Heat Transfer Control," U.S. Army Research Office Report No. 1001, Research Triangle Park, North Carolina: U.S. Army Research Office, July 1978.

12. Stang, J. H., Woods, M. E., Geary, W. C., Williamson, A. S., and Updike, W. A., "Development of an Adiabatic Diesel Engine," Technical Report No. 12345, Warren, Michigan: U.S. Army Tank-Automotive Command Research and Development Center, January 1978.
13. Kamo, R., Woods, M. E., Geary, W. C., Williamson, A. S., Updike, W. A., Johnson, K. A., and Cheng, C., "Development of an Adiabatic Diesel Engine," Technical Report No. 12448, Warren, Michigan: U.S. Army Tank-Automotive Command Research and Development Center, March 1979.
14. Kirloskar, C. S., Chandorkar, S. B., and Narayan Rao, N. N., "The AV1 Series III Diesel - A Differentially - Cooled Semi-Adiabatic Engine Below 10 kW," Presented at the Off-Highway Vehicle Meeting and Exposition, September 1979, SAE Paper No. 790844.
15. Murray, R. G. and Hoecker, N. E., "Characterization of Heat Transfer in Ceramic Coated Internal Combustion Engines," U.S. Army Research Office Report No. 1, Research Triangle Park, North Carolina: U.S. Army Research Office, February 1981.
16. Bryzik, W., Glance, P., Klein, R. F., Raffa, C. J., and Rostam-Abadi, F., Diesel Engine Cycle Simulation, FY80 ILIR Year End Report, Propulsion Systems Division In-House Laboratory Independent Research (ILIR) FY80 Report No. 12535, Warren, Michigan: U.S. Army Tank-Automotive Command Research and Development Center, September 1980.
17. Wallace, F. J., Kao, T. K., Alexander, W. D., Cole, A., and Tarabad, M., "Thermal Barrier Pistons and Their Effect on the Performance of Compound Diesel Engine Cycles," Presented at the International Congress and Exposition, February-March 1983, Paper No. 830312.
18. Scharnweber, D. H., and Hoppie, L. O., "Hypergolic Combustion in an Internal Combustion Engine," Presented at the International Congress and Exposition, Detroit, Michigan, February-March 1985, SAE Paper No. 850089.
19. Hoppie, L. O., "The Influence of Initial Fuel Temperature on Ignition Delay," SAE Paper No. 820356, 1982.
20. Lockwood, F. C., "The Modelling of Turbulent Premixed and Diffusion Combustion in the Computation of Engineering Flows," Combustion and Flame 29, (1977):111-122.
21. Lavoie, G. A., Heywood, J. B., and Keck, J. C., "Experimental and Theoretical Study of Nitric Oxide Formation in Internal Combustion Engines," Combustion Science and Technology, Volume 1, (1970):313-326.
22. Woschni, G., and Anisits, F., "Experimental Investigation and Mathematical Presentation of Rate of Heat Release in Diesel Engines Dependent Upon Engine Operating Conditions," SAE Paper No. 740086.

23. Sirignano, W. A., "One-Dimensional Analysis of Combustion in a Spark-Ignition Engine," Combustion Science and Technology, Volume 7, 1973, pp. 99-108.
24. Bracco, F. V. and Sirignano, W. A., "Theoretical Analysis of Wankel Engine Combustion," Combustion Science and Technology, Volume 7, 1973, pp. 109-123.
25. Bellan, J. R. and Sirignano, W. A., "A Theory of Turbulent Flame Development and Nitric Oxide Formation in Stratified Charge Internal Combustion Engines," Combustion Science and Technology, Volume 8, 1973, pp. 51-68.
26. Sirignano, W. A., "One-Dimensional Analysis of Combustion in a Spark-Ignition Engine," Presented at the 6th Intersociety Energy Conversion Engineering Conference, Boston, MA, August 1971, also in Combustion Science and Technology, Volume 7, 1973.
27. Bracco, F. V., "Theoretical Analysis of Stratified, Two-Phase Wankel Engine Combustion," Combustion Science and Technology, Volume 8, 1973, pp. 69-84.
28. Boni, A. A., Chapman, M. and Schneyer, G. P., "A One-Dimensional Variable Area Computer Simulation of Combustion in a Divided Chamber, Stratified Charge Engine," ASME Paper No. 75-WA/DGP-1, 1975.
29. Bellan, J. R. and Sirignano, W. A., "Combustion and NO Formation in a Stratified-Charge Engine: A Two-Turbulent Equations Model," Combustion Science and Technology, Volume 12, 1976, pp. 75-104.
30. Bracco, F. V., "Theoretical Analysis of Stratified, Two-Phase Wankel Engine Combustion," Combustion Science and Technology, Volume 8, 1973, pp. 69-84.
31. Annand, W. J. D. and Pinfold, D., "Heat Transfer in the Cylinder of a Motored Reciprocating Engine," Presented at the Congress and Exposition, February 1980, SAE Paper No. 800457.
32. Borgnakke, C., Arpaci, V. S., and Tabaczynski, R. J., "A Model for the Instantaneous Heat Transfer and Turbulence in a Spark Ignition Engine," Presented at the Congress and Exposition, February 1980, SAE Paper No. 800287.
33. Borgnakke, C., Davis, G. C., and Tabaczynski, R. J., "Predictions of In-Cylinder Swirl Velocity and Turbulence Intensity for an Open Chamber Cup in Piston Engine," Presented at the International Congress and Exposition, February 1981, SAE Paper No. 810224.

34. Davis, G. C. and Borgnakke, C., "The Effect of In-Cylinder Flow Processes (Swirl, Squish and Turbulence Intensity) on Engine Efficiency - Model Predictions," Presented at the International Congress and Exposition, February 1982, SAE Paper No. 820045.
35. Morel, T. and Keribar, R., "A Model for Predicting Spatially and Time Resolved Convective Heat Transfer in Bowl-in-Piston Combustion Chambers," Presented at the International Congress and Exposition, February-March 1985, SAE Paper No. 850204.
36. Griffin, M. D., Anderson, J. D., Jr., and Diwakar, R., "Navier-Stokes Solutions of the Flowfield in an Internal Combustion Engine," AIAA Paper No. 76-403, July 1976. Also, AIAA Journal, Volume 14, No. 12, December 1976, pp. 1665-1666.
37. Diwakar, R., Anderson, J. D., Jr., Griffin, M. D. and Jones, E., "Inviscid Solutions of the Flowfield in an Internal Combustion Engine," AIAA Journal, Volume 14, No. 12, December 1976.
38. Diwakar, R., Interaction of Combustion with the Aerodynamic Flowfield in an Internal Combustion Reciprocating Engine - A Two-Dimensional Numerical Solution, Ph.D. Thesis, Department of Aerospace Engineering, University of Maryland, 1977.
39. Griffin, M. D., Numerical Solutions for Two and Three-Dimensional Non-Reacting Flows in an Internal Combustion Engine, Ph.D. Thesis, Department of Aerospace Engineering, University of Maryland, 1977.
40. Griffin, M. D., Diwakar, R., Anderson, J. D., Jr., and Jones, E., "Computational Fluid Dynamics Applied to Flows in an Internal Combustion Engine," Presented at the AIAA 16th Aerospace Sciences Meeting, Huntsville, Alabama, January 1978.
41. Gosman, A. D. and Watkins, A. P., "A Computer Prediction Method for Turbulent Flow and Heat Transfer in Piston/Cylinder Assemblies," Presented at Symposium on Turbulent Shear Flows, Pennsylvania State University, April 1977.
42. Gosman, A. D. and Johns, R. J. R., "Development of a Predictive Tool for In-Cylinder Gas Motion in Engines," Presented at the Congress and Exposition, February-March 1978, SAE Paper No. 780315.
43. Gosman, A. D., Johns, R. J. R. and Watkins, A. P., "Assessment of a Prediction Method for In-Cylinder Processes in Reciprocating Engines," Proc. General Motors Research Symposium on Combustion Modelling in Reciprocating Engines, 1978.
44. Gosman, A. D., Johns, R. J. R., Tipier, W. and Watkins, A. R., "Computer Simulation of In-Cylinder Flow, Heat Transfer and Combustion: A Progress Report," Presented at the 13th CIMAC Conference, Vienna, 1979.

45. Arcoumanis, C., Bicen, A. F., Gosman, A. D., Morse, A. P., and Whitelaw, J. H., Velocity Characteristics of the Flow in Motored Engines, Report Grant No. DA-ERO-79-G-0030, London: European Research Office, U.S. Army, June 1980.
46. Gosman, A. D. and Johns, R. J. R., "Computer Analysis of Fuel-Air Mixing in Direct-Injection Engines," SAE Report No. 800091, 1980.
47. Ahmadi-Befrui, B., Gosman, A. D., Lockwood, F. C., and Watkins, A. P., "Multidimensional Calculation of Combustion in an Idealized Homogeneous Charge Engine: A Progress Report," SAE Report No. 810151, 1981.
48. Gosman, A. D. and Harvey, P. S., "Computer Analysis of Fuel-Air Mixing and Combustion in an Axisymmetric D.I. Diesel," Presented at the International Congress and Exposition, February 1982, SAE Report No. 820036.
49. Gosman, A. D., Tsui, Y. Y. and Watkins, A. P., "Calculation of Three-Dimensional Air Motion In Model Engines," SAE Paper No. 840229, 1984.
50. Gupta, H. C., Bracco, F. V. and Westbrook, C. K., "Mathematical Modeling of Two-Phase, Unsteady, Two-Dimensional Flows," Paper G5 presented at the Fifth International Colloquium on Gas-dynamics of Explosions and Reactive Systems, September 1975.
51. Bracco, F. V., Gupta, H. C., Krishnamurthy, L., Santavicca, D. A., Steinberger, R. L., and Warshaw, V., "Two-Phase, Two-Dimensional Unsteady Combustion in Internal Combustion Engines: Preliminary Theoretical-Experimental Results," Presented at the SAE Automotive Engineering Congress, February 1976, SAE Paper No. 760114.
52. Bracco, F. V., Gupta, H. C. and Westbrook, C. K., "Numerical Computations of Two-Dimensional, Unsteady Sprays for Application to Internal Combustion Engines," Paper No. 13, Presented at the Combustion Institute Eastern Section Fall Meeting, November 1976.
53. Bracco, F. V., "Modelling of Two-Phase, Two-Dimensional, Unsteady Combustion for Internal Combustion Engines," In-Stratified Charge Engines, I. Mech E. Conference Publications, 1976, p 167.
54. Gupta, H. C., Steinberger, R. L. and Bracco, F. V., "Combustion in a Divided Chamber, Stratified Charge, Reciprocating Engine: Initial Comparisons of Calculated and Measured Flame Propagation," Combustion Science and Technology, Volume 22, 1980, pp. 27-61.
55. Butler, T. D. and O'Rourke, P. J., "A Numerical Method for Two-Dimensional Unsteady Reacting Flows," Presented at the Sixteenth Symposium on Combustion, August 1976.

56. Butler, T. D., Cloutman, L. D., Dukowicz, J. K., and Ramshaw, J. D., "Multidimensional Numerical Simulation of Reactive Flow in Internal Combustion Engines," Prog. Energy Combustion Science, Volume 7, 1981, pp. 293-315.
57. Butler, T. D., Cloutman, L. D., Dukowicz, J. K. and Ramshaw, J. D., "Toward A Comprehensive Model For Combustion in a Direct-Injection Stratified-Charge Engine," Combustion Modeling in Reciprocating Engines, Presented at the Symposium on Combustion Modeling in Reciprocating Engines, 1978, New York: Plenum Press, 1980.
58. Haselman, L. C., "TDC - A Computer Code for Calculating Chemically Reacting Hydrodynamic Flows in Two-Dimensions," Lawrence Livermore Lab Report UCRL-25931, 1980.
59. Boni, A. A. and Nakayama, P. I., "Two-Dimensional Computer Simulation of Combustion in a Divided-Chamber Stratified Charge Engine," Paper G4 presented at the Fifth International Colloquium on Gasdynamics of Explosions and Reactive Systems, September 1975.
60. Boni, A. A., Chapman, M., Cook, J. L. and Schneyer, G. I., "Computer Simulation of Combustion in Stratified Charge Engines," Presented at the Sixteenth Symposium on Combustion, August 1976.
61. Boni, A. A., "Numerical Simulation of Flame Propagation In Internal Combustion Engines," Presented at the Congress and Exposition, February-March 1978, SAE Paper No. 780316.
62. MacCormack, R. W., "An Efficient Numerical Method for Solving the Time-Dependent Compressible Navier-Stokes Equations at High Reynolds Number," NASA TM X-73, 129, July 1976.
63. Rivard, W. C., Farmer, O. A. and Butler, T. D., "Rice: A Computer Program for Multicomponent Chemically Reactive Flows At All Speeds," Los Alamos Scientific Lab Report, LA-5812, 1975.
64. Hirt, C. W., Amsden, A. A. and Cook, J. L., "An Arbitrary Lagrangian-Eulerian Computing Method for all Flow Speeds," Journal of Computational Physics, Volume 14, No. 3, March 1974, pp. 227-253.
65. Ramos, J. I., Laminar Flow Calculations in Internal Combustion Engines, MAE Report No. 1409, Department of Mechanical and Aerospace Engineering, Princeton University, 1978.
66. Ramos, J. I., Turbulent Flow Calculations in Internal Combustion Engines, MAE Report No. 1410, Department of Mechanical and Aerospace Engineering, Princeton University, 1978.
67. Ramos, J. I. and Sirignano, W. A., "Axisymmetric, Unsteady Calculations in a Piston-Cylinder Configuration," Presented at the 1979 National Conference on Numerical Methods in Heat Transfer, University of Maryland, September 1979.

68. Ramos, J. I. and Sirignano, W. A., "Axisymmetric Flow Model With and Without Swirl in a Piston-Cylinder Arrangement With Idealized Valve Operation," SAE Paper No. 800284, 1980.
69. Ramos, J. I., "Axisymmetric Flow Model in a Piston-Cylinder Arrangement with Detailed Analysis of the Valve Region," Presented at the Congress and Exposition, February 1980, SAE Paper No. 800286.
70. Ramos, J. I. and Sirignano, W. A., "Turbulent Flow Field in Homogeneous-Charge, Spark-Ignition Engines," Presented at the Eighteenth International Symposium on Combustion, The Combustion Institute, 1981.
71. Bernard, P. S., "Computation of the Turbulent Flow in an Internal Combustion Engine During Compression," Journal of Fluids Engineering, Volume 103, March 1981, pp. 75-81.
72. Bernard, P. S., "A Method for Computing Two-Dimensional Turbulent Flows," SAIM Journal of Applied Mathematics, Volume 38, No. 1, February 1980, pp. 81-92.
73. Diwakar, R., "Multidimensional Modelling Applied to the Direct-Injection Stratified Engine - Calculation Versus Experiment," SAE Paper No. 810225, 1981.
74. Diwakar, R., "Direct Injection Stratified-Charge Engine Computations With Improved Submodels for Turbulence and Wall Heat Transfer," Presented at the International Congress and Exposition, February 1982, SAE Paper No. 820039.
75. Butler, T. D., Cloutman, L. D., Dukowicz, J. K. and Ramshaw, J. C., "CONCHAS: An Arbitrary Lagrangian-Eulerian Computer Code for Multi-Component Chemically Reactive Fluid Flows at All Speeds," Los Alamos Scientific Laboratories Report LA-8129-MS, November 1979.
76. Patankar, S. V., Numerical Heat Transfer and Fluid Flow, Washington, DC: Hemisphere Publishing Corporation, 1980.
77. Jones, W. P. and Launder, B. E., "The Calculation of Low-Reynolds Number Phenomena With a Two-Equation Model of Turbulence," International Journal of Heat and Mass Transfer, Volume 16, 1973, pp. 1119-1130.
78. Gosman, A. D. and Ideriah, F. J. K., "Teach-T: A General Computer Program for Two-Dimensional, Turbulent, Recirculating Flows," Department of Mechanical Engineering, Imperial College, London, England, June 1976.
79. Magnussen, B. F. and Hjertager, B. H., "On Mathematical Modeling of Turbulent Combustion with Special Emphasis on Soot Formation and Combustion," Presented at the 16th International Symposium on Combustion, The Combustion Institute, 1976.

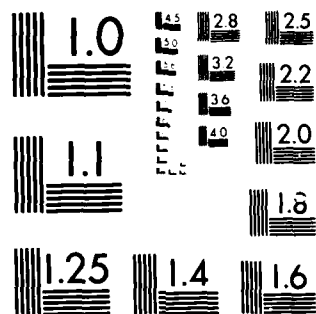
80. Launder, B. E. and Spalding, D. B., Mathematical Models of Turbulence, London: Academic Press Inc. Ltd., 1972.
81. Chute, R., Eaton Corporation, Engineering and Research Center, Southfield, Michigan, Personal Interview.
82. Shih, T. M., "Procedure to Debug Computer Programs," International Journal for Numerical Methods in Engineering, Volume 21, June 1985, pp. 1027ff.
83. Benson, R. S. and Whitehouse, N. D., Internal Combustion Engines, Volume 1, Oxford: Pergamon Press, 1979.
84. Jones, W. P., Lockwood, F. C. and Whitelaw, J. H., Notes for a Lecture Course Entitled, 'Modeling of Combustion Chambers and Furnaces Pennsylvania State University, June 1983.
85. Keating, E. L., "Internal and External Combustion Science: Principles and Applications" -- Lecture Notes, 1980-1981, U.S. Naval Academy.
86. Tribus, M., Thermostatistics and Thermodynamics, Princeton: Van Nostrand Co., 1961.
87. Patankar, S. V., "A Calculation Procedure For Two-Dimensional Elliptic Situations," Numerical Heat Transfer, Volume 4, 1981, pp. 409-425.
88. Roach, P. J., Computational Fluid Dynamics, Albuquerque: Hermosa Publishers, 1976.
89. Fox, R. W. and McDonald, A. T., Introduction to Fluid Mechanics, New York: John Wiley and Sons, Inc., 1978.
90. Rohsenow, W. M. and Hartnett, J. P., ed., Handbook of Heat Transfer, New York: McGraw-Hill Book Co., 1973.
91. Hughes, W. F. and Gaylord, E. W., Schaum's Outline Series: Basic Equations of Engineering Science, New York: McGraw-Hill Book Co., 1964.
92. Libby, P. A. and Williams, F. A., ed., Turbulent Reacting Flows, New York: Springer-Verlog, 1980.
93. Jones, W. P. and Launder, B. E., "The Prediction of Laminarization with a Two-Equation Model of Turbulence," International Journal of Heat and Mass Transfer, Volume 15, February 1972, pp. 304-314.
94. Morel, T. and Mansour, N. M., "Modeling of Turbulence in Internal Combustion Engines," Presented at the International Congress and Exposition, February 1982, Paper No. 830312.

AD-A165 003 NUMERICAL HEAT TRANSFER MODEL FOR A HEAT-BARRIER-PISTON 3/3
ENGINE WITH HYPER. (U) NAVAL ACADEMY ANNAPOLIS MD DIV
OF ENGINEERING AND WEAPONS D A BLANK FEB 86
UNCLASSIFIED USNA-EH-8-86 F/G 21/7 NL

END

FILMED

DTIC



MICROCOPY RESOLUTION TEST CHART
NATIONAL BUREAU OF STANDARDS 1963-A

95. Shih, T. M., Numerical Heat Transfer, Washington: Hemisphere Publishing Corporation, 1984.
96. Shih, T. M. and Ren, A. L., "Combined Convective and Radiative Recirculating Flows in Enclosures," Natural Convection in Enclosures - 1983-HTD, Volume 26, pp. 49-57.

END

FILMED

4-86

DTIC